②

Naval Research Laboratory
Washington, DC 20375-5000

NRL Memorandum Report 6163

The NRL Phase-Locked Gyrotron Oscillator Program for SDIO/IST

W. M. MANHEIMER, A. W. FLIFLET, S. H. GOLD
J. BURKE,* W. M. BLACK AND L. BARNETT†

High Power Electromagnetic Radiation Branch
Plasma Physics Division

**Burke Technologies, Inc.*
San Diego, CA 92111

†Department of Electrical Engineering
University of Utah
Salt Lake City, UT 84112

July 11, 1988

SECURITY CLASSIFICATION OF THIS PAGE

REPORT DOCUMENTATION PAGE

Form Approved
OMB No. 0704-0188

1a. REPORT SECURITY CLASSIFICATION: UNCLASSIFIED

1b. RESTRICTIVE MARKINGS

2a. SECURITY CLASSIFICATION AUTHORITY

2b. DECLASSIFICATION / DOWNGRADING SCHEDULE

3. DISTRIBUTION / AVAILABILITY OF REPORT: Approved for public release; distribution unlimited

4. PERFORMING ORGANIZATION REPORT NUMBER(S): NRL Memorandum Report 6163

5. MONITORING ORGANIZATION REPORT NUMBER(S)

6a. NAME OF PERFORMING ORGANIZATION: Naval Research Laboratory

6b. OFFICE SYMBOL (If applicable): Code 4740

7a. NAME OF MONITORING ORGANIZATION

6c. ADDRESS (City, State, and ZIP Code): Washington, DC 22217

7b. ADDRESS (City, State, and ZIP Code)

8a. NAME OF FUNDING / SPONSORING ORGANIZATION: SDIO/IST

8b. OFFICE SYMBOL (If applicable)

9. PROCUREMENT INSTRUMENT IDENTIFICATION NUMBER

8c. ADDRESS (City, State, and ZIP Code):
Room 2C086
2800 Powder Mill Road
Adelphi, MD 20783

10. SOURCE OF FUNDING NUMBERS

PROGRAM ELEMENT NO	PROJECT NO	TASK NO	WORK UNIT ACCESSION NO.
66000A	DN156-218		47-2700-00

11. TITLE (Include Security Classification): The NRL Phase-Locked Gyrotron Oscillator Program for SDIO/IST

12. PERSONAL AUTHOR(S): Manheimer, W.M., Fliflet, A.W., Gold, S.H., Burke,* J., Black, W.M., and Barnett,+ L.

13a. TYPE OF REPORT: Interim

13b. TIME COVERED: FROM ________ TO ________

14. DATE OF REPORT (Year, Month, Day): 1988 July 11

15. PAGE COUNT: 174

16. SUPPLEMENTARY NOTATION:
*Burke Technologies, Inc., San Diego, CA 92111
+Department of Electrical Engineering, University of Utah, Salt Lake City, UT 84112

17. COSATI CODES

FIELD	GROUP	SUB-GROUP

18. SUBJECT TERMS (Continue on reverse if necessary and identify by block number): Large scale phased array, Amplifiers, Synchronization of coupled oscillators, Veba driven, free running oscillators,

19. ABSTRACT (Continue on reverse if necessary and identify by block number)

This is the second annual report on the NRL phase-locked gyrotron oscillator program for SDIO/IST. The introduction summarizes the program as well as possible SDIO applications for high power phase-locked microwave and millimeter wave sources. It considers the different possible architectures for a phased array for an SDIO mission. Section II summarizes results in theory. The main accomplishment was the development of a slow time scale code which examines phase locking in time varying situations. Section III summarizes the experimental design of the low power experiment which will examine phase locking in overmode cavities. Section IV summarizes the results of the slotted cavity experiments. The axial slots allow for mode control. With a slotted cavity, a gyrotron oscillator has reliably generated 35 MW at 35 GHz in a standing TE_{13} mode. Section V summarizes results on the VEBA driven free running oscillator. This experiment has succeeded in generating 200 MW at 35 GHz in a TE_{62} mode. Section VI discusses experimental design of the VEBA fundamental mode three cavity phase-locked oscillator at 35 GHz. This experiment is expected to

(Continues)

20. DISTRIBUTION / AVAILABILITY OF ABSTRACT: ☐ UNCLASSIFIED/UNLIMITED ☒ SAME AS RPT ☐ DTIC USERS

21. ABSTRACT SECURITY CLASSIFICATION: UNCLASSIFIED

22a. NAME OF RESPONSIBLE INDIVIDUAL: Wallace M. Manheimer

22b. TELEPHONE (Include Area Code): (202) 767-3128

22c. OFFICE SYMBOL: Code 4740

DD Form 1473, JUN 86 Previous editions are obsolete. SECURITY CLASSIFICATION OF THIS PAGE

S/N 0102-LF-014-6603

3

19. ABSTRACTS (Continued)

produce phase-locked power at the 5 MW level. Section VII discusses the experimental results up to now on this experiment. Section VIII discusses the experimental design of the strongly coupled phase-locked oscillator experiment.

CONTENTS

I. INTRODUCTION 1

References for Section I 14

II. HIGH POWER GYROTRON THEORY 20

II.1 OVERVIEW OF THEORETICAL EFFORT 20

II.2 INTRODUCTION TO THE THEORY OF DRIVEN GYROTRON OSCILLATOR 23

II.3 PHASE-LOCKED OSCILLATOR THEORY 26

II.4 RESULTS OF CALCULATIONS FOR A DRIVEN OSCILLATORS 45

II.5 DISCUSSION OF DRIVEN OSCILLATOR THEORY AND RESULTS 51

REFERENCES FOR SECTION II 53

III. THE LOW POWER OSCILLATOR EXPERIMENTAL DESIGN 63

REFERENCES FOR SECTION III 77

IV. FEBETRON-GYROTRON SLOTTED CAVITY EXPERIMENTS 96

REFERENCES FOR SECTION IV 97

V. VEBA GYROTRON OSCILLATOR EXPERIMENT 98

VI. THREE-CAVITY PHASE-LOCKED GYROTRON CIRCUIT DESIGN 109

REFERENCES FOR SECTION VI 119

VII. VEBA THREE-CAVITY PHASE-LOCKING EXPERIMENT 131

A. Diagnostics 131
B. Apparatus 133

1. Cavities 133
2. Beam Formation 136

REFERENCES FOR SECTION VII 138

VIII. STRONGLY COUPLED OSCILLATOR EXPERIMENT 143

COUPLING OF HIGH-POWER HIGH-ORDER-MODE GYROTRON CAVITIES 145

CAVITY MODE EXCITATION 146

MODE SUPPRESSION BY THE SELECTION AND POSITIONING OF COUPLING 152

COUPLING CAVITY BETWEEN OSCILLATORS 155

DISTRIBUTION LIST 163

THE NRL PHASE-LOCKED GYROTRON OSCILLATOR PROGRAM FOR SDIO/IST

I. Introduction

This report is for the second year of the SDIO/IST project on high power phase-locked oscillators at the U. S. Naval Research Laboratory. We preface the actual report of progress with a brief discussion of the options available for a large scale phased array and a discussion of the reasons that such would be of interest for strategic defense.

There are three types of architecture available for a large scale phased array. These are architectures based on amplifiers, weakly driven phase-locked oscillators, and on strongly driven phase-locked oscillators. All other things being equal, amplifiers are the preferred choice since the high power source is the slave of the low power driver as regards both amplitude and phase. If the technological challenges in building an amplifier prove to be too difficult, the next choice is the weakly driven phase-locked oscillator. Here, the tubes oscillate on their own; however, their phases can be controlled by inputting a low power signal. It is important to note that in the weakly driven phase-locked oscillator, power flows only from the low power control to the high power oscillator, and not vice versa. Thus, as in the case of an amplifier, the control is isolated from the oscillator, and if a phased array is made, the oscillators are isolated from each other. The last type of architecture which we consider is that of the strongly coupled

---

Manuscript approved January 7, 1988

oscillator. In this case, two oscillators of equal strength phase lock each other. This is, of course, the analog of Huygen's observation that two clocks (oscillators of equal strength) will synchronize each other when placed on the same wall. Note that in this case, the power flows equally between the oscillators, and neither is isolated from the other. In a large scale phased array, the synchronization would undoubtedly be very complicated and take a very long time to achieve, since there are many possible cross communication channels. This problem of synchronization of strongly coupled oscillators gets very much into the area of chaos, on which so much fascinating work has been done lately. Schematics of the three basic types of architecture are shown in Figs. I.1, I.2, and I.3.

We now discuss the possible applications of such phase controlled sources and arrays to strategic defense. The first potential application is to directed energy at very high power. Consider, for example, an array of 1000 Gigawatt sources spread out so that the effective antenna area is 100 km^2. This would irradiate a target at a range of 1000 km with an irradiance of 10^{6}W/cm2. (Notice that such a large antenna focuses the radiation to a spot considerably smaller than the antenna itself, so that at the antenna, the irradiance on the antenna would be considerably less than the atmospheric breakdown limit.) To build such an array with today's technology, the most likely approach would be to use SLAC klystrons.[1] These are amplifiers and have been built at a frequency of 3 GHz, a power of 150 MW, an efficiency of 50% and a pulse length of 1 μsec. The authors of Ref. 1 claim that the power in the tube can be upgraded to 700 MW, so that as far as tube power goes, today's technology can take us just about where we want to go.

The opinion of the NRL group is that the role for innovative technology is to extend this capability, to the extent possible, to higher frequencies. For the large phased array for directed energy, this would reduce the antenna size, and thereby reduce the cost and complexity of the system considerably. For instance, at 10 GHz, the antenna size would go down to 3 km on a side, and at 30 GHz, it would further shrink to 1 km on a side.

In going to higher frequency, the temptation might be to use a klystron. However, a klystron has very unfavorable scaling with frequency. The scaling usually invoked is $P \sim f^{-5/2}$, so that at, say 30 GHz, the SLAC klystron of Ref. 1 would scale to a power of 2 MW. It could then be argued that the most prudent technique would be to develop a high power amplifier at high frequency. However, experience has shown that at high frequency, amplifiers are much more difficult to build than oscillators. Even in fundamental mode, it is difficult to suppress oscillation if the radiation can make many round trips in the structure. As the system gets more and more overmoded, suppressing spurious oscillation in every possible mode just becomes extraordinarily more difficult. Unlike a conventional klystron, for which the beam has no free energy in the absence of an input signal, nearly every source proposed for high frequency does have free energy to drive oscillation in the absence of an input signal. Thus, there is an even greater tendency for the cavity to oscillate, particularly at the large volume cavities necessary for high power.

Since oscillation is so difficult to prevent at high power and high frequency, the logical strategy is to use this oscillation, but to phase-lock it, rather than avoid it. Thus, the strategy of the NRL program is to investigate the innovative technology of high power, high frequency phase-locked oscillators. In order to control the phase, the idea is to use a low power signal in, for instance, a prebunching cavity and develop a weakly coupled phase-locked oscillator. This low power input signal would then be injected into a much smaller size, much more dissipative prebunching cavity, which would not oscillate on its own. We close this discussion by noting that two very powerful free electron laser amplifiers were developed millimeter waves; the LLNL FEL, which generated in excess of 1 GW at a frequency of 35 GHz[2] , and the NRL FEL, which generated about 20 MW at the same frequency.[3] However, each of these amplified only a very short pulse, shorter than the round trip pulse time in the device. Thus it is not known whether these amplifiers could operate at long pulse.

We now discuss additional applications of the weakly driven, high frequency phase-locked oscillator. First, we consider the disruption of enemy satellite communications. Disrupting a single satellite could provide tremendous leverage in a war or short of war situation, as many different communications are channeled through one satellite. The satellite does not have to be burned out, and, in fact, the data rate it transmits can be given only a small bit error rate to make the transmitted data useless. Furthermore, clock signals can be disrupted and thrown off by high power microwave interference. This error could throw off all positioning and navigational signals transmitted by that satellite to a large number enemy strategic and/or tactical assets.

Consider a ship based array of 300 sources, each at a power of 100 kW, and each at a frequency of 100 GHz, radiated through a 25 meter phased array. On a LEO satellite, this would give an irradiance of 10 W/cm^2, while on a geosynchronous satellite, it would give an irradiance of $2\text{x}10^{-4}$W/cm^2. Since geosynchronous satellites have antenna areas of typically 10^6 cm^2, the input power would be about 200 watts assuming a flat frequency response of the antenna. In Fig. I.4 is shown the response of a typical filter set for 1.7 GHz. Notice that even with the 60 db attenuation between 1.7 and 10 GHz, the 200 watt signal (attenuated by 60 db) would still swamp anything the receiver would normally see. However, above 10 GHz, the filter attenuation is typically 20-30 db, so the satellite would be even easier to disrupt. To make things easier, one could use intermodulation, that is, irradiate the satellite with two high frequency signals whose difference frequency corresponds to some natural frequency in the satellite. If this natural frequency is the transmitted frequency, it is easy to determine. If it is the I.F., we note that for U. S. satellites, the intermediate frequency is often published in the unclassified literature. We assume such information is available also for Soviet satellites.

By going to millimeter waves, and a ship based system, one could have the ultimate in surreptitious disruption of a satellite communication system. For frequencies $0 < f < 50$ GHz, and $70 < f < 110$ GHz, the one way attenuation through the atmosphere is less than 2 db, as long as the angle to the horizon is greater than 30 degrees. At higher angles, the frequency window can be increased considerably. However, these frequencies strongly attenuate at sea level, so there is almost no way that such a disrupter could be detected. By having the disrupter on more than one mobile source, for instance, on several ships, the problem of high frequency propagation through bad weather is minimized.

It is interesting to note that the Soviets already have a fleet of about 30 ships which could have this capability. In Fig. I.5 is shown a picture of the Kosmonavt Yuri Gagarin. The Soviets say that these ships are for satellite tracking, but if they also have a transmit function, they could have the potential of disrupting our own satellite communications also.

Another potential application of the high power, high frequency weakly coupled phase-locked oscillator is a space based radar. Here the high frequency has two important advantages; first, it implies a more tightly focused beam, so that the radar can give better spatial resolution, and second, at a frequency of 60 GHz, and above 120 GHz, the atmosphere is opaque, so interference from the ground is not possible. Virtually any radar more than the very simplest must have phase control to separate moving targets, form images, provide range resolution, etc.

A question is whether a phase-locked oscillator can provide the bandwidth necessary for a space based radar. While wide frequency separation might be required from pulse to pulse, and this could be achieved by using more than one oscillator, one of the most stressing bandwidth requirements in a single pulse is the requirement for range resolution. Generally if the pulse has bandwidth Δf, the range resolution ΔR is given roughly by

$$\Delta R = c/\Delta f.$$

Thus, for three meter range resolution, the required bandwidth is about 50 MHz. The bandwidth of a phase-locked oscillator is generally some fraction of its frequency. For instance the Adler relation gives

$$\Delta f/f = (1/Q)x(P_{in}/P_{out})^{1/2}$$

where P_{in} is the input locking power and P_{out} is the oscillator power. Typically then $\Delta f/f \sim 10^{-3}$, so that by using a phase-locked oscillator at high frequency, the bandwidth should be sufficient for space based radar applications.

We next consider the last architecture we have considered, the strongly coupled oscillators. The rationale for the strongly coupled oscillators must be that, just as an amplifier might be too difficult and thereby force one into a weakly coupled phase-locked oscillators, the weakly coupled phase-locked oscillator itself might be too difficult. For instance, at the gigawatt power level and at high frequency, the input driver itself could be a considerable technical challenge. Furthermore, a multigigawatt beam might just be too powerful to pass through, for instance, a prebunching cavity which is itself stable. Thus, if one could simply make the oscillators, link them together and have them self phase lock, there could be a considerable simplification. We point out that very little is known about the actual locking mechanism of a large number of self coupled oscillators. For instance, how would one electronically control each phase at the high power operation? Even if this can be done, how long will it take to achieve locking? If we consider the large array, if the array is three kilometers on a side, the one way transit time across it at the speed of light is 10 microseconds; it seems certain that the locking time would be much longer than this. Thus, the strongly coupled phase-locked oscillators do not seem well matched for a large scale array.

For the satellite disrupter, the power of the individual source is small enough that it is likely that a weakly coupled phase-locked oscillator would work. For the space based radar, an array is not necessarily needed, just accurate phase control of single high power (100 kW-1 MW) source. Thus, the strongly coupled oscillators do not appear to have any relevance to these SDIO missions either.

The principal application of the strongly coupled oscillators, it seems to us, is that it would allow one to utilize the full current capability of a pulse power accelerator. For instance, such accelerators typically have the capability of generating hundreds of kiloamps. However, the limiting beam current which can propagate is limited by the Alfven current, at best, tens of kiloamps. For a tube like a gyrotron, which relies on giving the beam transverse energy, the current limit is considerably less, typically around ten kiloamps. However, by putting more than one tube on an accelerator plate, one can propagate, say, 10 kiloamps in each, and thereby utilize much more of the current capability of the accelerator. It is important that these tubes phase lock each other in order that the output radiation is reproducible from shot to shot, and that the target is irradiated with a predictable radiation pattern.

Thus for the strongly coupled oscillators, it is less important for them to work in a large array, than it is for them to work as a small array of, say, ten or fewer elements. One could even envision a hybrid architecture for the large array. For instance, in Fig. I.2 each building could be a strongly coupled array of, say, ten individual oscillators, whose overall phase is controlled at low power by the central control.

The NRL SDIO/IST program in phase-locked oscillators is set up to examine the crucial issues regarding high power (hundreds of megawatts to one gigawatt) phase-locked oscillators at high frequency. The program is now set up on two tracks. The first is to develop a weakly coupled phase-locked oscillator at high frequency and at high power in a very overmoded cavity. The second is to develop two or more strongly coupled oscillators which phase lock each other. Each track has subtracks leading up to the final result, and at least one subtrack (a high power free running oscillator) is common to both tracks.

The first track has, as its end point, the development of a weakly coupled phase-locked oscillator at the hundreds of megawatt to one gigawatt level which utilizes a TE_{13} mode in the main oscillator cavity. The TE_{13} mode appears to us to be about as overmoded as it is prudent to go while both controlling the mode in the main cavity and stabilizing the prebunching cavity to all competing modes while also externally exciting the desired mode. Since we anticipate that the gain will not be much more than 30 db between locking signal and main oscillator power, an input signal of about 1 MW is required. This forces us to operate the main cavity at X-band, where the input source is readily available. We emphasize, however, that this is the main reason to operate at X-band rather than at higher frequency where we have typically operated in the past.

There are three separate subtasks leading up to this end point. First of all, there is the development of a free running oscillator in a standing TE_{13} mode. These experiments are being done at a frequency of 35 GHz and have achieved a power of 35-40 MW with a beam voltage of about 750 kV, current of about 2-3 kA on the NRL compact febetron accelerator. Follow up experiments at higher voltage and current are underway on the VEBA accelerator. The mode is generated in a standing pattern by the use of axial slots in the cavity wall. The second is the development of a low power phase-locked oscillator in a TE_{13} cavity mode with the use of a prebunching cavity. This has been designed, virtually all of the parts are in, and is being set up. The frequency is 85 GHz, and the anticipated power is about 50-100 kW. These experiments utilize a thermionic electron gun which is capable of high reprate. Although this will serve as a prototype for the high power oscillator, we also note that it could have direct relevance to both the satellite disrupter and the space based radar. If successful, it will be, by far, the most powerful compact source in this frequency range. The third subtask is the development of a fundamental mode three cavity phase-locked oscillator at a frequency of 35 GHz and an anticipated power of of 1-10 MW. This experiment will also be done on the VEBA facility and it should give the necessary experience in diagnosing phase locking at power and high frequency on a single shot experiment.

The second track which the project is on is the development of two strongly coupled phase-locked oscillators. These will operate in the TE_{62} mode, a mode which we have had good success with in the free running oscillator. This mode has achieved 100 MW when run on the febetron, and on VEBA experiments which are still underway, it has achieved more than 200 MW. One potential option for the program could be to increase the power by operating in yet a higher order mode, say a $TE_{15,2}$. However, we have not pursued this option. Doing so would require re-engineering large parts of the tube, and we felt that the limited resources available would be more effectively utilized in examining phase locking issues in cavity mode with which we have had experience. The next phase of this track of the program will be the linking of two free running oscillators to investigate under what conditions they will self lock.

The remainder of this report is divided into seven sections which will examine progress on theoretical issues, the low power experiment, the free running TE_{13} oscillator, the VEBA gyrotron experiments, the design of the three cavity phase-locked oscillator, the three cavity oscillator setup, and the strongly coupled oscillator. There are five appendices which are reprints and preprints of relevant published reports.

References for Section I

1. T.G. Lee, G.T. Konrad, Y. Okazaki, M. Watanobe, and H. Yonezawa, "The Design and performance of a 150-MW Klystron at S Band," IEEE Trans. on Plasma Science, **PS-13** (6), p. 545 (1985).
2. T.J. Orzechowski, B.R. Anderson, J.C. Clark, W.M. Fawley, A.C. Paul, D. Prosnitz, E.T. Scharlemann, and S.M. Yarema, "High-Efficiency Extraction of Microwave Radiation from a Tapered-Wiggler Free-Electron Laser," Phys. Rev. Lett. **57** (17) p. 2172 (1986).
3. S.H. Gold, D.L. Hardesty and A.K. Kinkead, "High-Gain 35 GHz Free-Electron Laser-Amplifier Experiment," Phys. Rev. Ltrs. **52** (14), p. 1218 (1984).

AMPLIFIERS

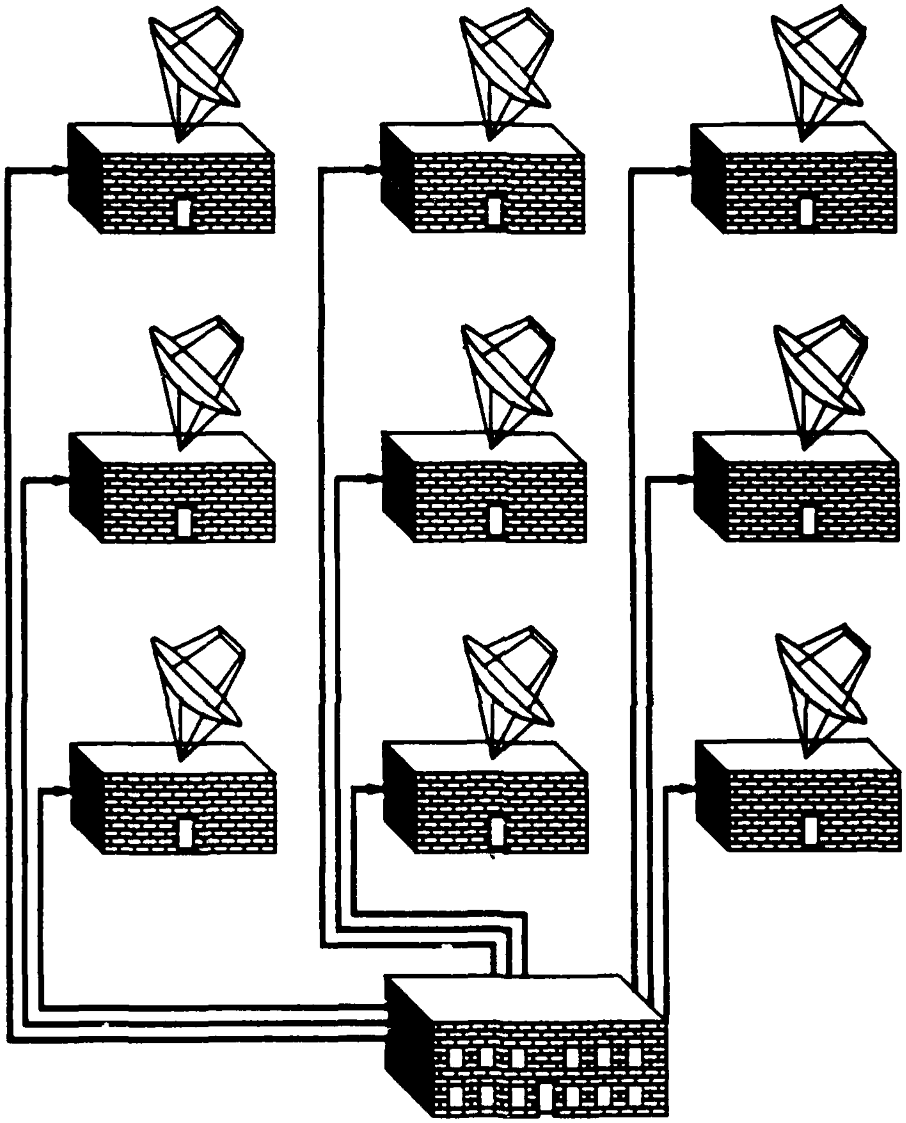

THE HIGH POWER SOURCES ARE ISOLATED FROM EACH OTHER AND ARE TOTALLY THE SLAVES OF THE LOW POWER CENTRAL CONTROL REGARDING BOTH AMPLITUDE AND PHASE.

Fig. I.1. Architecture for a phased array based on amplifiers.

DECOUPLED PHASE LOCKED OSCILLATORS

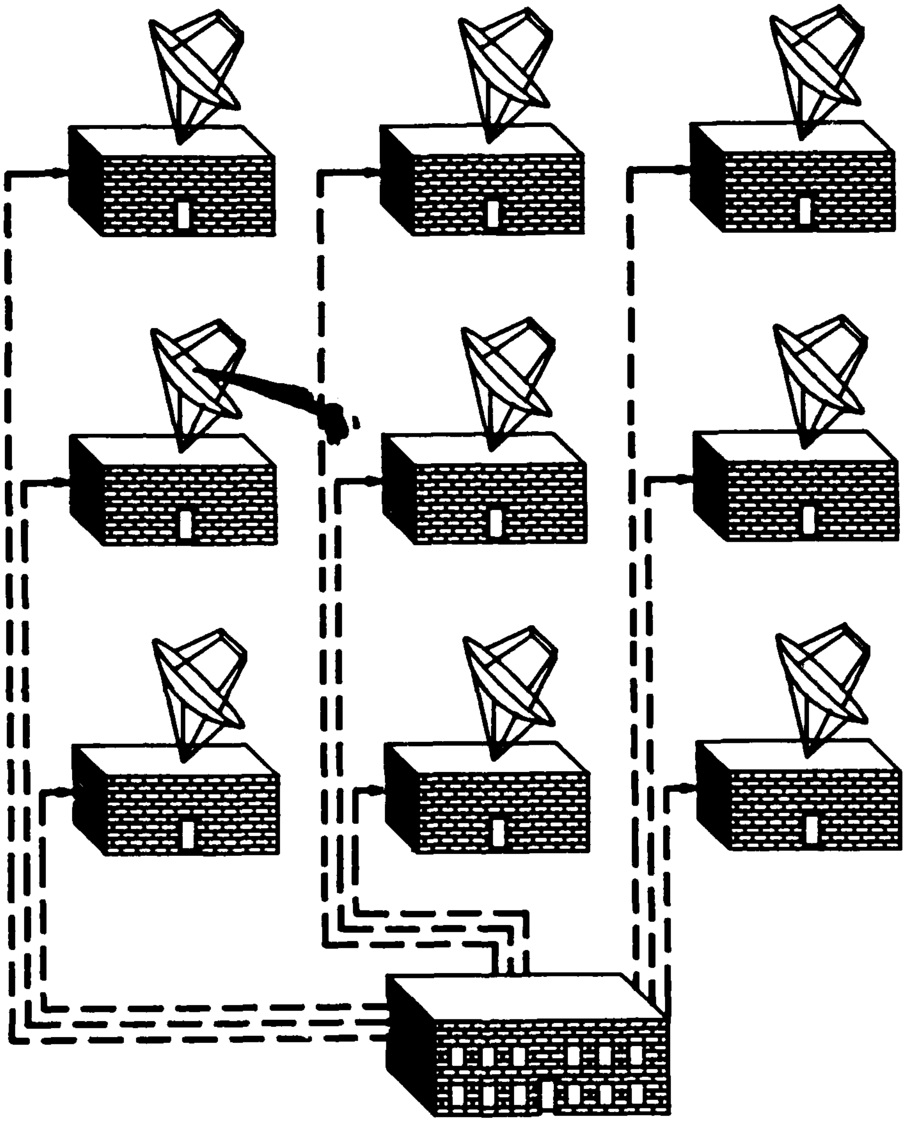

THE HIGH POWER SOURCES ARE ISOLATED FROM EACH OTHER BUT HAVE INDEPENDENT EXISTENCE. THEIR PHASES ARE DETERMINED AT LOW POWER BY THE CENTRAL CONTROL.

Fig. I.2. Architecture for a phased array based on weakly coupled oscillators.

STRONGLY COUPLED OSCILLATORS

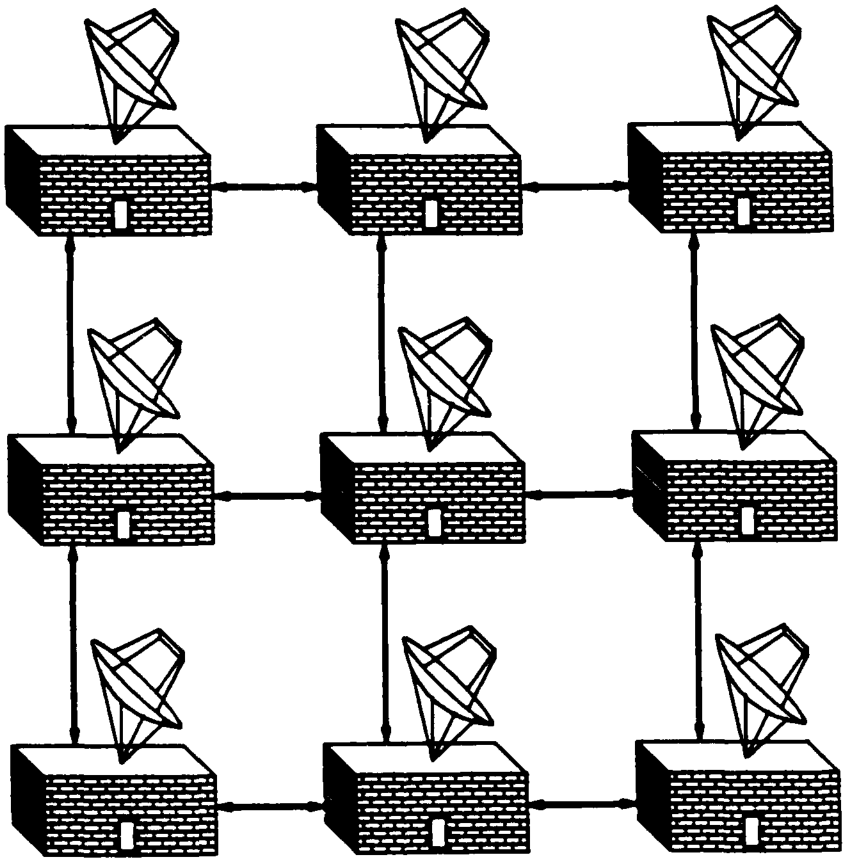

THESE LOCK AND CONTROL EACH OTHER IN SOME COLLECTIVE MANNER, CURRENTLY NOT WELL UNDERSTOOD.

Fig. I.3. Architecture for a phased array based on strongly coupled oscillators.

Diplexer Above Band Response Transmission J1 → J4

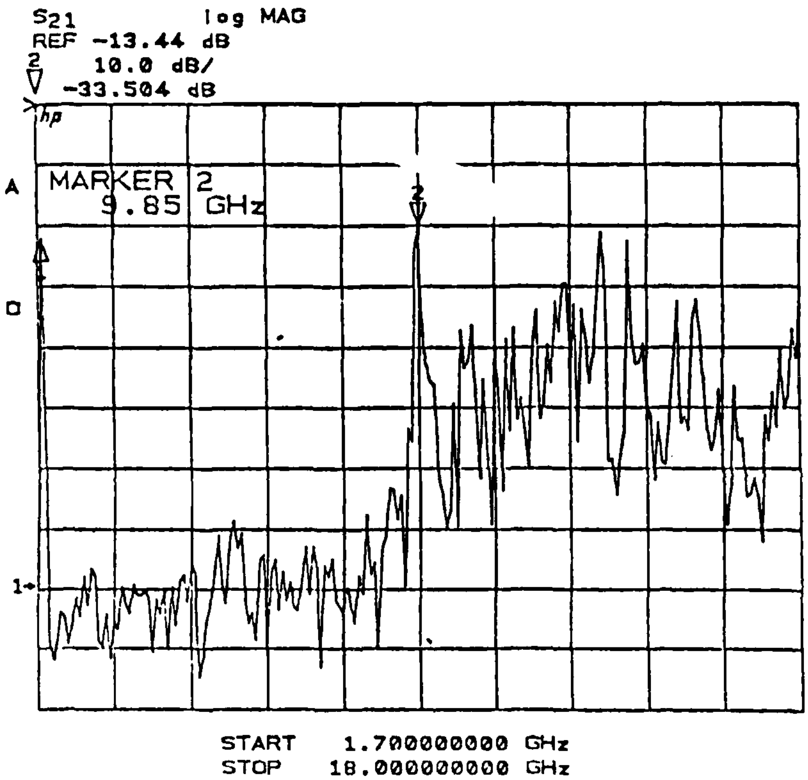

Fig. I.4. A filter response for 1.7-18 GHz showing the transmission for frequencies far above the design value.

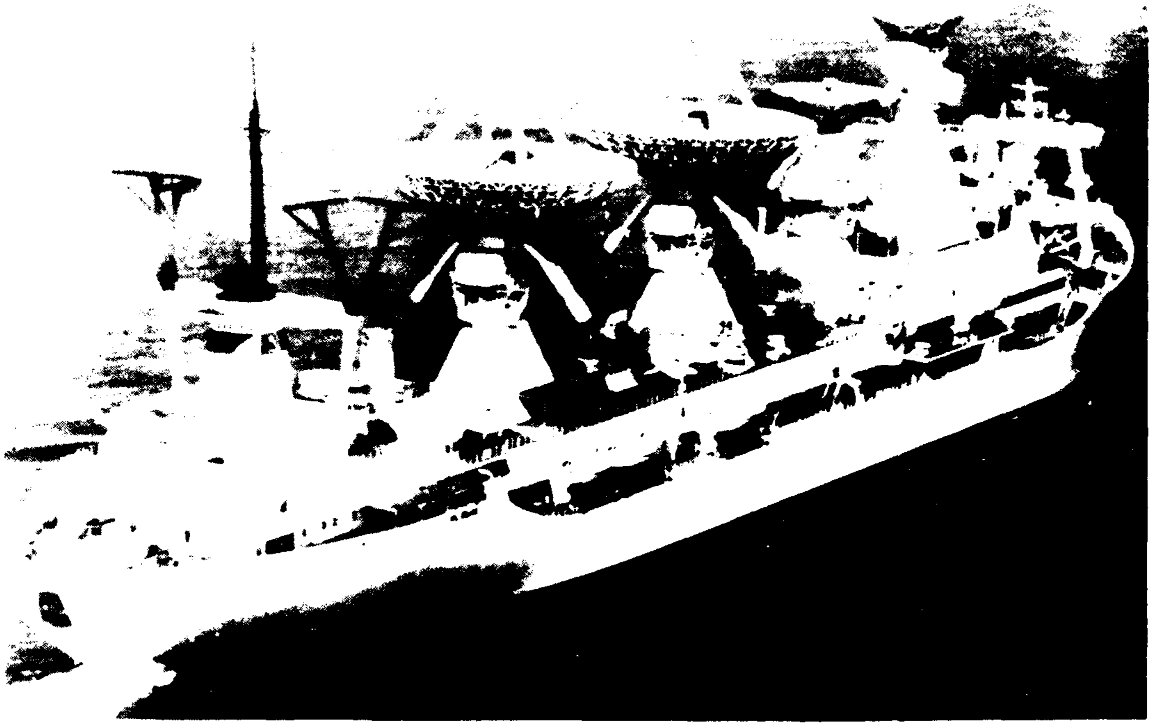

The Soviet *satellite* tracking ship *KOSMONAVT YURI GAGARIN is one of a fleet of Soviet Space Event Support Ships (SESS)* which are employed in civilian and military space and missile programs. The large, sophisticated ships of this type have secondary intelligence collection and political presence capabilities. Most of these ships are operated by civilian research institutes with a few being Navy manned

Fig. I.5. The Soviet satellite tracker ship Kosmonavt Yuri Gagarin.

II. HIGH POWER GYROTRON THEORY

II.1 OVERVIEW OF THEORETICAL EFFORT

Theoretical research at NRL in support of the development of high power phase-locked gyrotrons has recently emphasized the the theory and simulation of driven gyrotron oscillators, the design of cavities with axial slots to promote single mode operation, and the simulation of transient effects in pulseline accelerator gyrotrons with short, nonideal voltage waveforms. This work has had a direct impact on the design and analysis of the SDIO-IST high power phase-locked gyrotron experiments.

Considerable progress has been made on the theory of driven gyrotron oscillators. An analytical theory of the multi-cavity phase-locked oscillator based on a perturbation theory approach has been published by Manheimer.[1] A reprint of this work, which treats gyrotron operation in linearly polarized TE_{1n} modes and accounts for beam velocity spread, is included in this report as Appendix 1. The extension of this work to a realistic nonlinear, time-dependent model of a gyrotron driven by an external signal is essentially the topic of the following parts of this Section. In this work phase-locking by both directly injected radiation and by a driven prebunching cavity is considered and comparisons made. The accuracy of the perturbation theory approach to phase-locking with a prebunching cavity is investigated. The theory for direct injection phase-locking can be extended to the simulation of coupled gyrotron oscillators.

The control of mode competition is a fundamental issue for overmoded high power gyrotrons. The use of axial slots to promote stable operation in the TE_{13} mode was recently demonstrated at NRL as discussed in Section IV. The design of the slotted cavities used in this experiment required the calculation of the mode and slot angle dependent Q factor due to the slots. A powerful boundary integral method for computing transverse eigenfunctions of slotted gyrotron cavities with arbitrary cross sections was developed for this purpose by McDonald, Finn, Read and Manheimer.[2] A reprint of this paper is included as Appendix 2 of this Report.

Prior to the theory developed in this Section which emphasizes the relation between analytical and fully nonlinear theories of driven oscillators, a related slow-time-scale (STS), time-dependent, multimode theory was derived by Fliflet, Lee, Manheimer and Ott[3] for free-running oscillators and oscillators driven by prebunching cavities. Reference 3 is included in this report as Appendix 3. This work shows the feasibility and effect of phase-locking a gyrotron with a voltage ripple, an important issue for intense-beam gyrotrons. A comparison between the NRL STS time-dependent simulation code and the fast-time-scale particle simulation code developed by A.T. Lin at

UCLA has been carried out for an intense beam gyrotron.[4] The configuration modeled in this work, which is included as Appendix 4 of this Report, was the NRL 35 GHz, 100 MW Febetron-gyrotron experiment which is known to be dominated by nonstationary effects.[5] This joint UCLA-NRL theory effort provides an important validation of both codes for the single operating mode case. The UCLA particle code also shows interesting multimode and e-beam transit time effects which warrant further investigation.

II.2 INTRODUCTION TO THE THEORY OF DRIVEN GYROTRON OSCILLATORS

There is currently considerable interest in the development of high power phase-locked gyrotron oscillators. These devices have the potential to combine the high efficiency and power associated with oscillators with the coherence and phase control properties associated with amplifiers. Although previous theoretical work on steady-state gyrotron operation[6-13] has been successfully applied to the development of cw devices for heating of tokamak plasmas, the investigation of the phase locking of gyrotron oscillators driven by external signals has received much less attention. A consideration of the properties of driven oscillators necessarily involves the study of non-stationary operation. Time dependent effects can be studied using a particle-in-cell simulation code of the type developed by Lin and co-workers.[14] In this work an alternative nonlinear, slow-time-scale approach is used to study time-dependent effects in driven oscillators. Under certain approximations analytical estimates of such quantities as the locking bandwidth are obtained. For example, Adler's relation[15] is recovered for the case of phase locking by direct injection of radiation at the cavity output.

The time-dependent theory of gyrotrons has been considered by Nusinovich and co-workers,[16,17] mainly in the context of multimode operation and mode stability. A time-dependent multimode theory of quasi-optical gyrotrons has been developed by Bondeson et al.[18] Early work on mode selection and phase-locking of vacuum tube oscillators was carried out by Van der Pol[19] and Adler.[15] An analytical theory of the conditions for phase-locking gyrotrons has been presented by Manheimer.[1,20] The present work extends the theoretical approach developed by Manheimer to the nonlinear regime and incorporates slow-time-scale (STS) gyrotron dynamics.

The time dependent theory of driven gyrotron oscillators derived in this work is based on slow-time-scale equations for the electron motion similar to those used in steady-state models.[12,21] Slow-time-scale equations for the cavity rf field amplitude are obtained by expressing the time-dependent behavior relative to a reference frequency ω_o which is close to the operating frequency ω. The fact that the electron transit time through the cavity is short compared to the radiation field risetime is also exploited. The external signal is introduced either directly into the cavity output or via a beam prebunching cavity. Two approaches are investigated for the case of phase-locking with a prebunching cavity. In the first the induced ac current density due to the prebunching cavity is treated as a small perturbation on the ac current density in the oscillator. In this approach, which follows the work of Manheimer,[1] the equations for the time-dependent wave amplitude and phase are similar in structure to the equations for gyrotrons driven by direct injection and lead to a simple analytical estimate of the locking bandwidth. The accuracy of the perturbation approach is investigated by comparing it with the results of the second approach in which the beam prebunching is introduced in the initial conditions for integrating the equations-of-motion. This approach is well-known in the analysis of gyro-klystons.[22] The theory is applied to a high voltage gyrotron configuration similar to the NRL high voltage gyrotron experiment.[5]

The next part of this section of this paper describes the theoretical approach. The following part contains the results of calculations and the last part presents conclusions drawn from this research.

II.3 PHASE-LOCKED OSCILLATOR THEORY

Consider a gyrotron with a cylindrical resonator and a thin annular beam. The electrons follow helical trajectories in the applied axial magnetic field about guiding centers located at a radius R_o from the symmetry axis. The electron beam interacts with a TE resonator mode which is assumed to be near cutoff. It is convenient to look at time dependent effects which remain after a reference frequency ω_o has been factored out. These effects are characterized by time scales which are much longer than the wave period and are incorporated in a time dependent mode profile function f(z,t). Using complex notation, the transverse electric field is expressed in the form:

$$\mathbf{E}_t = f(z,t)\mathbf{e}_n(r,\theta;z)\exp(-i\omega_o t) \qquad (1)$$

where $\mathbf{e}_n$ is a transverse mode vector function defined in Ref. 21. The transverse electric field satisfies the wave equation:

$$\nabla^2 \mathbf{E}_t - \frac{1}{c^2}\frac{\partial^2 \mathbf{E}_t}{\partial t^2} = \mu_o \frac{\partial \mathbf{J}_t}{\partial t} \qquad (2)$$

where $\mathbf{J}_t$ is the transverse ac current density, c is the speed of light and μ_o is the permeability of free space. MKS units are used throughout except as noted.

There are two methods of phase-locking gyrotron oscillators: direct injection of a locking signal or by means of a modulated electron beam produced by a prebunching cavity. In the case of direct injection of radiation the wave amplitude function at the cavity output can be expressed in the form:

$$f(z,t) = A(t)e^{i[k_z z-\psi(t)]} + \beta e^{-ik_{zo}z} \tag{3}$$

where the first term on the right hand side of Eq.(3) represents the time-dependent oscillator output (an outgoing wave with amplitude A and wavenumber k_z; ψ is a slowly varying phase) and the second term represents a constant amplitude incoming wave with frequency ω_o due to the external signal. In the case of beam premodulation via a bunching cavity, the ac current density can be viewed as having two parts:

$$J_t = J + \delta J \tag{4}$$

where J is generated by the electric field in the oscillator cavity and δJ is the current density generated in the prebunching cavity. It is convenient to express the rf current density in the approximate form:[12]

$$J_t = (J_\omega + \delta J_\omega)\exp(-i\omega_o t) \tag{5}$$

where

$$J_\omega = \int_0^{2\pi} d(\omega_o t)\ J\ e^{i\omega_o t} \tag{6}$$

and similarly for δJ_{ω}. Substituting Eqs.(1) and (5) into Eq.(2), noting that $\partial f/\partial t \ll \omega_o f$, multiplying by $e_n{}^*$, and integrating over the resonator cross section one obtains:

$$\left[\frac{\partial^2}{\partial z^2} + \frac{\omega_o^2 - \omega_{c\,o}^2}{c^2} + 2i\frac{\omega_o}{c^2}\frac{\partial}{\partial t}\right] f(z,t) = -i\mu_o\omega_o \int da\; e_n^* \cdot (J_{\omega} + \delta J_{\omega}) \tag{7}$$

where $\omega_{c\,o}$ is the cut-off frequency of the resonant mode in the cavity.

To obtain slow-time-scale equations for a gyrotron oscillator driven by an external signal, multiply Eq.(7) by f^* and multiply the complex conjugate of Eq.(7) by f. Then first add and then subtract the resulting equations, and integrate the sum or difference over the axial extent of the cavity. The sum leads to:

$$\int_0^L dz \left[f^* \frac{\partial^2 f}{\partial z^2} + f \frac{\partial^2 f^*}{\partial z^2} + 2\frac{\omega_o^2 - \omega_{c\,o}^2}{c^2} ff^* + 2i\frac{\omega_o}{c^2}\left(f^* \frac{\partial f}{\partial t} - f \frac{\delta f^*}{\delta t}\right)\right] =$$

$$-i\mu_o\omega_o \int_V dadz \left[f^* e^* \cdot (J_{\omega} + \delta J_{\omega}) - fe \cdot (J_{\omega}{}^* + \delta J_{\omega}{}^*)\right] \tag{8a}$$

where V denotes integration over the cavity volume. The difference leads to:

$$\int_0^L dz \left[f^* \frac{\partial^2 f}{\partial z^2} - f \frac{\partial^2 f^*}{\partial z^2} + 2i \frac{\omega_o}{c^2} \frac{\partial |f|^2}{\partial t} \right] =$$

$$-i\mu_o \omega_o \int_V dadz \left[f^* \mathbf{e}^* \cdot (\mathbf{J}_\omega + \delta \mathbf{J}_\omega) + f \mathbf{e} \cdot (\mathbf{J}_\omega^* + \delta \mathbf{J}_\omega^*) \right] \tag{8b}$$

As will be shown, Eq.(8a) leads to an equation for the wave phase and Eq.(8b) leads to an equation for the wave amplitude. Integrating the first two terms on the right hand side of these equations by parts leads to:

$$\left. \frac{\partial |f|^2}{\partial z} \right|_0^L + \int_0^L dz \left[-2 \left| \frac{\partial f}{\partial z} \right|^2 + 2 \frac{(\omega_o^2 - \omega_{c\,o}^2)}{c^2} |f|^2 + 2i \frac{\omega_o}{c^2} \left(f^* \frac{\partial f}{\partial t} - f \frac{\partial f^*}{\partial t} \right) \right] =$$

$$-i\mu_o \omega_o \int_V dadz \left[f^* \mathbf{e}^* \cdot (\mathbf{J}_\omega + \delta \mathbf{J}_\omega) - f \mathbf{e} \cdot (\mathbf{J}_\omega^* + \delta \mathbf{J}_\omega^*) \right] \tag{9a}$$

and:

$$\left. \left[f^* \frac{\partial f}{\partial z} - f \frac{\partial f^*}{\partial z} \right] \right|_0^L + 2i \frac{\omega_o}{c^2} \int_0^L dz \frac{\partial |f|^2}{\partial t} =$$

$$-i\mu_o \omega_o \int_V dadz \left[f^* \mathbf{e}^* \cdot (\mathbf{J}_\omega + \delta \mathbf{J}_\omega) + f \mathbf{e} \cdot (\mathbf{J}_\omega^* + \delta \mathbf{J}_\omega^*) \right] \tag{9b}$$

respectively. The first term on the left hand side of Eq.(9a) is a boundary term which vanishes for a free running oscillator because $f \to 0$ at the cavity input ($z=0$) and $|f|$=constant at the cavity output ($z=L$) when there is only an outgoing wave. The boundary term does not vanish when there is an external signal incident at the cavity output, thus this term corresponds to phase-locking by direct injection of radiation. The boundary term in Eq.(9b) corresponds to the net power flow from the cavity.

In the case of direct injection of radiation (the case of phase-locking via beam prebunching is treated below), the boundary term in Eq.(9a) can be written in the form:

$$\left.\frac{\partial |f|^2}{\partial z}\right|_0^L = -\,4k_{zo}A(t)\beta\sin[2k_{zo}L-\psi(t)] \tag{10a}$$

and the boundary term in Eq.(9b) can be written in the form:

$$\left.\left[f^*\frac{\partial f}{\partial z} - f\frac{\partial f^*}{\partial z}\right]\right|_0^L = 2ik_{zo}(A(t)^2-\beta^2) \tag{10b}$$

where Eq.(3) has been used and the difference between k_z and k_{zo} has been neglected. The wave amplitude function inside the cavity can written in the form:

$$f(z,t) = a(t)e^{-i\psi(t)}h(z) \tag{11}$$

where $h(z)$ is the axial profile function. In what follows, $h(z)$ will be assumed to have a gaussian form: $h(z)=\exp[-(\kappa_z z)^2]$, centered at the cavity midpoint, where κ_z is the effective axial wavenumber inside the cavity. Using Eq.(11) in Eq.(9a) and (9b) and substituting Eq.(10a) or (10b) for the boundary terms leads to:

$$-4k_{zo}A(t)\beta\sin[2k_{zo}L-\psi(t)] + 2N\left[\frac{\omega_o^2-\omega_{ro}^2}{c^2}\,a(t)^2 + 2\frac{\omega_o}{c^2}a(t)^2\dot{\psi}\right] =$$

$$-i\mu_o\omega_o a(t)\int_V dadz\,h(z)\left[e^*\cdot J_\omega e^{i\psi} - e\cdot J_\omega^* e^{-i\psi}\right] \qquad (12a)$$

from Eq.(9a); and

$$2k_{zo}[A(t)^2-\beta^2] + 4\frac{\omega_o}{c^2}a(t)\dot{a}(t)N =$$

$$-\mu_o\omega_o a(t)\int_V dadz\,h(z)\left[e^*\cdot J_\omega e^{i\psi} + e\cdot J_\omega^* e^{-i\psi}\right] \qquad (12b)$$

from Eq.(9b);

where:

$$N = \int_0^L dz\,|h(z)|^2 \simeq \sqrt{\frac{\pi}{2}}\,\frac{L}{2} \qquad (13)$$

for a gaussian profile, and ω_{ro} is the cold cavity eigenfrequency of the interacting mode.

To calculate the ac current density, the interaction with the electron beam is treated in the single particle approximation. A considerable simplification of the general time dependent problem results if one uses the fact that the characteristic rise time of fields in the resonator is much longer than the electron transit time in the cavity. In this case one can use a quasi-steady-state approximation in which the electron trajectories are calculated for rf fields with fixed amplitude, $f(\tau_o)$, and linearized phase, $\psi_n \simeq \psi_n(\tau_o) + \psi_n'(\tau_o)(\tau - \tau_o)$. The slow-time-scale nonlinear electron equations of motion for an electron in a thin annular beam interacting at a particular harmonic with a single circularly polarized TE mode are readily deduced from previous steady-state analyses[12,21] and are given by:

$$\frac{du_t}{d\bar{z}} = -\frac{\gamma}{u_z} f \, J_s'(\bar{k}_t \bar{r}_L) \, \mathrm{Re}\left[\left(h + i\frac{u_z}{\gamma\bar{\omega}_o}\frac{dh}{d\bar{z}}\right)e^{-i[\Lambda+\psi]}\right] \tag{14a}$$

$$\frac{d\Lambda}{d\bar{z}} = -\frac{s\gamma}{u_z u_t} f \, \frac{sJ_s(\bar{k}_t \bar{r}_L)}{\bar{k}_n \bar{r}_L} \mathrm{Re}\left[\left(h + i\frac{u_z}{\gamma\bar{\omega}_o}\frac{dh}{d\bar{z}} - \frac{\bar{\omega}_{co}^2 u_t^2}{s\bar{\Omega}\bar{\omega}_o\gamma}h\right) e^{-i[\Lambda+\psi]}\right] + \bar{\omega}_o\left(1 - \frac{s\Omega}{\bar{\omega}_o\gamma}\right) \tag{14b}$$

$$\frac{du_z}{d\bar{z}} = \frac{u_t}{u_z \bar{\omega}_o} \; f \; J_s'(\bar{k}_t \bar{r}_L) \operatorname{Re}\left[i \frac{dh}{d\bar{z}} \quad e^{-i[\Lambda+\psi]} \right] \tag{14c}$$

where $u_t = \gamma v_t / c$ is the normalized transverse momentum amplitude, $u_z = \gamma v_z / c$ is the normalized axial momentum, Λ is a slowly varying transverse momentum phase, s is the harmonic number, γ is the relativistic mass ratio, k_t is the mode transverse wavenumber, r_L is the Larmor radius of the orbit, J_s (J_s') is (the derivative of) a regular Bessel function, Ω is the nonrelativistic cyclotron frequency, and f is the normalized rf field amplitude:

$$f = \frac{|e|}{m_o c^2} \; x_{mn}' C_{\text{[illegible]}} \; {}_{m-s}(k_t R_o) \; a \tag{15}$$

Quantities with a "-" have been normalized according to: $\bar{z} = z/r_{wo}$, $\bar{r}_L = r_L/r_{wo}$, $\bar{\Omega} = \Omega r_{wo}/c$, $\bar{\omega}_o = \omega_o r_{wo}/c$, and $\bar{k}_n = k_n r_{wo}$. R_o denotes the orbit guiding center radius, e is the electron charge, m_o is the electron mass, m is the mode azimuthal index, x_{mn}' is a zero of J_m', and r_{wo} is an arbitrary normalization factor. The transverse TE mode normalization coeficient

$$C_{mn} = \left[\sqrt{[\pi(x_{mn}'^2 - m^2)]} \, J_m(x_{mn}') \right]^{-1} \tag{16}$$

The ac current density is obtained by integrating Eqs.(14) for an appropriate set of initial conditions at the cavity input at z_o. For a cold, phase-mixed electron beam: $u_t(z_o)=u_{to}$, $u_z(z_o)=u_{zo}$, and $\Lambda(z_o)=\Lambda_o$ is uniformly distributed in the interval $[0,2\pi]$. For a thin annular beam the transverse ac current density is given by

$$J_t = -\frac{I_o}{v_z}v_t \tag{17}$$

Substitution of Eqs.(17) and (6) into Eqs.(12) and using the prescription developed in previous work[12] leads to the following equations for the time-dependent wave and phase:

$$-4k_{zo}A(t)\beta\sin[2k_{zo}L-\psi(t)] + 2N\left[\frac{\omega_o^2-\omega_{ro}^2}{c^2}a(t)^2 + 2\frac{\omega_o}{c^2}a(t)^2\dot{\psi}\right] = \tag{18a}$$

$$-4\mu_o I_o\omega_o C_{mn}J_{m-s}(k_tR_o)a(t)\int_0^L dzh(z)\left\langle\frac{\partial J_s(k_tr_L)}{\partial r_L}\frac{u_t}{u_z}\sin(\Lambda+\psi)\right\rangle_{\Lambda_o}$$

from Eq.(12a); and, from Eq.(12b),

$$2k_{zo}[A(t)^2-\beta^2] + 4\frac{\omega_o}{c^2}a(t)\dot{a}(t)N =$$

$$4\mu_o I_o \omega_o C_{mn} J_{m-s}(k_t R_o)a(t)\int_0^L dzh(z)\left\langle\frac{\partial J_s(k_t r_L)}{\partial r_L}\frac{u_t}{u_z}\cos(\Lambda+\psi)\right\rangle_{\Lambda_o} \quad (18b)$$

where $\langle\ \rangle_a$ denotes an average with respect to the variable a. The cavity field amplitude can be related to the external field amplitude via the output diffraction Q factor according to:

$$A(t) = \sqrt{\frac{N}{k_{zo}Q}}\,\frac{\omega_o}{c}\,a(t) \quad (19)$$

Substituting Eq.(19) into Eqs.(18), the equations for the time-dependent phase and amplitude can be written in the form:

$$\frac{d\psi}{d\tau} = -\frac{\Delta\omega_o}{\omega_o} - \frac{I}{f}\int_0^{\bar{L}} d\bar{z}h(\bar{z})\left\langle J_s'(\bar{k}_t\bar{r}_L)\frac{u_t}{u_z}\sin(\Lambda+\psi)\right\rangle_{\Lambda_o}$$

$$+\frac{1}{Q}\frac{f_L}{f}\sin[\psi-\Phi_o] \quad (20a)$$

$$\frac{df}{d\tau} = -\frac{1}{2Q}\frac{f^2-f_L{}^2}{f} + I\int_0^{\bar{L}} d\bar{z}h(\bar{z})\left\langle J_s'(k_t r_L)\frac{u_t}{u_z}\cos(\Lambda+\psi)\right\rangle_{\Lambda_o} \quad (20b)$$

where $\Delta\omega_o=\omega_o-\omega_{ro}$, $\Phi_o=k_{zo}L$, f_L is an effective field amplitude due to the locking signal given by:

$$f_L = \frac{|e|}{m_o c} x'_{mn} C_{mn} J_{m-s}(k_t R_o) \sqrt{\frac{2\mu_o Q P_L}{N\omega_o}} \tag{21}$$

where P_L is the locking signal power, and I is the normalized current parameter:

$$I = \frac{|e|\mu_o}{m_o c\bar{\omega}_o} \frac{r_{wo} \; J^2_{m-s}(k_t R_o)}{\pi(1-m^2/x'^2_{mn})J^2_m(x'_{mn})N} I_o \tag{22}$$

To treat the case of phase-locking via beam prebunching, the current density perturbation is assumed to be due to phase bunching. The ac current density perturbation can then be expressed in the form:

$$\hat{\delta J} \equiv \delta J_x + i\delta J_y = -I_o \frac{v_{to}}{v_{zo}} e^{-i(\omega_o t-\delta\Lambda)} \delta(r-R_o) \tag{23}$$

where

$$\delta\Lambda = \frac{\omega_o-\Omega}{v_{zo}}z + \theta_o - q\sin\theta_o - \Phi_o \tag{24}$$

where q is the bunching parameter and Φ_o is a phase factor determined by the locking signal. Evaluating the terms in Eqs.(9) involving δJ in the same manner as the terms involving J and using Eq.(23) leads to:

$$\frac{c^2\mu_o}{4N\omega_o a(t)^2}\int_V dadz\left[f^* e^* \cdot \delta J_\omega \pm fe \cdot \delta J_\omega^*\right] =$$

$$\begin{Bmatrix}-1\\-i\end{Bmatrix}\frac{I}{r_{wo}f}\,\frac{v_{to}}{v_{zo}}J_s'(k_t r_{Lo})\int_o^L dzh(z)\left\langle\begin{Bmatrix}\cos\\\sin\end{Bmatrix}(\delta\Lambda+\psi)\right\rangle_{\theta_o} \qquad (25)$$

where the "+" ("-") sign on the left hand side of Eq.(25) is associated with the upper (lower) quantities in the brackets on the right hand side. Substituting Eq.(24) into (25), and performing the phase average yields:

$$\frac{c^2\mu_o}{4N\omega_o a(t)^2}\int_V dadz\left[f^* e^* \cdot \delta J_\omega \pm fe \cdot \delta J_\omega^*\right] = \qquad (26)$$

$$\begin{Bmatrix}-1\\i\end{Bmatrix}\frac{I\,v_{to}}{r_{wo}fv_{zo}}J_s'(k_t r_{Lo})\int_o^L dzh(z)J_1(q)\begin{Bmatrix}\sin\\\cos\end{Bmatrix}\left(\frac{\omega_o-\Omega}{v_{zo}}z+\psi-\Phi_o\right)$$

Under the assumption of phase bunching only, the bunching parameter has no z-dependence in the cavity region and assuming a gaussian form for the profile function h(z), the axial integration can be carried out to obtain:

$$\frac{c^2\mu_o}{4N\omega_o a(t)^2}\int_V dadz\left[f^* e^* \cdot \delta J_\omega \pm fe \cdot \delta J_\omega^*\right] \simeq \qquad (27)$$

$$\begin{Bmatrix}-1\\i\end{Bmatrix}\frac{\sqrt{\pi}I}{\kappa r_{wo}f}\,\frac{v_{to}}{v_{zo}}J_s'(k_t r_{Lo})e^{-\left[\frac{\omega_o-\Omega}{2v_{zo}\kappa}\right]^2}J_1(q)\begin{Bmatrix}\sin\\\cos\end{Bmatrix}(\psi-\Phi_o)$$

where the cavity axial wavenumber defines an effective interaction length according to $\kappa \equiv 2/L$. Substituting Eq.(27) into Eqs.(9) leads to the counterparts of Eqs.(20) for the case of phase-locking via a prebunched beam:

$$\frac{d\psi}{d\tau} = - \frac{\Delta\omega_o}{\omega_o} - \frac{I}{f}\int_0^{\bar{L}} d\bar{z}\, h(\bar{z}) \left\langle J_s'(\bar{k}_t \bar{r}_L)\, \frac{u_t}{u_z}\, \sin(\Lambda+\psi) \right\rangle_{\Lambda_o} + \frac{\pi^{\frac{3}{2}}}{x'_{mn}} \frac{L}{\lambda} \frac{I}{f} \frac{v_{to}}{v_{zo}} J_s'(k_t r_{Lo})\, e^{-\left[\frac{\omega_o - \Omega}{2 v_{zo} \kappa}\right]^2} J_1(q) \cos(\psi - \Phi_o) \tag{28a}$$

$$\frac{df}{d\tau} = - \frac{f}{2Q} + I \int_0^{\bar{L}} d\bar{z}\, h(\bar{z}) \left\langle J_s'(k_t r_L)\, \frac{u_t}{u_z}\, \cos(\Lambda+\psi) \right\rangle_{\Lambda_o} + \frac{\pi^{\frac{3}{2}}}{x'_{mn}} \frac{L}{\lambda}\, I\, \frac{v_{to}}{v_{zo}} J_s'(k_t r_{Lo})\, e^{-\left[\frac{\omega_o - \Omega}{2 v_{zo} \kappa}\right]^2} J_1(q) \sin(\psi - \Phi_o) \tag{28b}$$

Eqs.(28) have been derived in part to show the similar structure of the phase and amplitude equations for a gyrotron driven by a directly injected rf signal or by a premodulated beam. As discussed by Manheimer,[1] these equations also lead to analytical estimates of the maximum frequency bandwidth for phase-locking, i.e., Adler's relation [Eq.(30) below], and of the exponentiation time in the approach to phase-lock. To carry out nonlinear numerical calculations of the temporal evolution of an oscillator driven by a premodulated beam it is more accurate to incorporate the beam premodulation directly into the wave equation source term via the initial conditions on the electron equations of motion. In this approach a nonuniform initial phase distribution is used of the form:

$$\Lambda_o = \theta_o - q\sin\theta_o - \Phi_o \tag{29}$$

where θ_o is uniformly distributed in the interval $[0,2\pi]$.

Eqs.(20) and (28) can be used to obtain estimates of the maximum frequency bandwidth for obtaining phase-locked operation for given system parameters. The wave amplitude and frequency shift due to beam loading for the free-running oscillator during steady-state operation are given by:

$$f_o = \left[2QI\int_0^{\bar{L}} d\bar{z}\,h(\bar{z}) \left\langle J_s'(k_t r_L)\,\frac{u_t}{u_z}\,\cos(\Lambda+\psi)\right\rangle_{\Lambda_o}\right]_{ss} \tag{30a}$$

$$\frac{\Delta\omega_{FRO}}{\omega_o} = -\frac{I}{f_o}\left[\int_0^{\bar{L}} d\bar{z}\,h(\bar{z})\left\langle J_s'(\bar{k}_t \bar{r}_L)\,\frac{u_t}{u_z}\,\sin(\Lambda+\psi)\right\rangle_{\Lambda_o}\right]_{ss} \tag{30b}$$

where $\Delta\omega_{FRO}=\omega_{r1}-\omega_{ro}$ and ω_{r1} is the beam loaded resonant frequency of the free-running oscillator.

For an oscillator operating near steady-state conditions and driven by a weak external signal with frequency ω_o, Eqs.(30) can be used to rewrite Eq.(20a) as:

$$\frac{\partial \Psi}{\partial \tau} \simeq -\frac{\Delta\omega}{\omega_o} - \frac{1}{Q}\frac{f_L}{f_o}\sin(\Psi) \qquad (31)$$

where $\Delta\omega \approx \omega_o - \omega_{r1}$ and $\Psi = \psi - \Phi_o + \pi$. *The condition for phase-locked* operation, $\partial\Psi/\partial\tau = 0$, implies:

$$\frac{\Delta\omega}{\omega_o} = -\frac{1}{Q}\frac{f_L}{f_o}\sin(\Psi_o) \qquad (32)$$

where Ψ_o denotes the phase during phase-locked operation. Since f_o nd f_L are proportional to the square root of the oscillator output power and locking power, respectively, Eq.(32) leads to Adler's relation for the frequency pulling bandwidth of a phase-locked oscillator driving a matched load:

$$\frac{|\Delta\omega|}{\omega_o} \leq \frac{1}{Q}\sqrt{\frac{P_L}{P_{ss}}} \qquad (33)$$

As discussed by Manheimer,[1] for frequencies satisfying Eq.(33), Eq.(32) has a stable solution of the form: $\Psi = \Psi_o + \delta e^{-\tau/T}$, where δ is a small perturbation, indicating that the approach to phase-locked operation is exponential. The time constant is given by:

$$\Upsilon = Q\sqrt{\frac{P_{osc}}{P_L}}\left[1 - \left(\frac{\Delta\omega Q}{\omega_o}\right)^2 \frac{P_{osc}}{P_L}\right]^{-1/2} \qquad (34)$$

Eq.(34) shows that Υ becomes large, and thus the time to achieve phase-lock becomes long, for frequencies near the bandwidth limit.

Similarly, in the case of phase-locking by beam pre-modulation, a similar analysis based on Eqs.(28) leads to the following equations describing the time-dependent amplitude and phase for operation near the oscillator steady-state:

$$\frac{d\Psi}{d\tau} \approx -\frac{\Delta\omega}{\omega_o} - \frac{\sqrt{\pi}}{2}\,\frac{\mu I_G}{Q\;F}\,J_1(q)\,e^{-\left[\frac{\Delta\mu}{4}\right]^2}\left\{\frac{2^s\,s!}{s^s\,\beta_{to}^{s-1}}\,J_s'(s\beta_{to})\right\}\sin\Psi \qquad (35a)$$

$$\frac{dF}{d\tau} \approx \frac{(F_o - F)}{2Q} + \frac{\sqrt{\pi}}{2}\,\frac{\mu I_G}{Q}\,J_1(q)\,e^{-\left[\frac{\Delta\mu}{4}\right]^2}\left\{\frac{2^s\,s!}{s^s\,\beta_{to}^{s-1}}\,J_s'(s\beta_{to})\right\}\cos\Psi \qquad (35b)$$

In deriving Eqs.(35) the following scaled "universal" gyrotron field amplitude, current, interaction length, and cyclotron resonance detuning parameters defined by Danly and Temkin[13] have been introduced:

$$F = \frac{\beta_{to}^{s-4}}{\gamma_o}\left[\frac{s^s}{2^{s-1}s!}\right]\frac{f}{x'_{mn}} \tag{36a}$$

$$I_G = \left[\frac{2}{\pi}\right]^{\frac{3}{2}} \frac{Q\ \bar{\omega}_o}{\gamma_o\,\beta_{to}^{s(3-s)}}\ \frac{N}{r_{wo}}\ \frac{\lambda}{L}\left[\frac{s}{2^s s!}\right]^2 I \tag{36b}$$

$$\mu = \pi\,\frac{\beta_{to}^2}{\beta_{zo}}\,\frac{L}{\lambda} \tag{36c}$$

$$\Delta = \frac{2}{\beta_{to}^2}\left(1 - \frac{s\Omega}{\omega_o}\right) \tag{36d}$$

The factor in Eqs.(35) involving the Bessel function $J'_s(s\beta_{to})$ reduces to unity when the small argument expansion of the Bessel function is valid. This is a good approximation for weakly relativistic beams and low-order harmonic interactions but can lead to inaccuracies in the relativistic gyrotron regime of interest here. The condition for phase-locked operation, $\partial\Psi/\partial\tau=0$, implies:

$$\frac{\Delta\omega}{\omega_o} = -\frac{\sqrt{\pi}}{2}\,\frac{\mu I_G}{QF_{do}}\,J_1(q)\,e^{-\left[\frac{\Delta\mu}{4}\right]^2}\left\{\frac{2^s\,s!}{s^s\,\beta_{to}^{s-1}}\,J_s'(s\beta_{to})\right\}\sin\Psi_o \qquad (37)$$

where the amplitude of the driven oscillator F_{do} is given by:

$$F_{do} = F_o + \sqrt{\pi}\,\mu I_G\,J_1(q)\,e^{-\left[\frac{\Delta\mu}{4}\right]^2}\left\{\frac{2^s\,s!}{s^s\,\beta_{to}^{s-1}}\,J_s'(s\beta_{to})\right\}\cos\Psi_o \qquad (38)$$

Eqs.(36) and (37) show that, unlike the case of direct injection, the amplitude of the driven oscillator has a dependence on the locking frequency. Eq.(36) leads to the counterpart of Adler's relation for phase locking via a prebunched beam:

$$\frac{|\Delta\omega|}{\omega_o} \leq \frac{\sqrt{\pi}}{2}\,\frac{\mu I_G}{QF_{do}}\,J_1(q)\,e^{-\left[\frac{\Delta\mu}{4}\right]^2}\left\{\frac{2^s\,s!}{s^s\,\beta_{to}^{s-1}}\,J_s'(s\beta_{to})\right\} \qquad (39)$$

A corresponding result was obtained by Manheimer[1] (using different notation) for the case of a gyrotron in a linearly polarized TE_{1n} mode. The time constant for the approach to phase-locked operation is given by:

$$\Upsilon = \left[\frac{|\Delta\omega|^2_{max}}{\omega_o^2} - \frac{\Delta\omega^2}{\omega_o^2} \right]^{-1/2} \qquad (40)$$

where $|\Delta\omega|_{max}/\omega_o$ is given by Eq.(39) with the equality sign.

Tran et al.[22] have used single-particle theory in the small signal approximation to calculate the bunching parameter q. Their result for the case of a single prebunching cavity with a gaussian axial field profile and circular mode polarization is:

$$q = \sqrt{\pi}\ F_1\ \mu_1\ e^{-\left[\frac{\Delta_1 \mu_1}{4}\right]^2} \left[\frac{\sqrt{3}}{2} \mu_1 + \mu_d \right] \qquad (41)$$

where parameters with a "1" subscript denote bunching cavity parameters and μ_d is the normalized distance from the end of the bunching cavity to the beginning of the oscillator cavity.

II.4 RESULTS OF CALCULATIONS FOR A DRIVEN OSCILLATOR

Calculations have been carried out for a driven gyrotron oscillator using the theory developed in Section II. Phase locking by both direct injection and using a prebunching cavity has been simulated and the accuracy of simple theoretical estimates of locking bandwidth has been investigated. The dependence of the bandwidth for phase-locking on gyrotron operating parameters is shown.

The configuration analyzed is a high voltage 35 GHz gyrotron similar to the NRL experiment recently reported by Gold et al.[5] The peak voltage and current of the annular beam are taken to be 650 kV and 1.5 kA, respectively, which are typical operating parameters. The beam guiding center radius is R_o=1.16 cm, the cavity radius is 1.6 cm, and the longitudinal profile of the cavity fields is assumed to be guassian with effective length L=4 cm. The operating mode is the TE_{621} circular mode with polarization counter-rotating to the beam rotation. The beam pitch ratio $\alpha \equiv v_t/v_z = 1$. The cavity Q factor Q=250. Spreads in beam guiding center and pitch ratio are neglected as are space-charge effects. The cold cavity eigenfrequency for the TE_{621} mode is 35.08 GHz.

The calculated efficiency, output power and frequency shift due to beam loading of the free-running oscillator (FRO) are shown as a function of magnetic field in Figure 1. The corresponding transverse efficiency and normalized cavity wave amplitude are shown as a function of the detuning parameter Δ in Figure 2. The electronic efficiency η is obtained from the transverse efficiency η_t according to: $\eta=\eta_t[\beta^2{}_{to}/2(1-\gamma_o{}^{-1})]$ where in the present case $\gamma_o=2.27$ and $\beta_{to}=0.63$. The transverse efficiency and normalized wave amplitude are related according to: $F^2=\eta_t I_G$. The normalized operating current is $I_G=0.238$. The normalized oscillation threshold current is also shown in Figure 2.

The case of direct injection of radiation is treated by integrating Eqs.(20). The injected locking power is taken to be 0.5 MW. The magnetic field is 2.5 Tesla [$\Delta=0.60$] and the cavity is seeded with a low amplitude field ($E=1$ kV/cm) at the beginning of the simulation. The time evolution of the driven oscillator output power is shown in Figure 3. This Figure shows that the steady state output power (140 MW) is achieved after about 5 nsec. The time evolutions of the driven oscillator frequency and phase are shown for three different locking frequencies in Figure 4. The oscillator frequency is expressed as the shift $\Delta\omega/\omega_o\equiv(\omega-\omega_o)/\omega_o\equiv d\psi/d\tau$ which vanishes when phase-locked operation is achieved. The initial locking frequency detuning $\Delta\omega_o/\omega_o\equiv(\omega_{FRO}-\omega_o)/\omega_o$ is $1\text{x}10^{-4}$, $2\text{x}10^{-4}$, and $3\text{x}10^{-4}$ in Figures 4(a), 4(b), and 4(c), respectively. According to Adler's relation [Eq.(33)], the maximum locking frequency shift for this magnetic field is $|\Delta\omega_o|_{max}/\omega_o=2.4\text{x}10^{-4}$. As expected, the oscillator evolves toward phase-locked operation in Figures 4(a) and 4(b), whereas phase-locked operation is not obtained in Figure 4(c). Comparison of Figures 3 and 4 shows that the time to achieve the equilibrium phase during phase-locked operation is much longer than the output power risetime. This confirms the validity of the assumptions made in obtaining Eq.(31) which in turn leads to Adler's relation.

The dependence of the phase angle for phase-locked operation on the locking frequency shift is shown in Figure 5 for the same oscillator parameters and locking power as above. The solid curve shows the analytical theory result [Eq.(32)] and the open circles indicate the results of slow-time-scale (STS) simulations. The angles plotted in Figure 5 correspond to the difference between the code result at each frequency shift and the code result for driving the oscillator at the free-running oscillator frequency. The dashed vertical lines indicate the minimum locking frequency shift for which phase-locked operation could not be obtained. This shift is found to be in good agreement with the maximum frequency shift predicted by Eq.(33),i.e., Adler's relation. Similar agreement was obtained between time-dependent calculations and Eq.(32) for a magnetic field of 2.4 Tesla. Since the oscillator is in the hard excitation regime for this magnetic field ($I<I_{thr}$), the cavity was seeded with the steady-state field amplitude in the time-dependent calculations. The phase-locking bandwidth for direct injection as a function of detuning parameter calculated using

Eq.(32) is shown in Figure 6. This Figure shows that the bandwidth is insensitive to the interaction detuning.

Phase-angle vs. locking frequency shift results for a gyrotron oscillator driven via a prebunching cavity are shown in Figure 7. The solid curve is based on Eq.(37) and the open squares are the results of integrating Eqs.(28) which are based on the perturbation theory (PT) approach. The open circles show results based on the klystron (K) approach in which the last terms on the RHS of Eqs.(28) are omitted and the beam phase bunching is introduced as initial conditions for the beam equations-of-motion. This avoids the approximation of separating the ac current density into two terms [cf. Eq.(4)]. The effect of the prebunching cavity, assuming phase bunching only, is represented by the bunching parameter $q_B=0.16$. This choice for q_B was used so the locking bandwidth prediction based on Eq.(39) for a magnetic field of 2.5 Tesla is the same as the direct injection result using 0.5 MW locking power. The time-dependent calculations based on perturbation theory are in good agreement with the results based on Eq.(37) except for negative frequency shifts near the bandwidth limit. The locking bandwidth obtained from the simulations is about 8% less than the result obtained using Eq.(39) which is considered to be good agreement considering the complexity of the time-dependent calculations. On the other hand the locking bandwidth obtained from simulations using the klystron approach is about 80% wider than the result obtained from Eq.(39) for this magnetic field. This difference is attributed to the approximation inherent in the perturbation theory approach.

The effect on the locking bandwidth of varying the magnetic field detuning parameter is shown in Figure 8 for phase-locking using a prebunched beam. According to Eq.(39) the locking bandwidth based on perturbation theory decreases rapidly as the detuning is increased. This behavior is shown in Figure 8 and implies a constraint on efficiency optimization. The decrease in bandwidth with increase in Δ obtained from simulations based on the klystron method is less pronounced than the perturbation theory results. The results of the two approaches converge and finally cross as the detuning is decreased. Comparison of Figures 6 and 8 shows a much stronger dependence on detuning parameter for phase locking with a perbunching cavity than by direct injection which is essentially independent of the detuning parameter. Figure 8 also shows the dependence of the exponentiation time constant, given in dimensionless form by Eq.(40), for the approach to phase-locked operation on the detuning parameter. The time constant plotted in Figure 8 corresponds to a locking frequency shift of one half the maximum frequency shift for obtaining phase-locked operation. To obtain the time constant in seconds, the result given by Eq.(40) should be divided by the operating frequency. Figure 8 shows that for the present configuration operating at 35 GHz and Δ=0.6 the efolding time is 21 nsec for a bunching parameter of 0.16. This time can be decreased to a few nanoseconds by increasing the bunching parameter and decreasing the detuning parameter.

II.5 DISCUSSION OF DRIVEN OSCILLATOR THEORY AND RESULTS

The extension of slow-time-scale steady-state gyrotron theory to time-dependent analysis of gyrotron oscillators driven by an external signal is demonstrated in this work. Calculations based on this theory yield the time evolution of the driven oscillator output frequency and phase for either the approach to phase-locked operation or for unphase-locked operation. These results should facilitate the investigation of driven intense-beam gyrotrons which are characterized by short pulselengths.

In the case of phase locking by direct injection, the maximum locking frequency shift which allows phase-locked operation obtained by integrating the STS time-dependent equations for the radiation amplitude and phase is in good agreement with Adler's relation. The simulations demonstrate the validity of the conceptual model which treats the phase-locking process as a perturbation of the free-running oscillator operation. Such calculations for frequencies near the maximum allowed frequency shift are costly since the time constant for the exponential approach to the phase-locked equilibrium phase becomes large in this limit. An important objective in carrying out the calculations shown, for example, in Figure 5 was to establish the time and space increments and number of phases needed to obtain accurate results from the time-dependent simulations.

In the case of phase locking using a prebunching cavity, the time-dependent calculations show that the perturbation theory approach underestimates the frequency shift bandwidth for phase locking except at small detuning parameters. The analytical bandwidth estimates based on the perturbation theory approach are nevertheless extremely useful for design purposes. The generality of the results has been increased by expressing the results in terms of well-known dimensionless gyrotron parameters.[13] The present results for a circularly polarized mode also extend the results obtained previously by Manheimer for a TE_{1n} linearly polarized mode.

References For Section II

1. W.M. Manheimer, Int. J. Electron. 63, 29-47 (1987).
2. S.W. McDonald, J.M. Finn, M.E. Read, and W.M. Manheimer, Int. J. Electron. 61, 795-822 (1986)
3. A.W. Fliflet, R.C. Lee, W.M. Manheimer, and E. Ott, NRL Memorandum Report 6064, 1987.
4. A.T. Lin, C.-C. Lin, Z.H. Yang, K.R. Chu, A.W. Fliflet, and S.H. Gold, to be published in the IEEE Special Issue on High Power Microwave Generation, (1988)
5. S.H. Gold, A.W. Fliflet, W.M. Manheimer, R.B. McCowan, W.M. Black, R.C. Lee, V.L. Granatstein, A.K. Kinkead, D.L. Hardesty, and M. Sucy, Phys. Fluids 30, 2226-2238 (1987).
6. P. Sprangle and W.M. Manheimer, Phys. Fluids 18, 224 (1975).
7. E. Ott and W.M. Manheimer, IEEE Trans. Plasma Sci. PS-13, 1 (1975).
8. V.A. Flyagin, A.V. Gaponov, A.V. Petelin, and V.K.Yulpatov, IEEE Trans. Microwave Theory Tech. MTT-25, 514 (1977).
9. P. Sprangle and A.T. Drobot, IEEE Trans. Microwave Theory Tech. MTT-25, 528 (1978).
10. K.R. Chu, Phys. Fluids 21, 2354 (1978).
11. K.R. Chu, A.T. Drobot, H.H. Szu, and P. Sprangle, IEEE Trans. Microwave Theory Tech. MTT-28, 313 (1980).
12. A.W. Fliflet, M.E. Read, K.R. Chu, and R. Seeley, Int. J. Electron. 53. 505 (1982).
13. B.G. Danly and R.J. Temkin, Phys. Fluids 29, 561 (1986).

14. M. Caplan, A.T. Lin, and K.R. Chu, Int. J. Electron. 53, 659 (1982).

15. R. Adler, Proc. Inst. Radio Engrs. 34, 351 (1946).

16. M.A. Moiseev and G.S. Nusinovich, Isvestia VUZ. Radiofizika 17, 1709 (1974) [Radio Phys. Quant. Electron. 17, 1305 (1976)].

17. N.S. Ginzburg, G.S. Nusinovich, and N.A. Zavolsky, Int. J. Electron. 61, 881 (1986).

18. A. Bondeson, W.M. Manheimer, and E. Ott, Phys. FLuids 26, 285 (1983).

19. B. van der Pol, Phil. Mag. 3, 65 (1927).

20. M.E. Read, R. Seeley, and W.M. Manheimer, IEEE Trans. Plasma Sci. PS-13, 398 (1985).

21. A.W. Fliflet, Int. J. Electron. 61, 1049 (1986).

22. T.M. Tran, B.G. Danly, K.E.Kreischer, J.B. Schutkeker, and R.J. Temkin, Phys. Fluids 29, 1274 (1986)

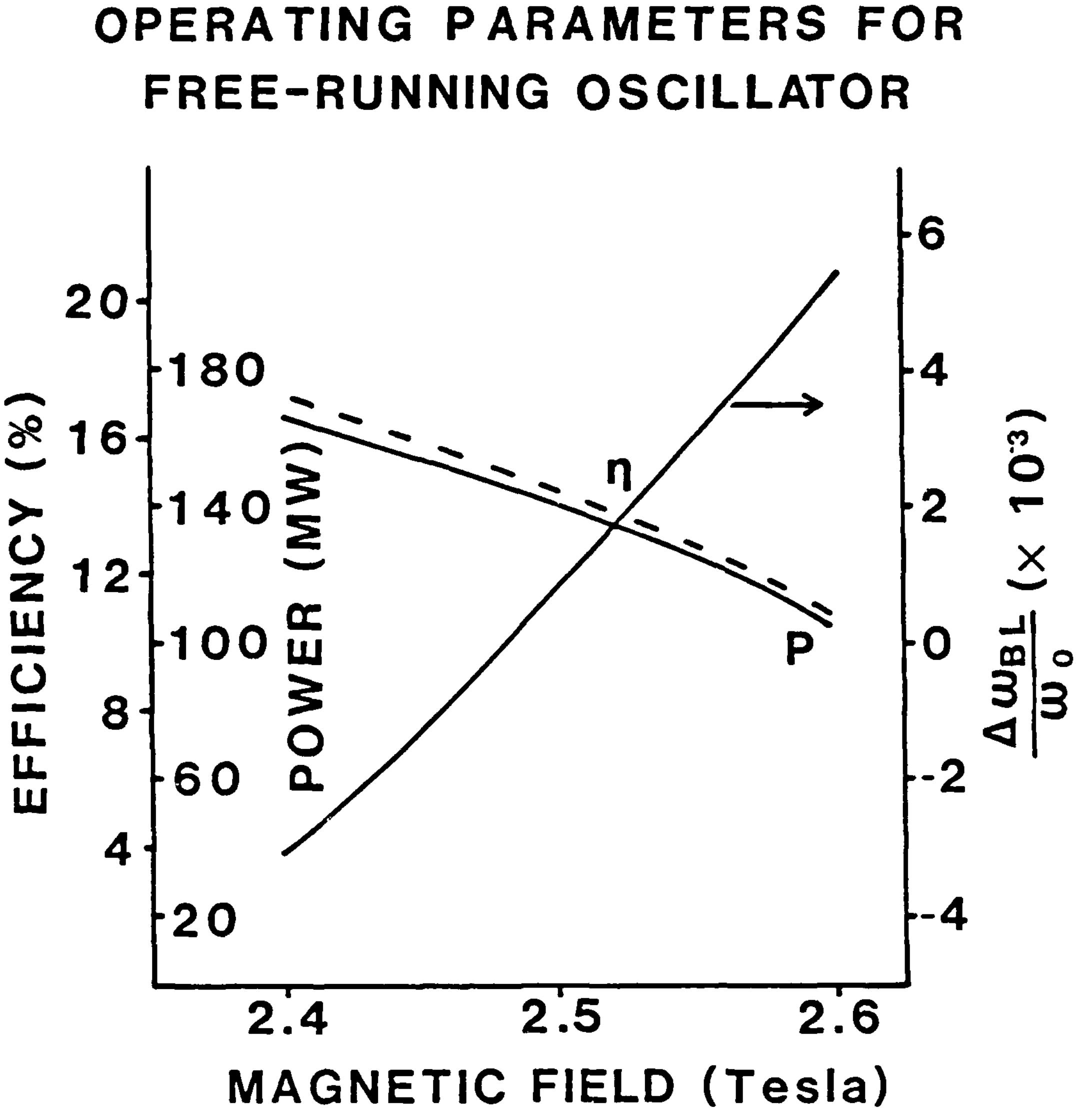

OPERATING PARAMETERS FOR FREE-RUNNING OSCILLATOR

Figure II.1. Efficiency, output power, and frequency shift due to beam loading for the free-running oscillator as a function of magnetic field.

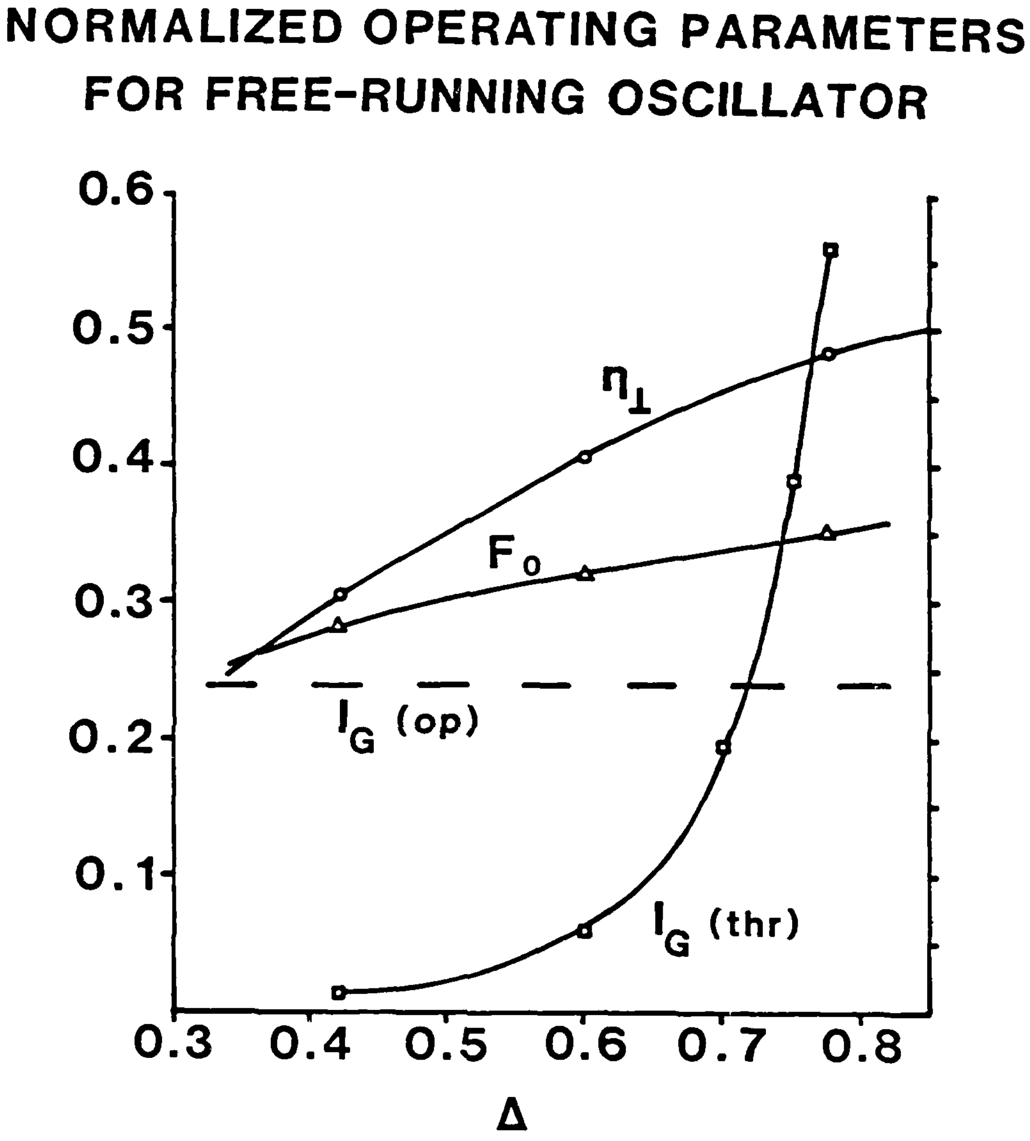

Figure II.2. Normalized operating parameters for the free-running oscillator.

OUTPUT POWER OF DRIVEN GYROTRON OSCILLATOR

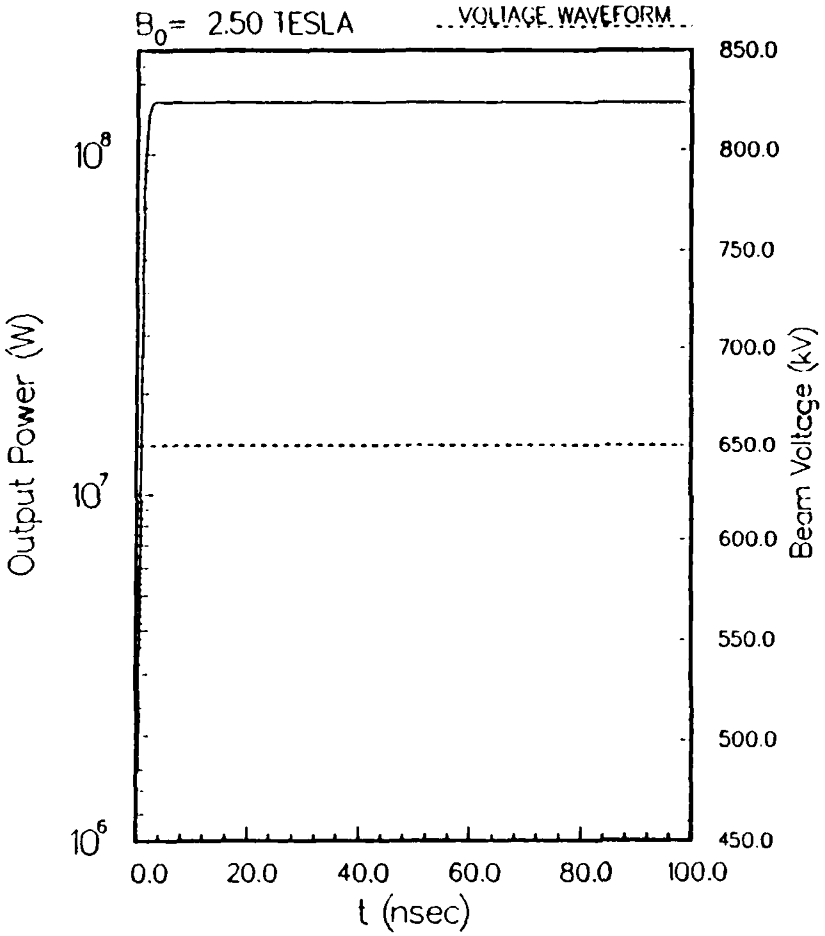

$V = 650$ kV

$I = 1500$ Amp

$\eta_{osc} = 14.5\%$

$\frac{\Delta \omega_0}{\omega_0} = 2 \times 10^{-4}$

$P_L = 0.5$ MW

$P_{osc} = 140$ MW

$Q = 250$

Figure II.3. Time evolution of the output power of the oscillator driven by 0.5 MW directly injected signal. The locking frequency detuning is 7 MHz and the magnetic field is 25 kG.

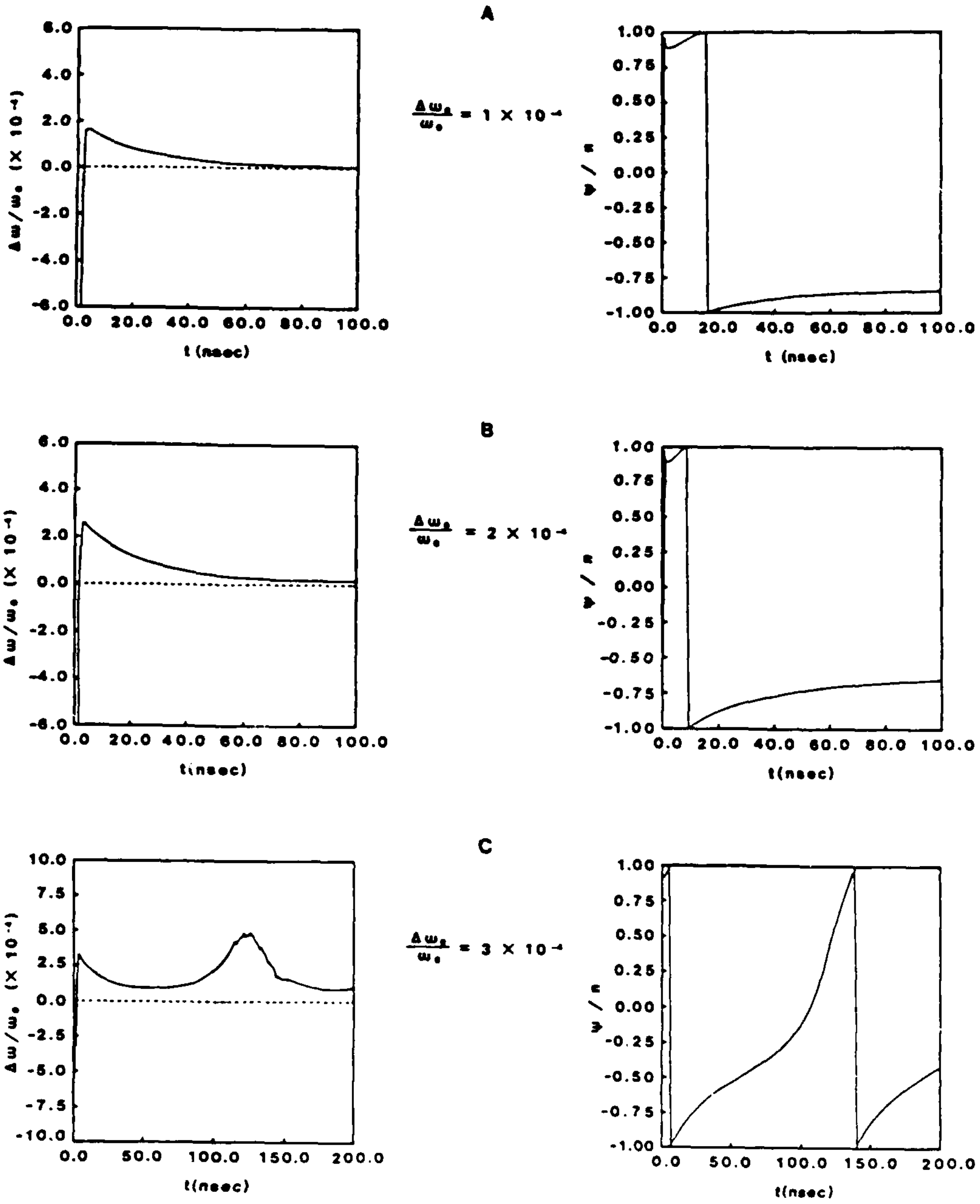

FREQUENCY AND PHASE OF A RELATIVISTIC GYROTRON DRIVEN BY DIRECT INJECTION

Figure II.4. Time evolution of the frequency and phase of the driven oscillator for three locking frequency detunings, (a): 3.5 MHz, (b): 7 Mhz, (c): 10.5 MHz. Operating parameters are the same as for Figure 3.

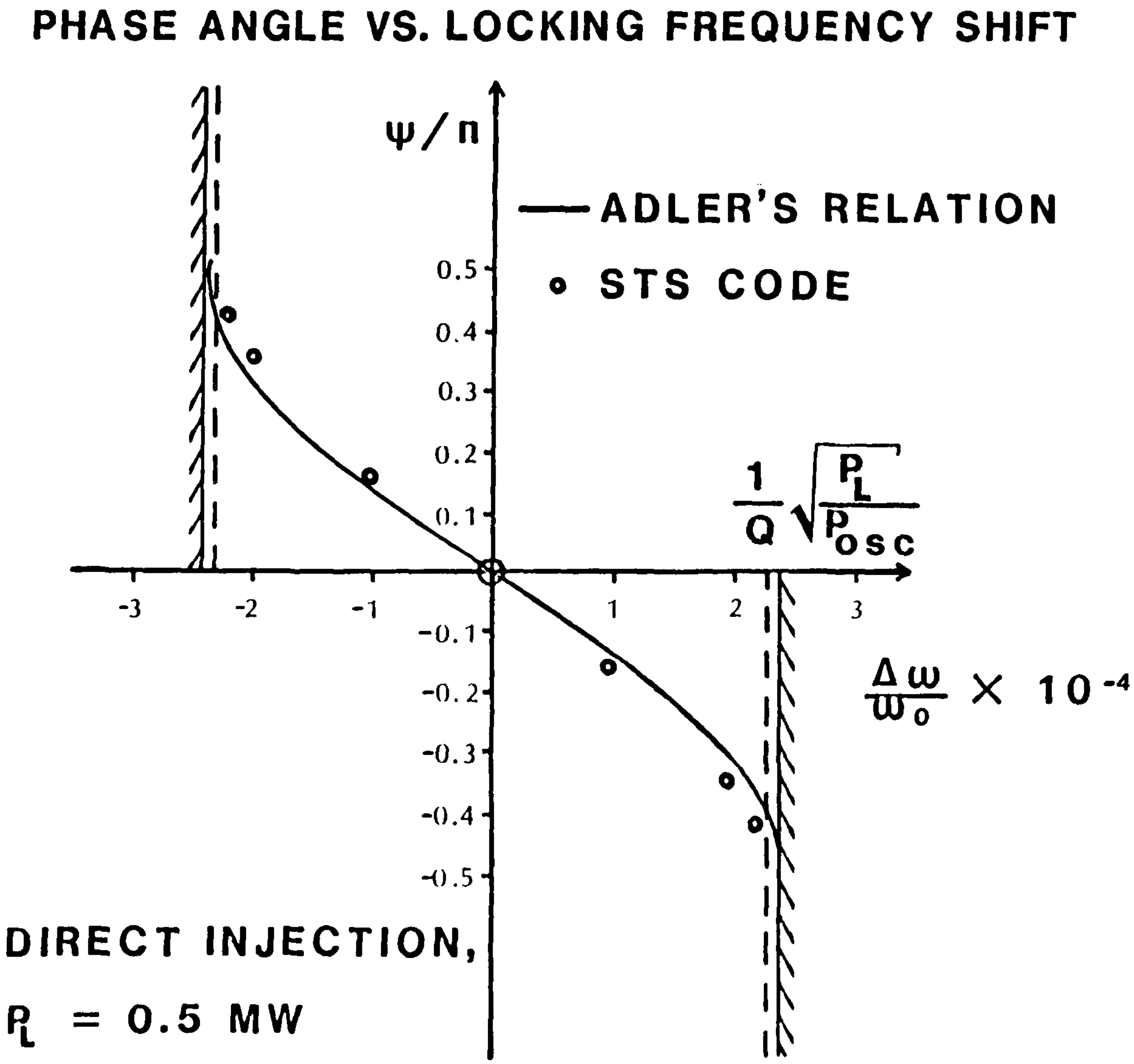

Figure II.5. Equilibrium phase angle versus frequency shift for the oscillator driven by 0.5 MW directly injected signal. Solid curve: analytical theory, circles: time-dependent simulation results. Shaded regions: Locking frequencies excluded by Adler's relation, dashed lines: upper and lower bounds for locking bandwidth from time-dependent simulations.

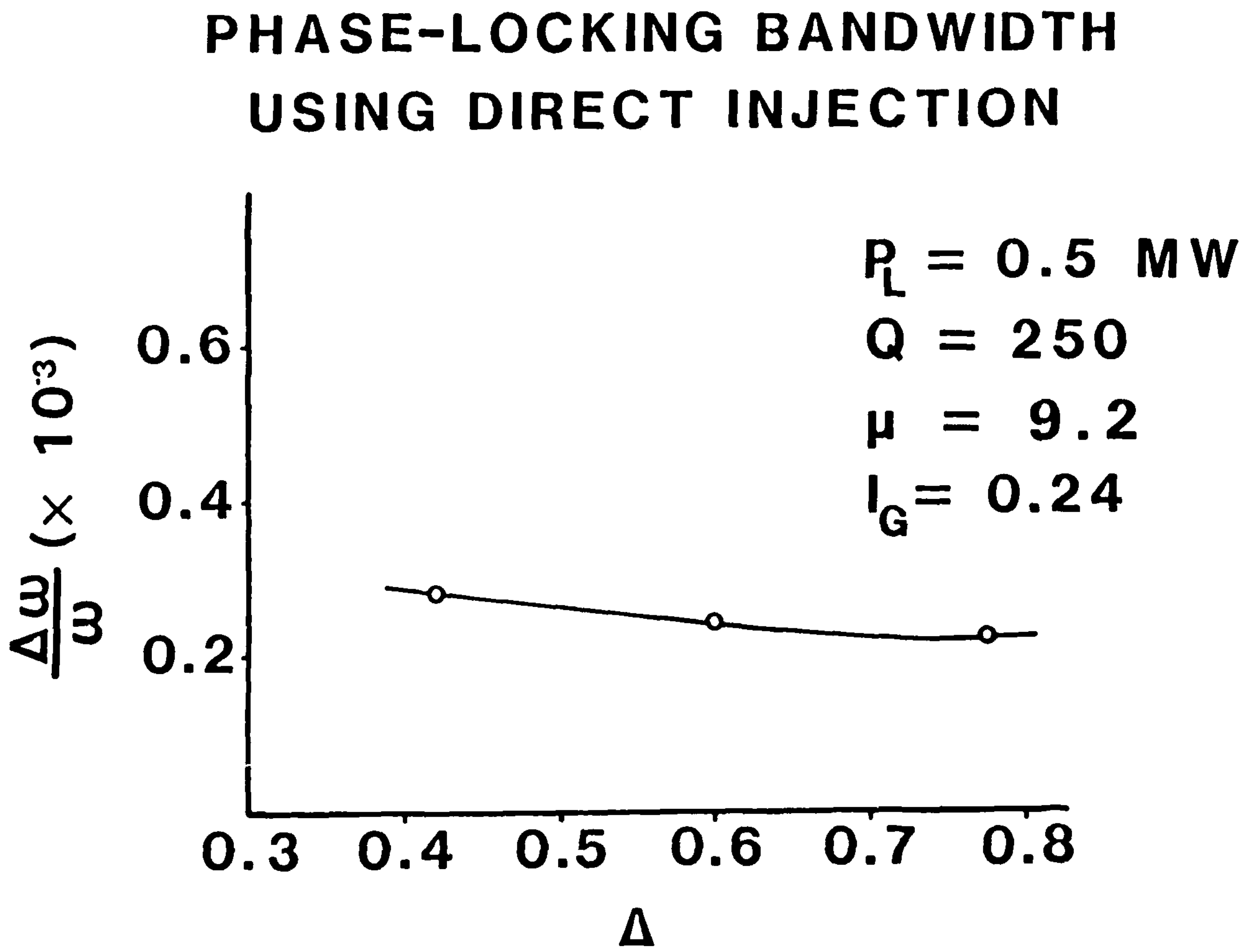

Figure II.6. Phase-locking bandwidth as a function of detuning parameter for the oscillator driven by 0.5 MW directly injected signal.

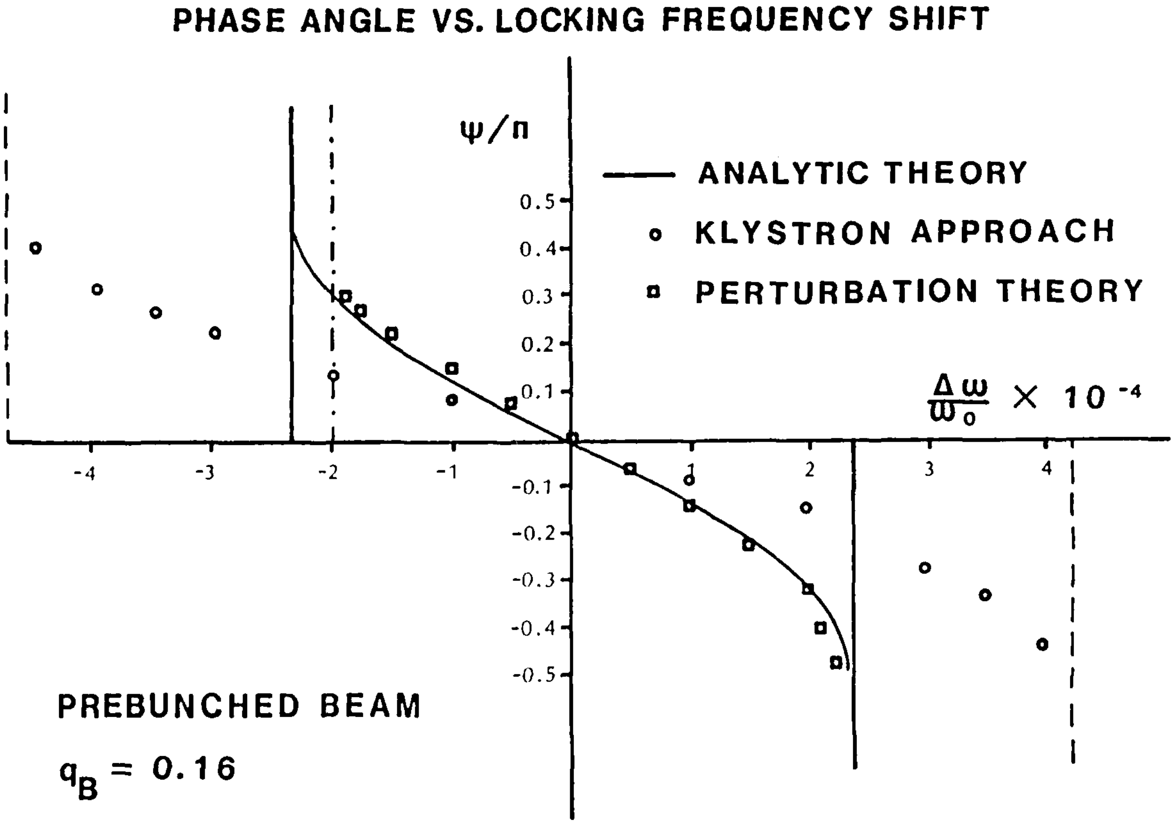

Figure II.7. Equilibrium phase angle versus frequency shift for the oscillator driven by prebunched beam with q_B=0.16. Solid curve: analytical theory, squares: time-dependent simulation results based on perturbation theory, circles: time-dependent simulation results based on klystron theory. Dashed line: upper and lower bounds for locking bandwidth based on klystron approach, solid vertical lines: maximum bandwidth based on analytical perturbation theory, dash-dot-dash line: lower bound for locking bandwidth from time-dependent simulations based on perturbation theory.

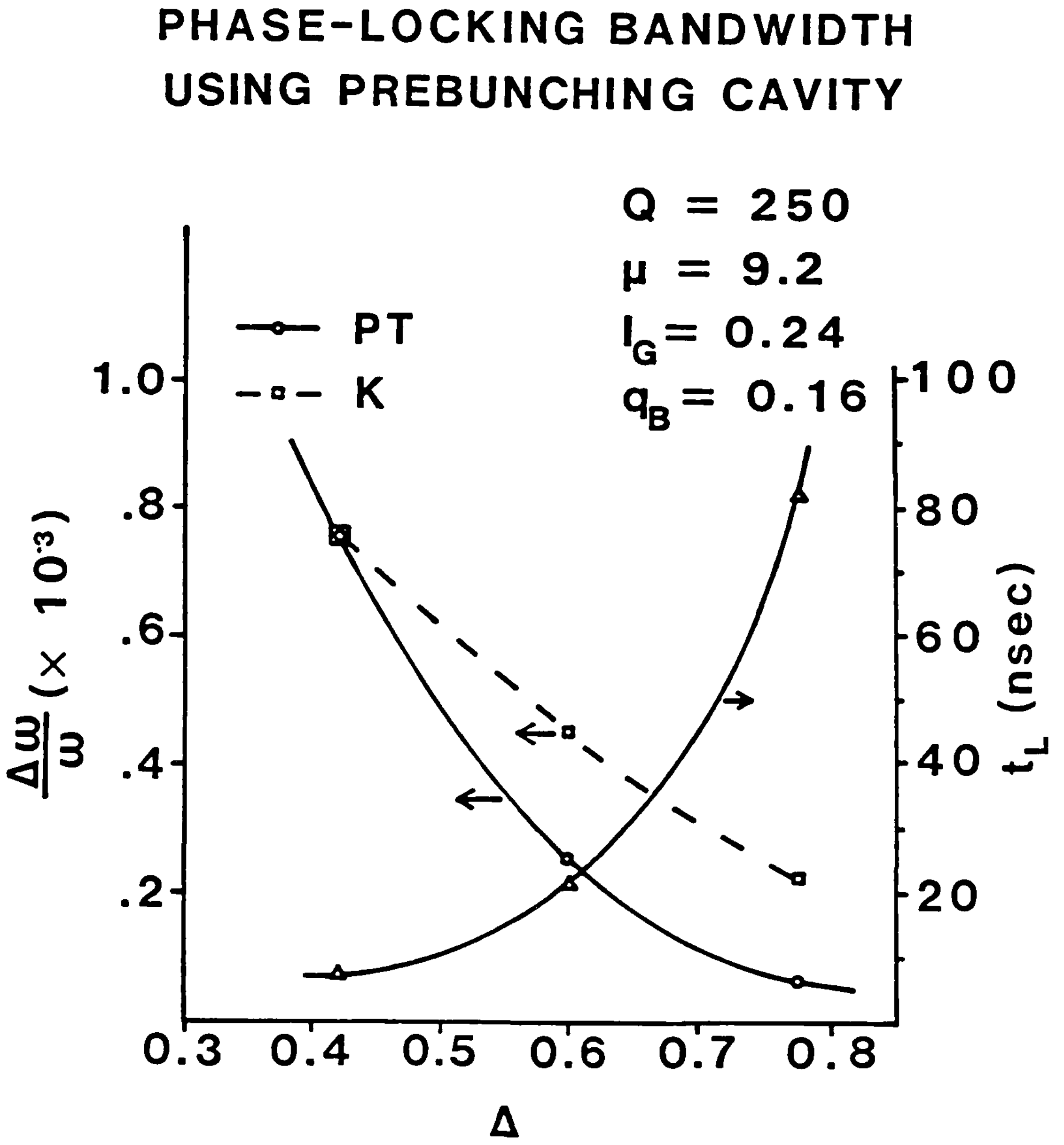
PHASE-LOCKING BANDWIDTH USING PREBUNCHING CAVITY

Figure II.8. Phase-locking bandwidth as a function of detuning parameter for the oscillator driven by a prebunched beam with q_B=0.16. Solid curve associated with left hand axis: perturbation theory result, dashed curve: klystron approach result, solid curve associated with right hand axis: exponentiation time constant based on perturbation theory.

III. The Low Power Oscillator Experimental Design

The goal of the low power experiment is to study a phase-locked oscillator in the actual mode at which the high power phase-locked oscillator will run. The phase locking signal will be injected into an input cavity where it will prebunch the beam. Although direct injection through a circulator is a possible strategy for this experiment, it will not be used because first, utilizing one or more prebunching cavities is expected to increase the locking bandwidth, and second, a circulator is not a viable option for the high power experiment of which this will be a low power prototype. The mode of operation will be the TE_{13} mode in both the main cavity and in the prebunching cavity. A TE_{13} mode is about as overmoded as seems prudent to operate in a first experiment. Furthermore, a TE_{1n} mode has the additional advantage that it is relatively simple to convert to a fundamental TE_{11} mode which is then quite easy to radiate. This experiment is designed using a thermionic electron beam and will be operable at high rep rate. In addition to being a prototype for the gigawatt power level phase-locked oscillator, it is of interest in its own right as the satellite disrupter and the space based radar. A schematic of the experimental design is shown in Fig III.1.

This experiment has taken longer to design than we had originally anticipated. The complications have been due to the fact that both the oscillator and prebunching cavity have had to operate in a very overmoded configuration. Recently, it has been shown that with careful design, a high power free running gyrotron oscillator can operate in a single very high order mode.[1,2] However, operation as a phase-locked oscillator puts many more constraints on the design than does operation as a free running oscillator. In addition to selecting the proper mode in the oscillator cavity, the phase-locked oscillator must be designed so as to suppress oscillation in the input cavity, launch the proper mode in the input cavity, and suppress communication between the input and oscillator cavities. Furthermore, the length of the drift section between the two cavities is limited by the thermal spread on the beam, as discussed in the previous section and elsewhere.[3] These design problems have proven to be very difficult and time consuming to solve. Using zero order design principles would quickly doom the experiment to failure. For instance, it might be thought that one could always stabilize the prebunching cavity simply by making it short enough. However, if one uses sudden changes in the cavity radius to define the cavity, one can make the cavity very short, but one will have a great deal of mode conversion at the cavity edges. This mode conversion will both lower the Q of the input cavity and also effectively trap any radiation which leaks out of the main oscillator cavity. Alternatively, one could use gentle tapers to define the cavity. This is, in fact, necessary to minimize mode conversion and our design does incorporate gentle tapers, and so will the gigawatt design. However, now one has fringe fields which extend far into the taper region, so that the effective cavity length is not simply the length of the straight section between the tapers, but is much longer. Even for zero straight section length, the effective length of the prebunching cavity can be considerable.

The longer one makes the taper on the cavity wall, the less mode conversion there will be. However, the taper cannot be made arbitrarily long either. For one thing, this makes the effective length of the prebunching cavity very long, and thereby more difficult to stabilize. Also, a long taper means a long drift section, so that thermal spread on the beam would greatly reduce the phase locking bandwidth. Thus, before the experiment can be set up, it is clear that a very careful, time consuming design is required.

Certain basic principles have become clear as we have proceeded with this design. First of all, our original strategy was to maximize the phase locking bandwidth by maximizing the field in the input cavity. This implied using a fairly high Q cavity for the input, and our original design choice was for a Q of five to ten thousand, not much less that the Ohmic Q. It was expected that the input cavity would have a lower start oscillation current, but that the input cavity would be stable because the magnetic field would be too high for it to oscillate. That is the input cavity would be very short, so that above a critical field B_∞ it would be stable. The main cavity would be longer and would oscillate at higher fields. The start oscillation current for the input cavity and the main cavity as a function of the magnetic field, for our original design, is shown schematically in Fig. (III.2). One disadvantage of such design is immediately apparent. On the I-B parameter space of a single cavity gyrotron, the regime of most efficient operation is shown in Fig. (III.3). Clearly, the high Q input cavity does not allow the main cavity to access the regime of most efficient operation. Furthermore, one is in danger of having the input cavity self oscillate due to operating in magnetic fields which are slightly incorrect. Finally it was realized that even though the inherent bandwidth of the oscillator is larger, it is still limited by the low bandwidth of the input cavity.

For all of these reasons, the design was switched to a low Q input cavity design with less inherent locking bandwidth. The I-B parameter space of the phase-locked oscillator with the low Q input cavity is shown schematically in Fig. (III.4). The operating regime now encompasses the regime of most efficient operation, and furthermore, there is no danger of the input cavity self oscillating at any magnetic field. While the inherent bandwidth is reduced, it also seems clear, in principle at least, that it can be increased by going to a multi-input-cavity configuration. By injecting the power in the first input cavity, one achieves amplification, so that the field in the second cavity is greater. This amplified field then prebunches the beam for the final oscillator cavity.

The total number of cavities is not limited by the thermal spread on beam; thermal spread on the beam only limits the intercavity spacing. At each intermediate cavity, an amplified field rebunches the beam at higher bunching parameter, so that on exiting one intermediate cavity, the beam effectively has no memory of the bunching in the cavities before. What does limit the number of cavities however is mode conversion. In the oscillator cavity, there is some mode conversion from, for instance, the TE_{13} to the TE_{12}. This TE_{12} mode propagates freely through the drift tube and through all of the prebunching cavities. As it passes each prebunching cavity, some of it is reconverted to the TE_{13} in the prebunching cavity and is then trapped there. If all prebunching cavities are identical, the same fraction of the leaked out mode is trapped in all prebunching cavities. Specifically, some will be trapped in the first cavity. As long as the power trapped in the first cavity is significantly less than the injected power, it should work as a multicavity phase-locked oscillator. Once the trapped power becomes comparable to the injected power, phase-locked operation clearly becomes nonviable. Thus, in an overmoded phase-locked oscillator, the mode conversion at the cavity tapers limits the number of prebunching cavities. This is in contrast to a fundamental mode oscillator or amplifier where there is no such limitation. For instance, the SLAC klystron has seven cavities altogether. It is unlikely that a TE_{13} phase-locked oscillator could ever have nearly that many. However, it could probably have three, and this would be a potential follow on project to this if there is interest in enhancing the locking bandwidth.

The parameters of the low power oscillator are a frequency of 85 GHz, the operating mode is a TE_{13} standing mode, the beam voltage is 70 kV, the current is 6 Amps or less, the output cavity Q is about 2000, the input cavity Q is about 1000, the isolation between the cavities is about 45 dB, the input power, from a Varian 85 GHz EIO is 500-1000 watts, and the output power will be 50-100 kW. The performance of the low power phase-locked oscillator has been examined using both the analytic theory for a TE_{13} standing mode, and also the slow time scale theory for a TE_{13} rotating mode. The analytic theory gives the result that

$$\frac{\Delta\omega}{\omega} = \frac{0.17\ I(\mathrm{Amps})}{E(\mathrm{kV/cm})}\,(U^2 + V^2)^{1/2}$$

where E is the field in the oscillator cavity. Taking I=4 and E=250, we find that

$$\frac{\Delta\omega}{\omega} = 2.7\times10^{-3}\,(U^2 + V^2)^{1/2}$$

For a beam with no thermal spread, $(U^2 + V^2)$ is a function of two parameters, the frequency mismatch and the field in prebunching cavity S. The parameter S is proportional to the bunching parameter Q_b. The slow time scale code predicts frequency width as a function of bunching parameter Q_b for $m(\gamma\omega - \Omega)r_p/p\cos\alpha_o = 2$ as shown below:

Q_b	$\Delta\omega/\omega$
0.25	2x10-4
0.5	4x10-4
1.0	1.1x10-3

In Fig. (III.5) is shown a contour plot of $(U_2 + V_2)^{1/2}$. Also shown are the positions of Q_b equal to 0,25, 0.5 and 1.0. Clearly, the analytic theory and the slow time scale code are in reasonable agreement for the low power, 85 GHz phase-locked oscillator experiment.

One of the most important things to quantify in designing the experiment is the mode conversion at the tapers, and equivalently, the cavity Q due to mode conversion. The mode conversion codes available to us did not account for standing modes in either the axial or azimuthal direction. Accordingly, these codes had to be modified to account for the actual mode structure. An example of the design is shown in Fig. (III.6).

There, for a cavity with a straight section length of 0.19 cm, the Q due to mode conversion and the maximum magnetic field for oscillation (B_∞) are tabulated as a function of taper length. This latter quantity is calculated using the actual computed axial field profile, as it exists in the cavity and as it spills over into the drift section. There the minimum wall radius is 0.4 cm, and the maximum wall radius is 0.5 cm. Another important factor which contributes to the cavity Q is the slot angle of the cavity. This will be chosen to load down all the competing modes, but to allow the desired TE_{13} mode to be excited, but not self oscillate. The cavity Q as a function of slot angle for the TE_{13} (desired) and TE_{42}, and TE_{71} (main competing) modes is shown in Fig. (III.7).

Since the input cavities have a large number of requirements regarding mode conversion, slot Q, mode excitation, and overall stability, we have minimized the risks by designing three different input cavities. These will be cold tested and optimized on the actual experimental setup before it is pumped down. The coupling hole will be machined slightly too small, so that it can be easily enlarged. This cold test will determine the input cavity Q and the coupling from the EIO to the cavity. The coupling hole will be determined so as to optimally match the into the cavity. That is, the contribution to Q arising from the coupling hole will be equal to the contribution to Q from everything else. This will be cold tested on the three cavities.

The wall radius, slot angle, effective length and predicted total Q for the three cavities are shown in Figs. (III.8a, b, and c). At optimal coupling, of course, the actual Q will be half of those values. Also shown are the computed axial field profiles. Notice that the effective length is not that strong a function of the physical length of the straight section of the cavity. The reason is that the evanescent region of the fields extend well into the drift section. Notice that the first cavity, the shortest one, has a very high predicted Q. This might appear incorrect because the large amount of mode conversion in the short taper would imply low Q. However, there is mode conversion at each taper, and it is possible that destructive interference between the forward converted TE_{12} mode at the right taper and the backward converted TE_{12} mode at the left taper could occur, thereby raising the Q. That is the basis of the design in Fig. (III.8a) and the reason the predicted Q is so high. Whether this will actually work as predicted will be answered in the series of cold tests. In Fig. (III.9a, b and c) are shown the start oscillation currents of the three cavities for the TE_{12} and TE[illegible] mode. Also shown is the start oscillation of the main oscillator cavities. Clearly there is a large range of currents where the input cavities will not oscillate at any value of magnetic field.

We now turn to the design of the main oscillator cavity. As this cavity will self oscillate at high power, it is particularly important that the mode conversion in the input taper be very small, so that it be isolated from the prebunching cavities. In Fig. (III.10) is shown the mode conversion from the TE_{13} to TE_{12} as a function of the input taper length. Also shown is the shift in the peak of the electric field profile. This shift essentially adds on to the physical separation of the two cavities. Since the mode conversion of the TE_{12} back to TE_{13} in the input cavities is always less than 15 dB (as quantified by the standard mode conversion codes for traveling waves) an input taper length of 0.4 cm will give at least 45 dB of isolation between two cavities. In Fig. (III.11) are shown the wall radius, field amplitude and phase as a function of axial distance for the output cavity.

We now turn to some issues of the mechanical and electrical design of the low power phase-locked oscillator. A mechanical drawing of the experiment is shown in Fig. (III.12). Notice that the input waveguide is pumped out in two places, at it entry to the tube, and also in a special pump out section near the input window. A preferable design would have been not to evacuate the input waveguide at all, but severe mechanical constraints prevents the use of a vacuum window inside the two inch bore of the superconducting magnet. Thus the only option is to put the input window outside of the magnet, and use an additional pumping port on the input waveguide. The electron gun to be used is the Varian VUW 8010 (Seftor) gun. This has been used in many experiments at NRL and is an extremely reliable piece of apparatus with which we have had a great deal of experience. Notice that after the gun, there is a space for the input and output cavity. For each, special cavity holders had to be designed, and the cavities themselves had to be designed to fit into them. The output cavity holder is the much more complicated and expensive holder, and the input cavity is the much more complicated and expensive cavity, for reasons we will go into shortly. There are also two current breaks, the first one, which is inside the magnet must be made of a nonmagnetic material; for the second, which is outside, can be either magnetic or non magnetic. The radiation leaves the tube through a beryllium oxide window.

We now turn to the input cavity. For all input cavities, the outside shape is the same, so the cavity holder is relatively simple to design. The cavity itself is quite massive. The inside shape is machined to match the design of the inside wall which we have just discussed. Since the cavity is slotted, a thick piece of absorber must be used to absorb any microwave radiation coming out of the slot. This is a piece of ceralloy. Since the dielectric constant of the ceralloy is high, a matching piece of macor is used to eliminate reflections. This matching interface must be an odd number of quarter wavelengths thick. The frequency it is matched to is 92 GHz, the frequency of the TE_{42} mode, the main competing mode. The bandwidth of the macor matching plate gets smaller as its thickness increases. For this reason, the most preferable thickness is one quarter wavelength. At this thickness, it will also be a good absorber for 85 GHz radiation; if the thickness is three quarters of a wavelength, there will be significant reflection there. However, machining such a thin, cylindrical piece of macor could be difficult, and it may be that we will have to settle for a thicker piece. A machine drawing of the input cavity is shown in Fig. (III.13).

The output cavity holder is one of the most complicated pieces to machine. To see this, note that there are three frequencies in the problem, the EIO frequency, the input cavity frequency, and the output cavity frequency. Clearly, one can only have a phase-locked oscillator if these three frequencies coincide to a very high degree of accuracy. The EIO is mechanically tuneable over about 2 GHz. The input cavities are not designed to be tuneable, because the complications of hooking up the input microwaves would make a mechanical tuning scheme extremely complicated. Therefore the output cavity must be tuneable, so that all frequencies are tuned to the input cavity. To make to output cavity tunable, we have utilized a slotted cavity design. A mechanical pusher compresses the cavity and slightly changes its shape and therefore its frequency (and cavity Q also). This plunger must be vacuum compatible. We have found that the mechanical design of the cavity which provides for reasonable amounts of compression (a few mills) with a reasonable force (a few pounds) is one in which the slots are brought all the way to the end of the cavity. Electrically, it is of course greatly preferable to bring the slots all the way to the narrow end of the cavity where there will be no microwave power. The output cavity holder then must be designed to transmit mechanical force through a vacuum enclosure. The actual transmitter will be a small bellows in the cavity holder which is machined separately form the rest of the cavity holder and welded on. A mechanical drawing of the cavity holder is shown in Fig. (III.14).

Notice that while the cavity is slotted, the main reason for the slots is not to provide mode control, but to allow for mechanical tuning. We have shown earlier that a TE_{13} mode gyrotron at 70 kV can run with little mode competition in an unslotted cavity.[1] Thus, the output cavity holder has no provision for using absorbers outside the slots. The actual output cavity, with slots and the axial tapers is three dimensional, and cannot be analyzed economically. What can be analyzed are two two dimensional approximations to it. First, we can use the slotted cavity code to calculate cavity frequency and Q as a function of slot width. The result of this calculation is shown in Fig. (III.15). Secondly, we can use the tapered cavity code (without slots) to calculate the frequency and Q as the cavity wall pivots about the end of the slots. The result of this calculation is also shown in Fig. (III.15). Clearly, compression of a few mills will give the sort of tuneability required, while not greatly affecting the Q. A machine drawing of the main oscillator cavity is shown in Fig. (III.16). Shown in Fig. (III.17) is a photograph of the input cavity holder, output cavity holder, and output cavity.

Finally, we turn to a discussion of the diagnostics of the low power phase-locked oscillator. Since this is a long pulse reprated experiment which will operate at high data rate, the diagnostics are simpler than in the single shot experiments which will be done at the megawatt and hundreds of megawatt level. A schematic of the diagnostic setup is shown in Fig. (III.18). The Varian EIO is launched through an isolator into the prebunching cavity of the gyrotron. The reflected power will be monitored. Another portion of the EIO signal will be branched off for comparison with the gyrotron signal. The two signals are sent through variable attenuators so that the signals are of equal strength. They are then mixed in a balanced mixer, and the difference frequency signal is extracted. If the oscillator is phase-locked, then this signal will be a constant, which can be nulled by the use of a phase shifter in one of the lines. Another diagnostic line will sent the signal from both the EIO and gyrotron to a spectrum analyzer so as to to measure the spectrum of each in phase-locked as well as free running oscillation.

References for Section III

1. M. Rhinewine and M.E. Read, "A $TE_{1,3}$ Gyrotron at 85 GHz," Int. J. Electronics **61** (6), p. 729 (1986).
2. K.E. Kreischer and R.J. Temkin, "Single-Mode Operation of a High-Power, Step-Tunable Gyrotron," Phys. Rev. Lett. **59** (5), p. 547 (1987).
3. W.M. Manheimer, "Theory of the multi-cavity phase locked gyrotron oscillator," Int. J. Electronics **63** (1), p. 29 (1987).

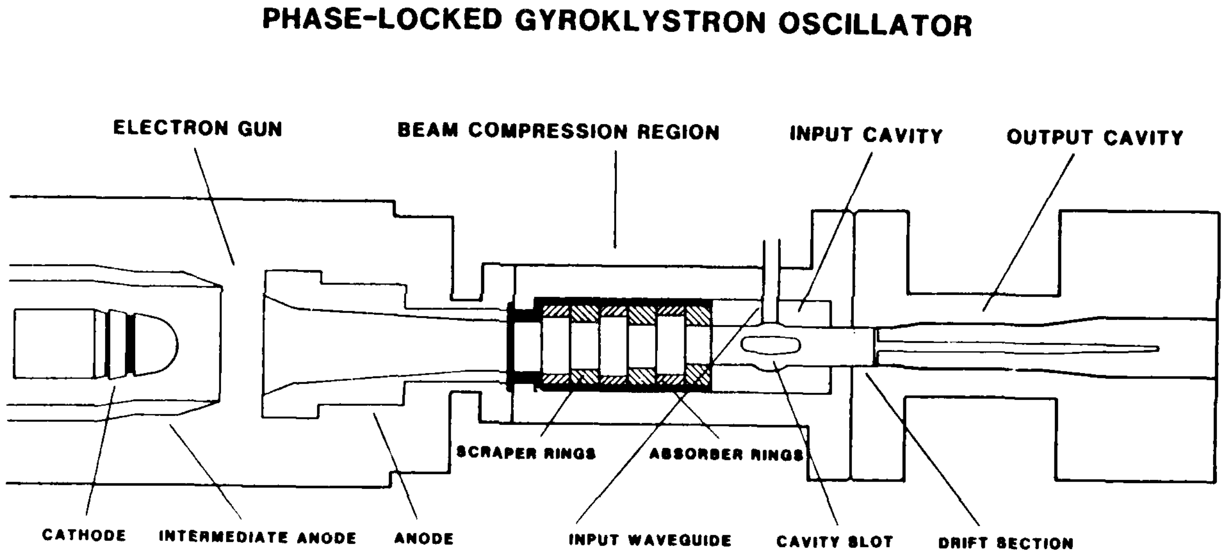

Fig. III.1. Schematic of the low power experiment.

ORIGINAL I-B PARAMETER SPACE
FOR DOUBLE CAVITY PHASE LOCKED OSCILLATOR

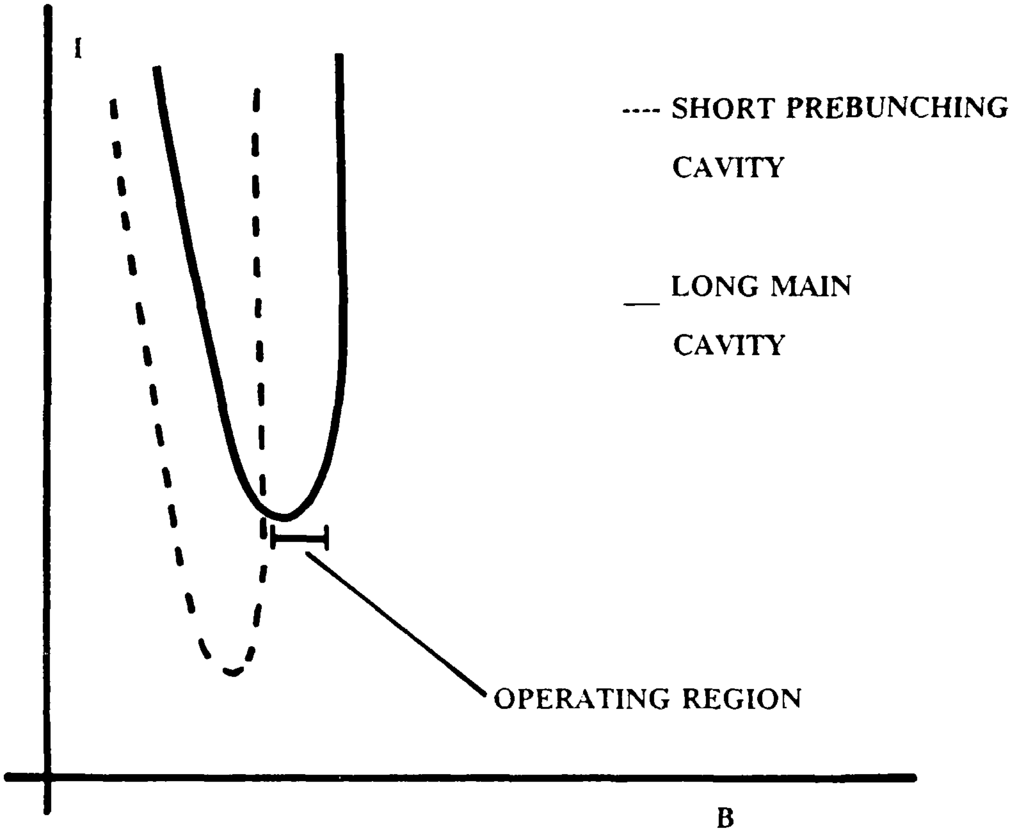

- MAIN CAVITY OPERATES IN LOW EFFICIENCY REGION BECAUSE PREBUNCHING CAVITY HAS LOW THRESHOLD CURRENT BECAUSE OF ITS HIGH Q.

- GETTING A SIZEABLE PARAMETER WINDOW WHERE THE PREBUNCHING CAVITY IS STABLE PROVED VERY DIFFICULT.

Fig. III.2. Original high Q input cavity design.

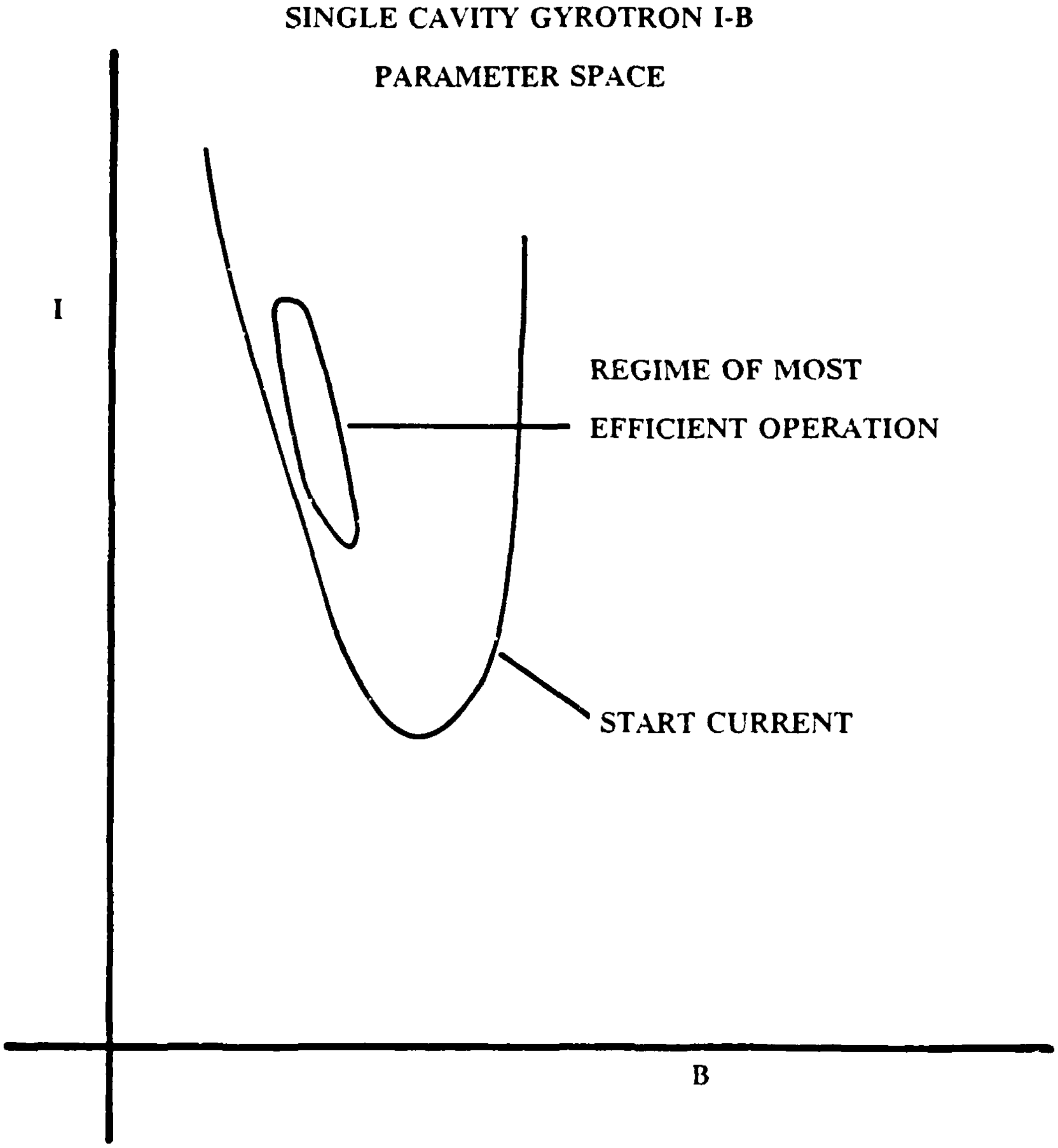

Fig. III.3. Operating parameter space for a gyrotron.

I-B PARAMETER SPACE FOR DOUBLE CAVITY
REVISED DESIGN OF PHASE LOCKED OSCILLATOR

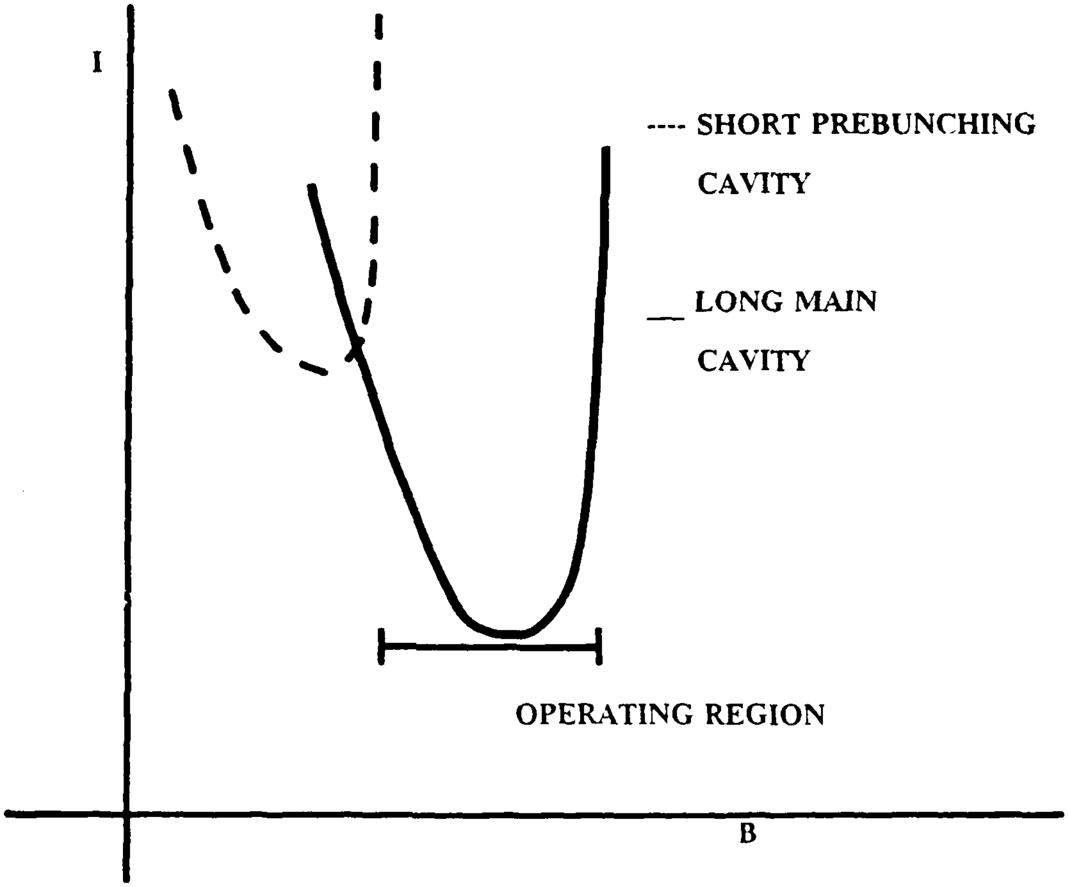

- OPERATING REGION NOW ENCOMPASSES HIGH EFFICIENCY OPERATION.
- CAN OPERATE BELOW MINIMUM START CURRENT OF PREBUNCHING CAVITY.
- INPUT FIELD CAN BE INCREASED BY GOING TO 3 CAVITIES. THIS SHOULD CONSIDERABLY INCREASE LOCKING BANDWIDTH.

Fig. III.4. Revised low Q input cavity design.

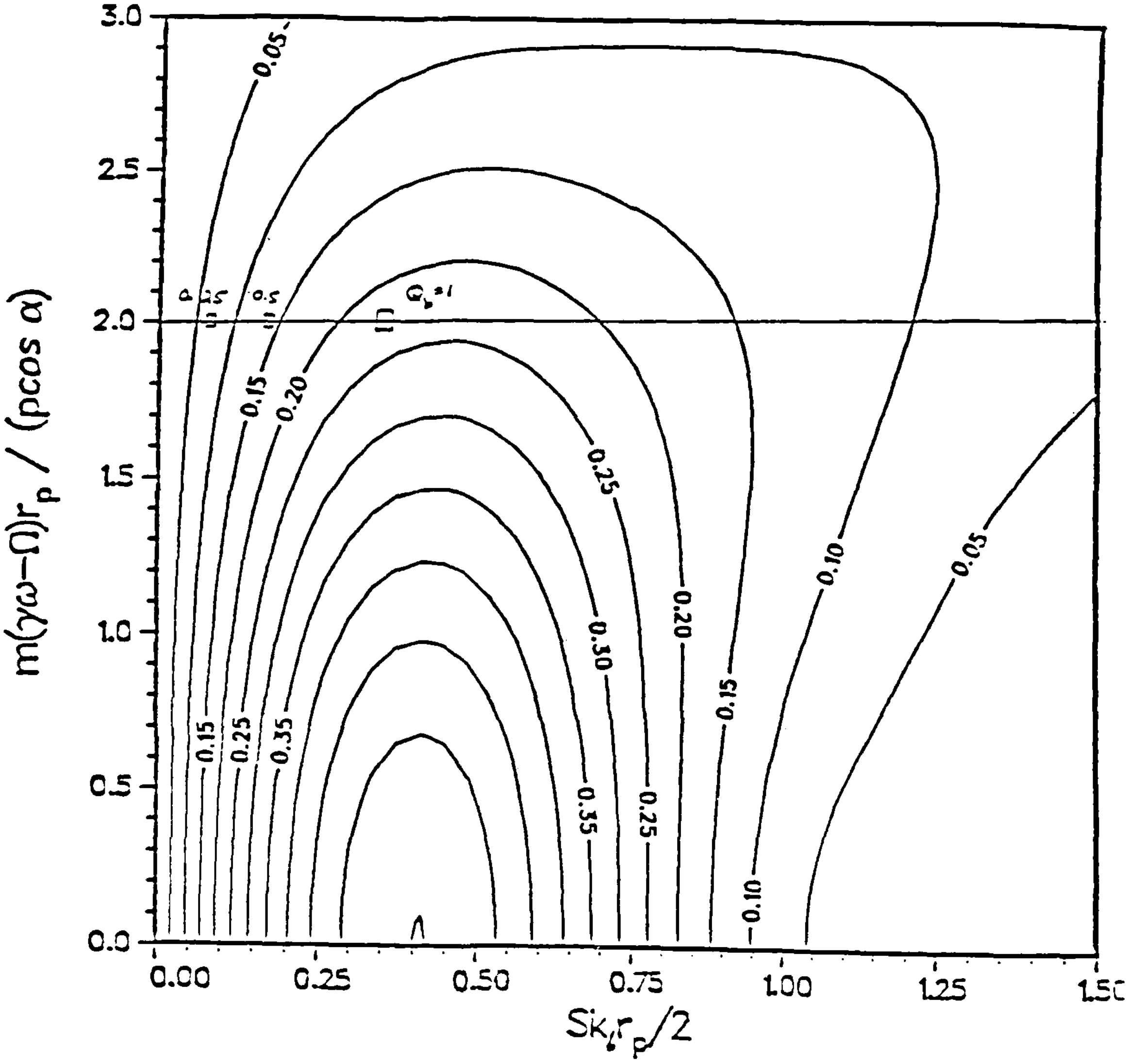

Fig. III.5. Contours of $(U^2 + V^2)^{1/2}$. The values of $Q_b = 0.25$, 0.5 and 1.0 correspond to the values of S shown.

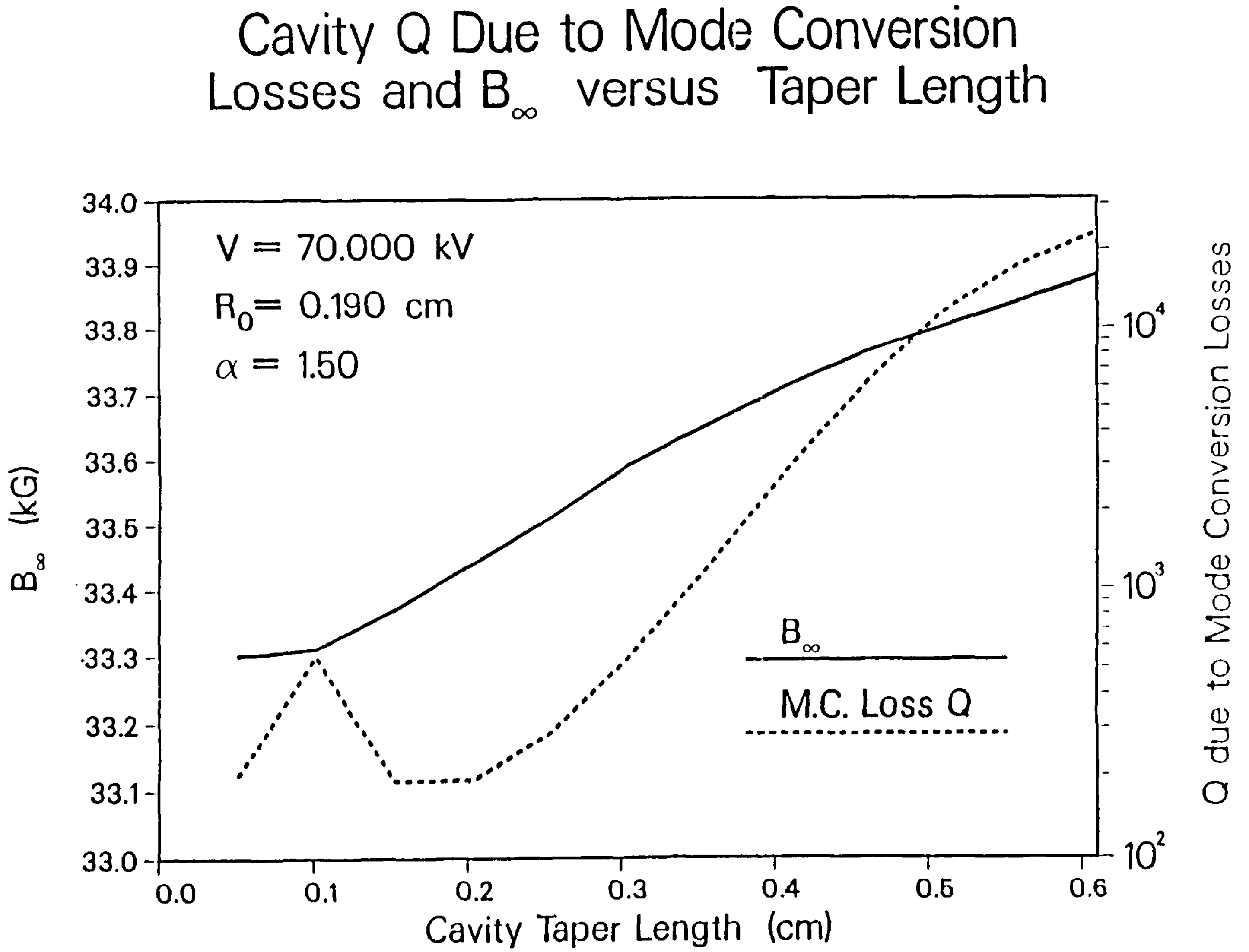

Fig. III.6. Mode conversion and critical field as a function of taper length.

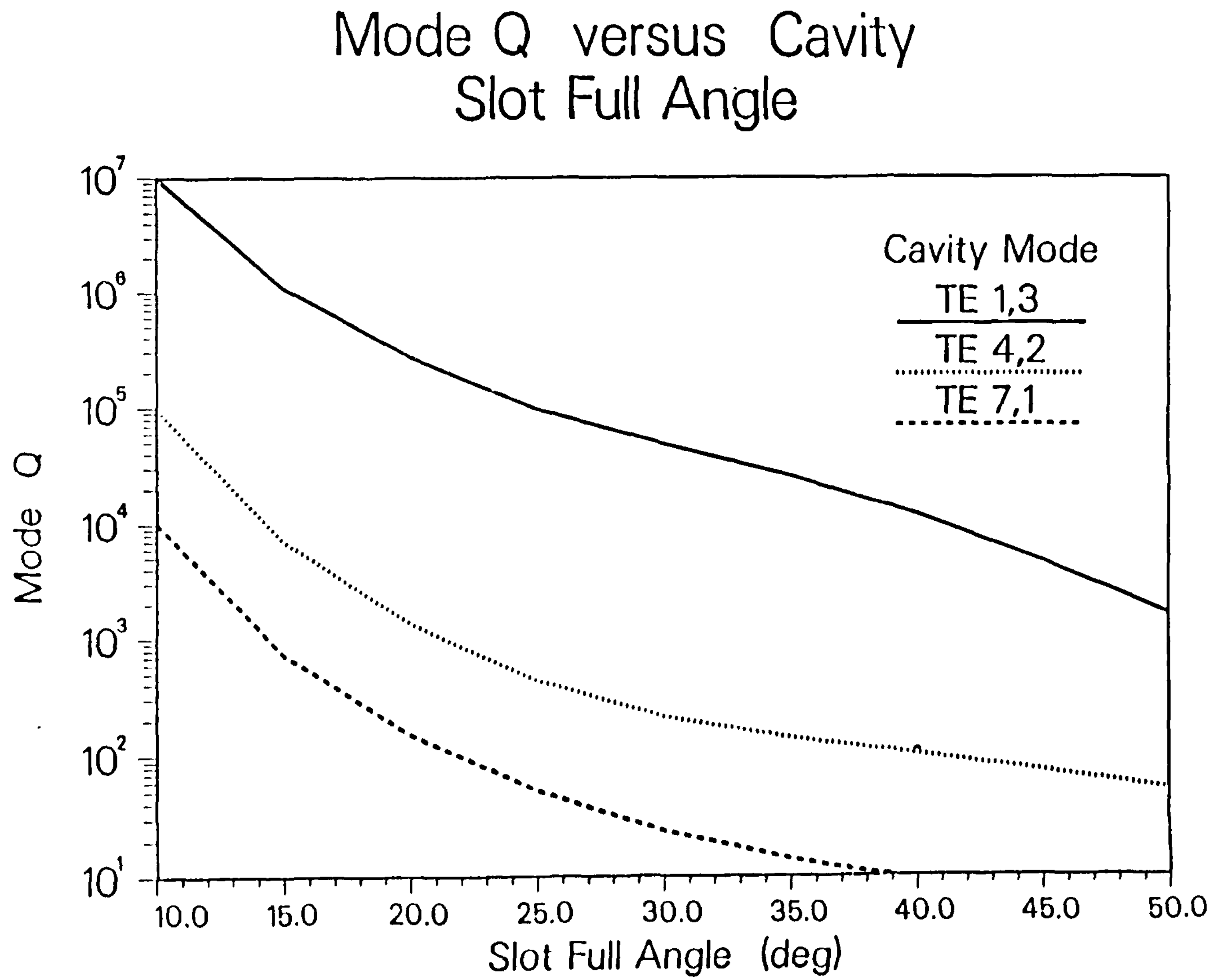

Fig. III.7. Slotted cavity Q.

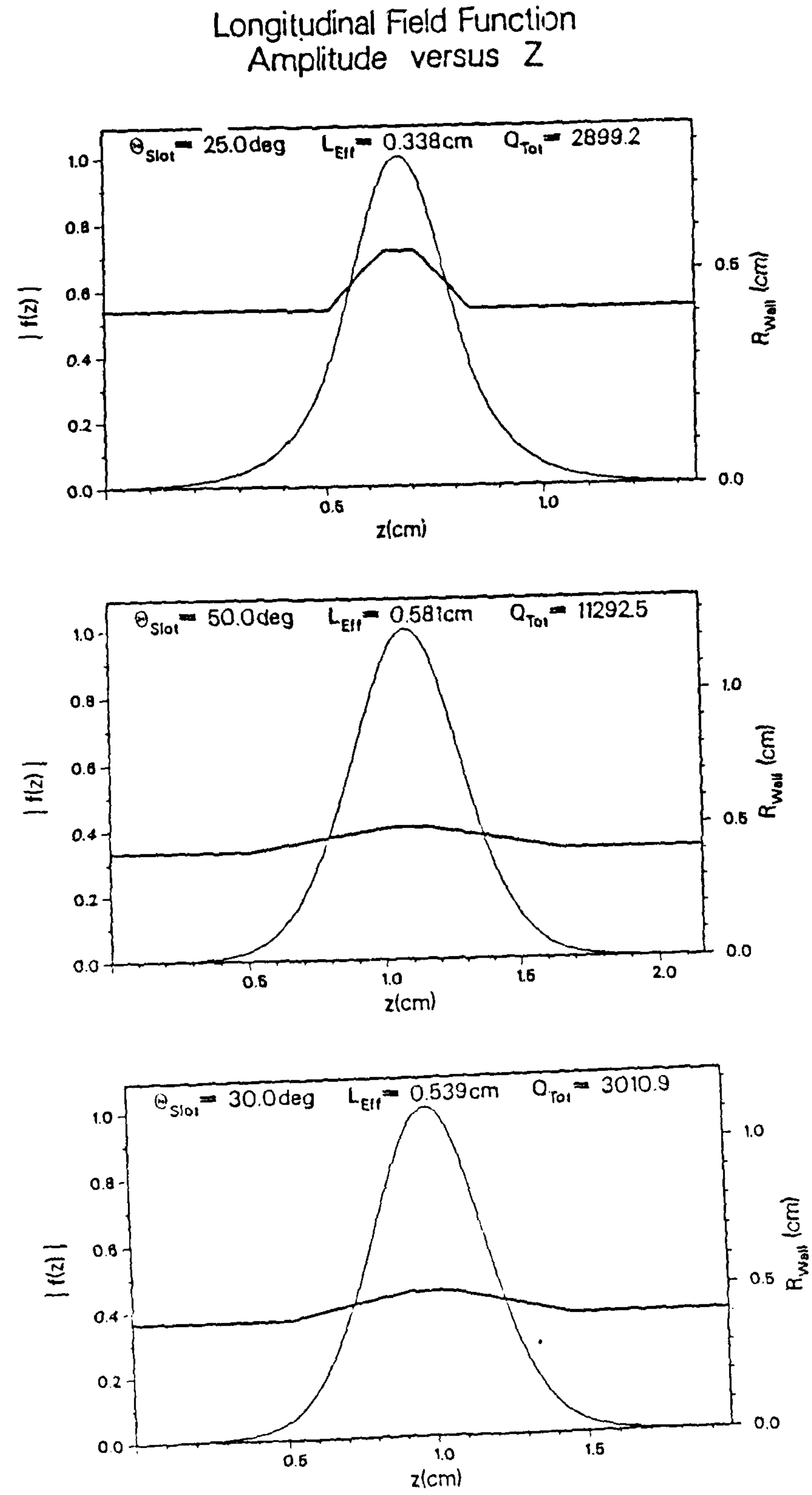

Fig. III.8. The three input cavities.

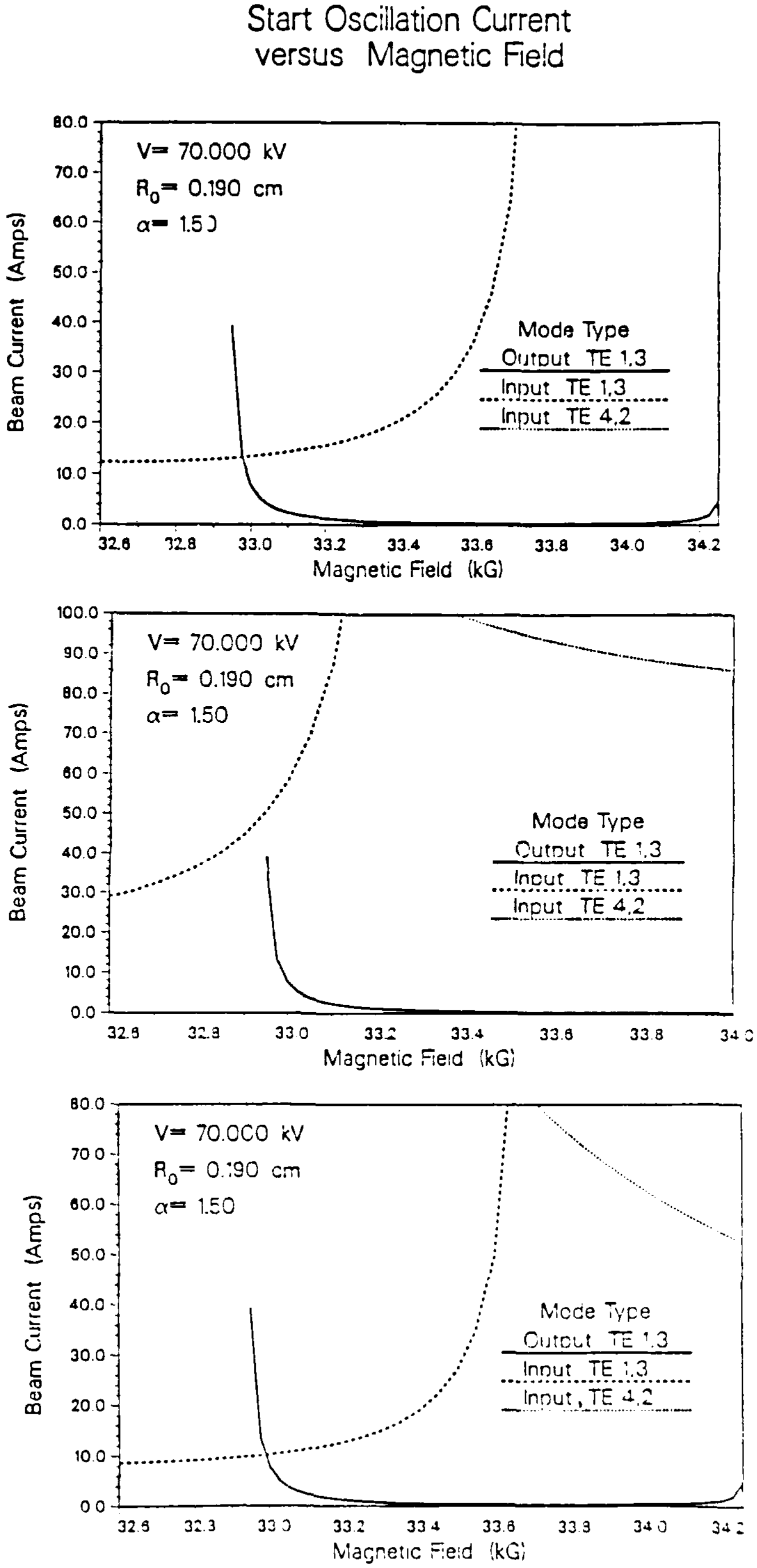

Fig. III.9. Start currents for the input cavities.

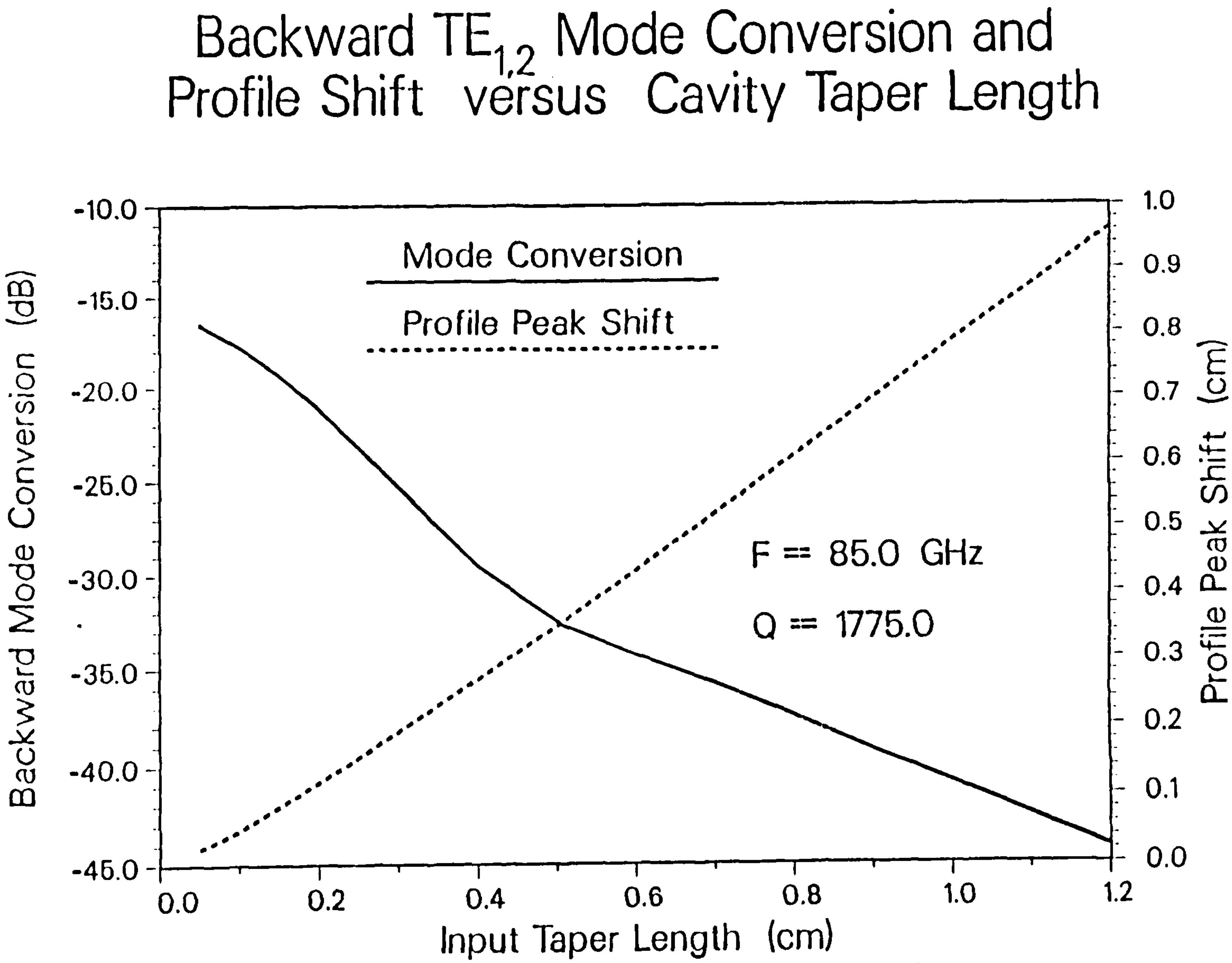

Backward $TE_{1,2}$ Mode Conversion and Profile Shift versus Cavity Taper Length

Fig. III.10. Mode conversion in oscillator cavity.

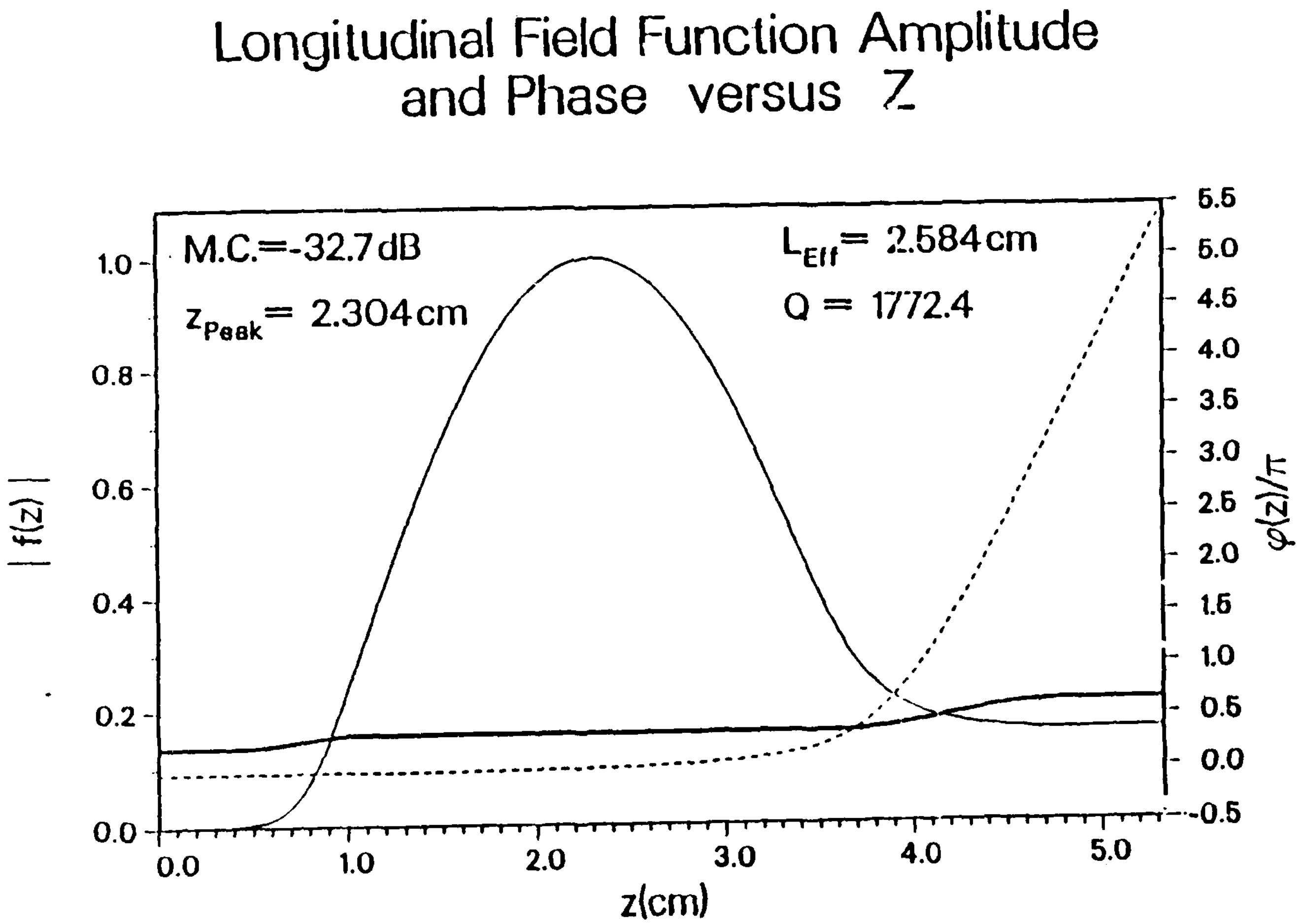
Longitudinal Field Function Amplitude and Phase versus Z

Fig. III.11. The oscillator cavity.

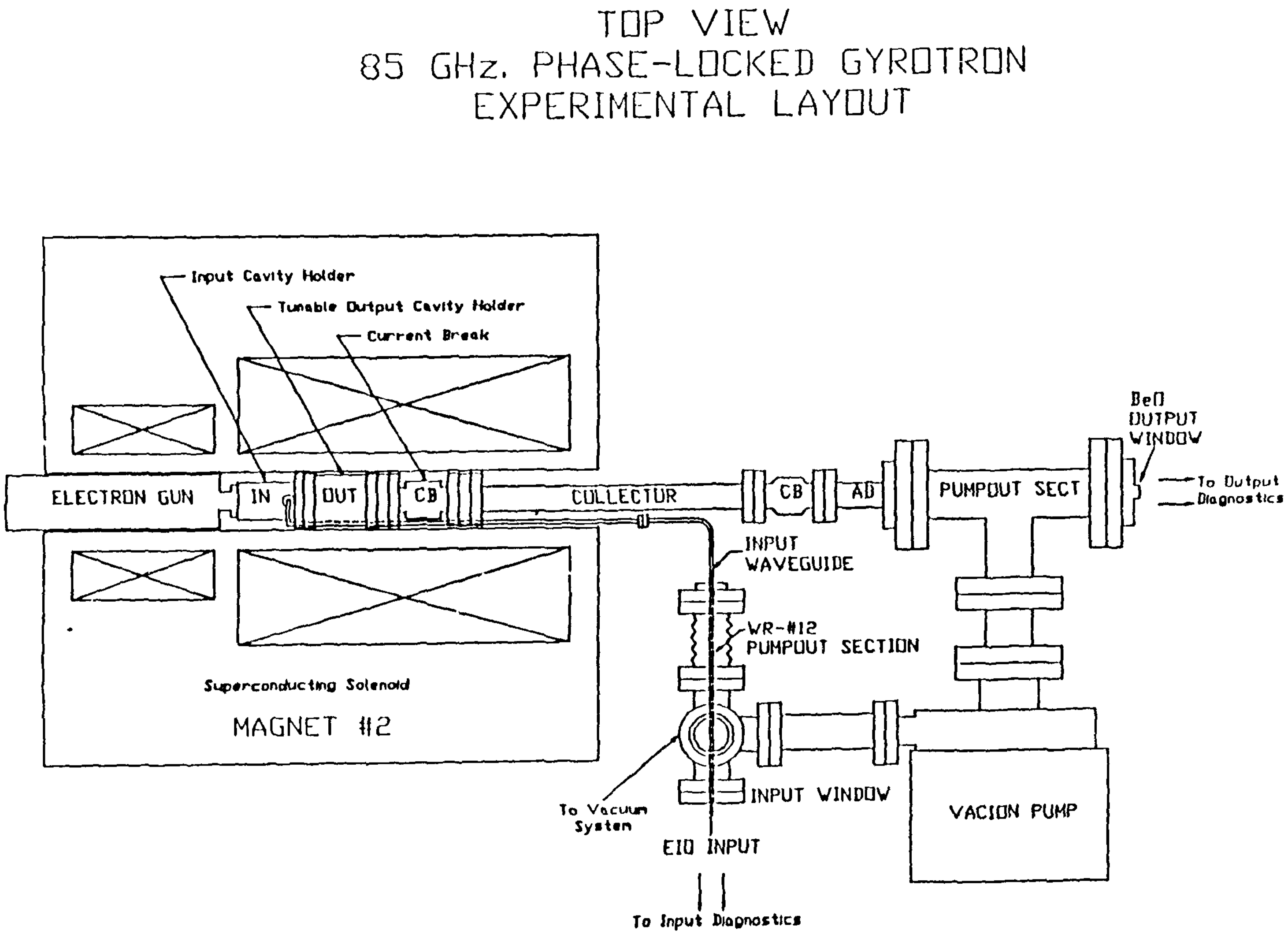

Fig. III.12. Mechanical design of the low power phase-locked oscillator.

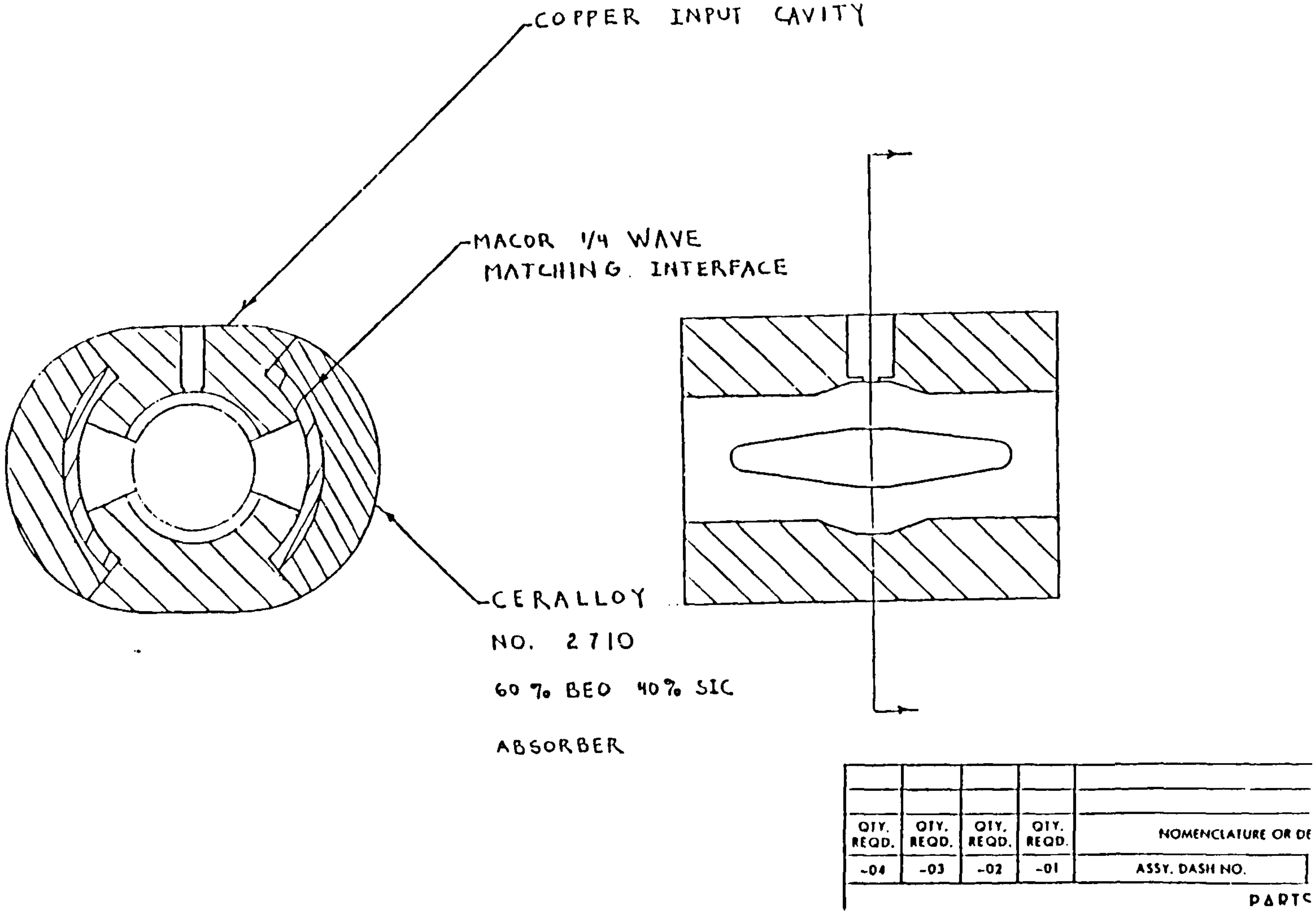

Fig. III.13. The input cavity.

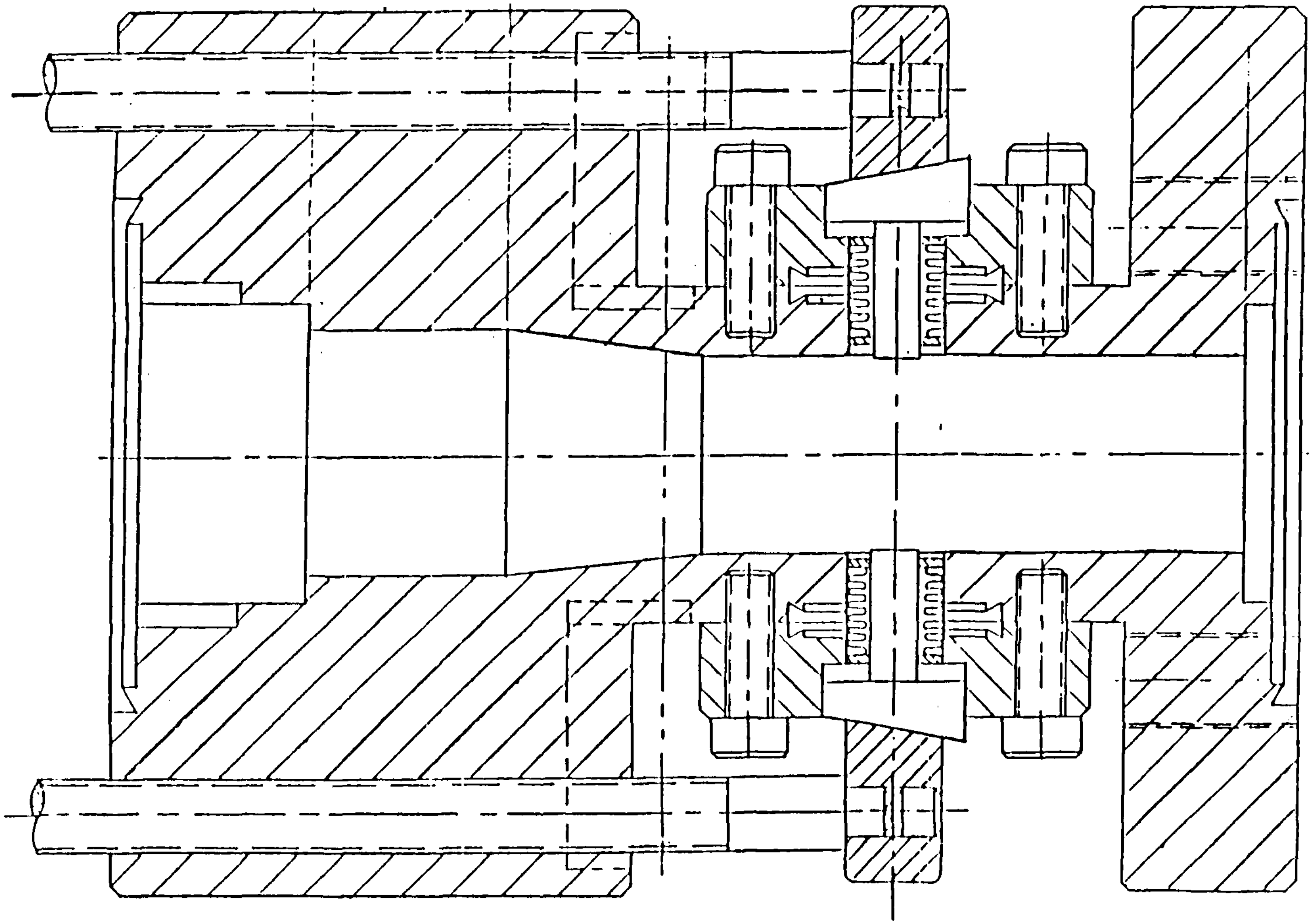

Fig. III.14. The output cavity holder.

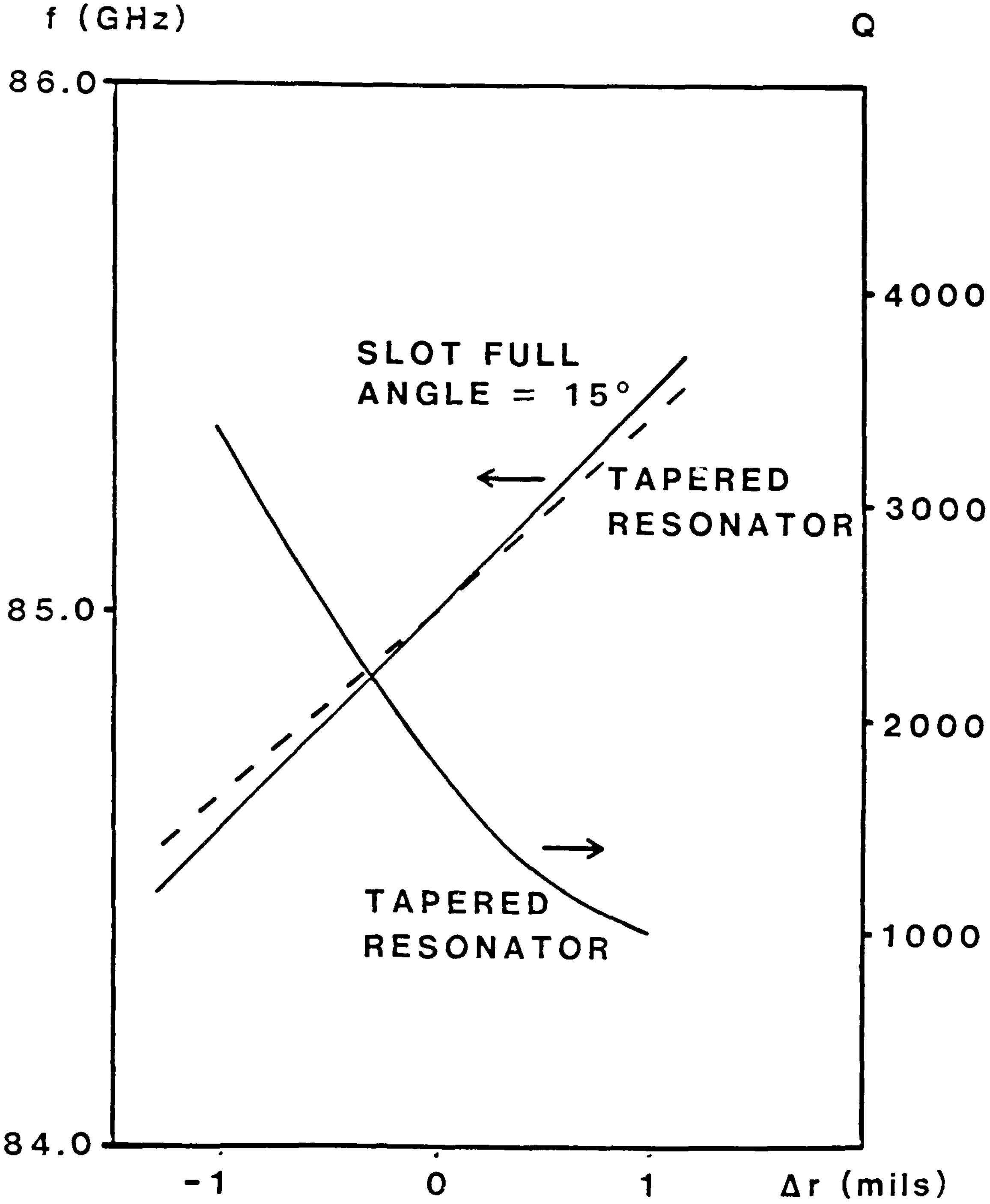

Fig. III.15. Frequency as a function of slot width and taper displacement and cavity Q for the tapered cavity.

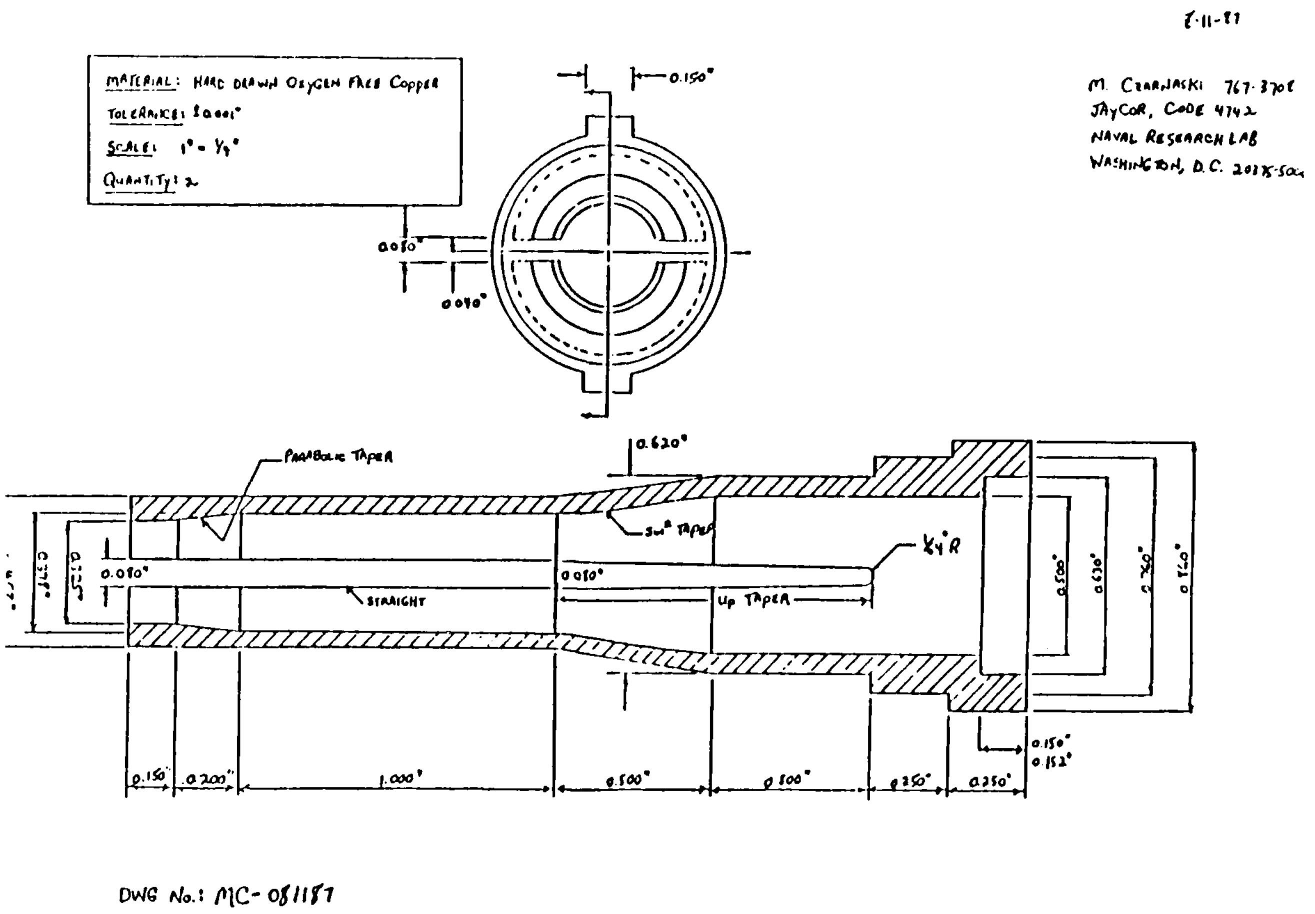

Fig. III.16. The main oscillator cavity.

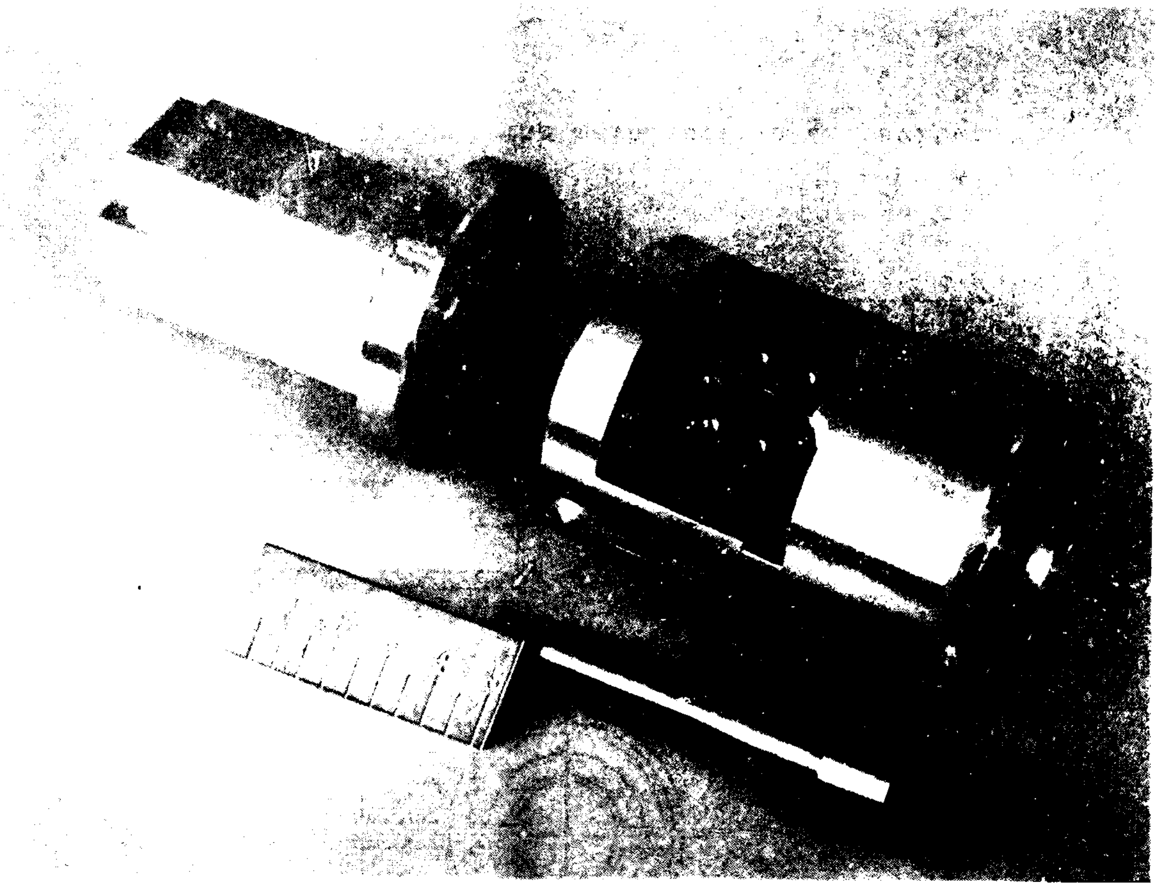

Fig. III.17. The input and output cavity holder and the main cavity.

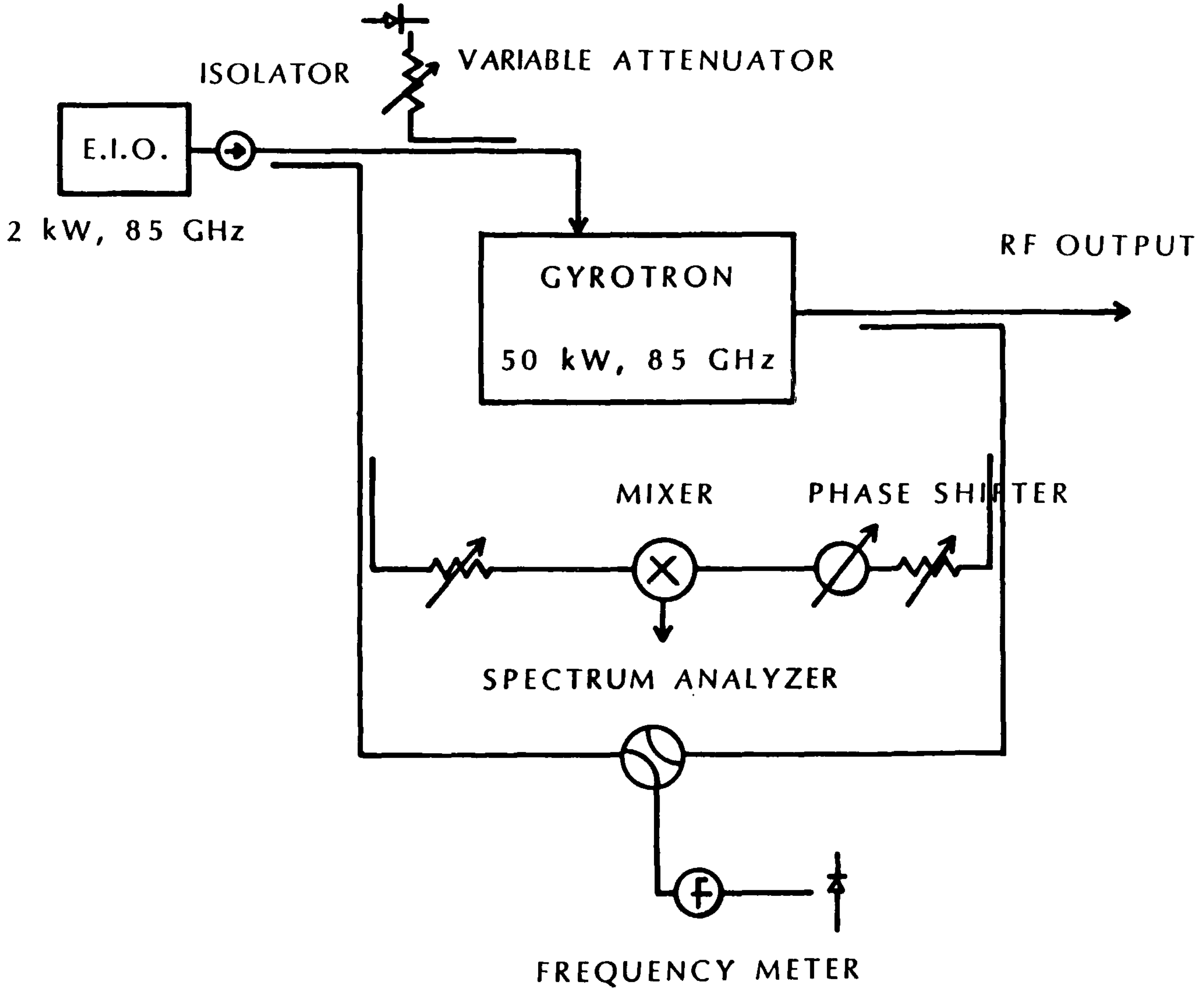

Fig. III.18. Schematic of the diagnostic set up.

IV. Febetron-Gyrotron Slotted Cavity Experiments

An experiment was carried out on the Febetron gyrotron facility to investigate TE_{13} operation at 35 GHz through use of axial wall slots in the cavity to suppress competition with "whispering-gallery" modes. An earlier experiment produced 100 MW in a circularly-polarized TE_{62} mode, and demonstrated frequency tuning over the range 28 to 49 GHz by operating in a family of TE_{m2} modes, with the azimuthal index "m" ranging from 4 to 10.[1] This experiment employed a 900 keV, 640 A electron beam, and successfully operated in the TE_{13} mode at a power level of 35 MW, using a 2.34-cm-diameter cavity with a pair of opposing 45° axial wall slots. In the absence of slots, significant mode competition was observed from the TE_{42} mode, so that stable operation in a circularly-polarized TE_{13} mode was not possible. Through use of a cavity with 33° axial wall slots, it was possible to operate in a linearly-polarized TE_{62} mode at ~48 GHz, while in the absence of slots it was straightforward to tune the interaction through the TE_{42}, TE_{52}, and TE_{62} modes. These modes were observed through a gas breakdown technique, that permitted straightforward observation of the azimuthal index of the mode as well as the presence or absence of linear polarization. The results of this research have been accepted for publication in the IEEE Trans. Plasma Sci. A copy of the manuscript is attached as Appendix 5.

References for Section IV

1. S.H. Gold, A.W. Fliflet, W.M. Manheimer, R.B. McCowan, W.M. Black, R.C. Lee, V.L. Granatstein, A.K. Kinkead, D.L. Hardesty, and M. Sucy, Phys. Fluids, vol. 30, pp. 2226-2238, 1987.

V. VEBA Gyrotron Oscillator Experiment

Two sets of gyrotron oscillator experiments have been carried out, or are currently under way, on the NRL VEBA facility. The motivation for these experiments is to pursue higher peak power through higher current, higher voltage operation than was possible on the Febetron accelerator, as well as to operate with a longer, flatter voltage pulse, in order to produce a more robust and more easily characterized output microwave pulse. Figure V.1 shows the experimental setup for the VEBA gyrotron experiments.

The first set of experiments were carried out from September to December, 1986, and produced an estimated peak power of 150 MW at 35 GHz in the TE_{62} mode, while operating at ~1.1 MeV and ~2 kA. The power estimate was produced by making measurements at the peak of the mode pattern in E_r, and assuming that the output mode pattern at the vacuum window was unchanged from the pattern observed on the TE_{62} Febetron gyrotron experiments. Before a definitive set of measurements could be completed, the VEBA facility became inoperable due to required maintenance that was estimate to take two months to complete. At that time, experimental effort was transferred back to the Febetron facility for the TE_{13} experiments discussed in Section IV.

The second set of experiments began in June 1987 and are still ongoing. Dr. Gold originally attempted to carry out these experiments in parallel with preparing the three-cavity phase-locking experiment, but since the latter experiment had the highest priority, this experiment could not be operated very frequently. Initial results were very disappointing, since the power appeared to have fallen by a factor of 4 from the earlier VEBA gyrotron experiment. In October, Dr. Murray Black was asked to begin operating this experiment, and the results soon improved substantially, returning first to approximately the same point as the first VEBA gyrotron run, at which point a complete scan of the mode in E_r and E_θ across the output window radius was taken. The approximate beam position and a map of the radial dependence of the coupling coefficients to the $TE_{\pm 6\,2}$ and $TE_{\pm 10,1}$ modes is shown in Fig. V.2. Principal coupling should be to the $TE_{-6\,2}$ mode, as was the case in the Febetron-gyrotron experiments employing 1.6-cm-radius cavities. Figure V.3 shows a set of typical experimental traces from the gyrotron. The radial scan demonstrated 115 MW at 35 GHz, with a somewhat scrambled mode pattern (see Fig. V.4). This may be compared to the predicted $TE_{6\,2}$ mode pattern in Fig. V.5. Clearly, substantial mode conversion has taken place, and additionally, based on the observed mode pattern, the possibility of coupling to the $TE_{10,1}$ mode cannot be ruled out. Subsequently, measurements performed at the radial peak of the mode pattern demonstrated a further factor of two increase to an estimated 225 MW. A calculation was performed of the mode conversion process in the 5° cavity output taper, the 10-cm-diameter output waveguide, and the 4.77° output taper ending the the 30-cm-diameter vacuum window (see Fig. V.6). This calculation suggests that substantial mode conversion should take place with only ~45% remaining content in the original TE_{62} mode, and substantial TE_{61} and TE_{63} mode energy present. The additional power near the wall could be explained by TE_{61} mode content, generated by mode conversion from an operating TE_{62} mode. For diagnostic purposes, a smaller horn combined with an attenuating output window, such as was used in the Febetron-gyrotron experiment, would reduce the mode conversion and improve the measured mode pattern. However, if air breakdown on the output window is to be avoided, there is no easy alternative to a very large output window when the full power is to be extracted into air.

In order to investigate the effect of improved beam quality on the gyrotron operation, and to eliminate the unknown space charge effects present in the original experiment, in which a substantial fraction of the diode current is reflected before reaching the gyrotron cavity and may cause space charge problems before being collected on the drift tube wall, a new diode was designed in which an annular beam is extracted through an anode scraper plate. Figure V.7 contains a schematic diagram of the new cathode and anode. In this configuration, the current will be controlled, and the beam quality should be improved, since emission will occur from the face of the cathode and be along the axial magnetic field, rather than from the edge of the cathode at some average angle to the axial magnetic field. Furthermore, any reflected current should be collected on the back of the scraper plate. By improving the beam quality, it should be possible to operate the experiment at higher average α, thus improving its performance. This is because the "pump" magnet has the effect of greatly magnifying the original velocity spread on the beam, and because adiabatic compression is always reflecting the highest α particles. The new diode should permit some combination of higher current and/or higher average α than has been possible in the foilless configuration used up to this point, which should result in improved gyrotron operation.

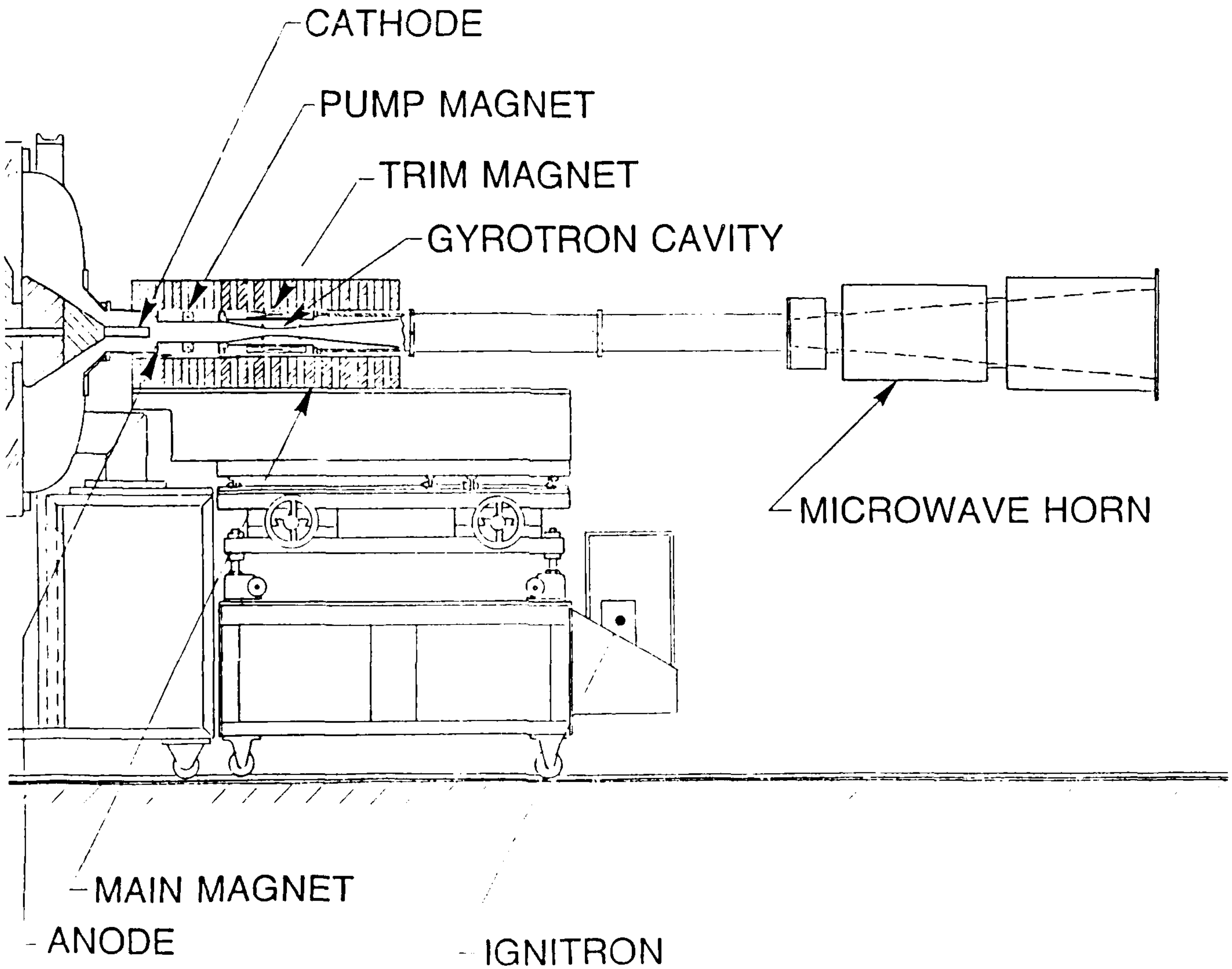

Fig. V.1. Experimental setup for the VEBA gyrotron experiments.

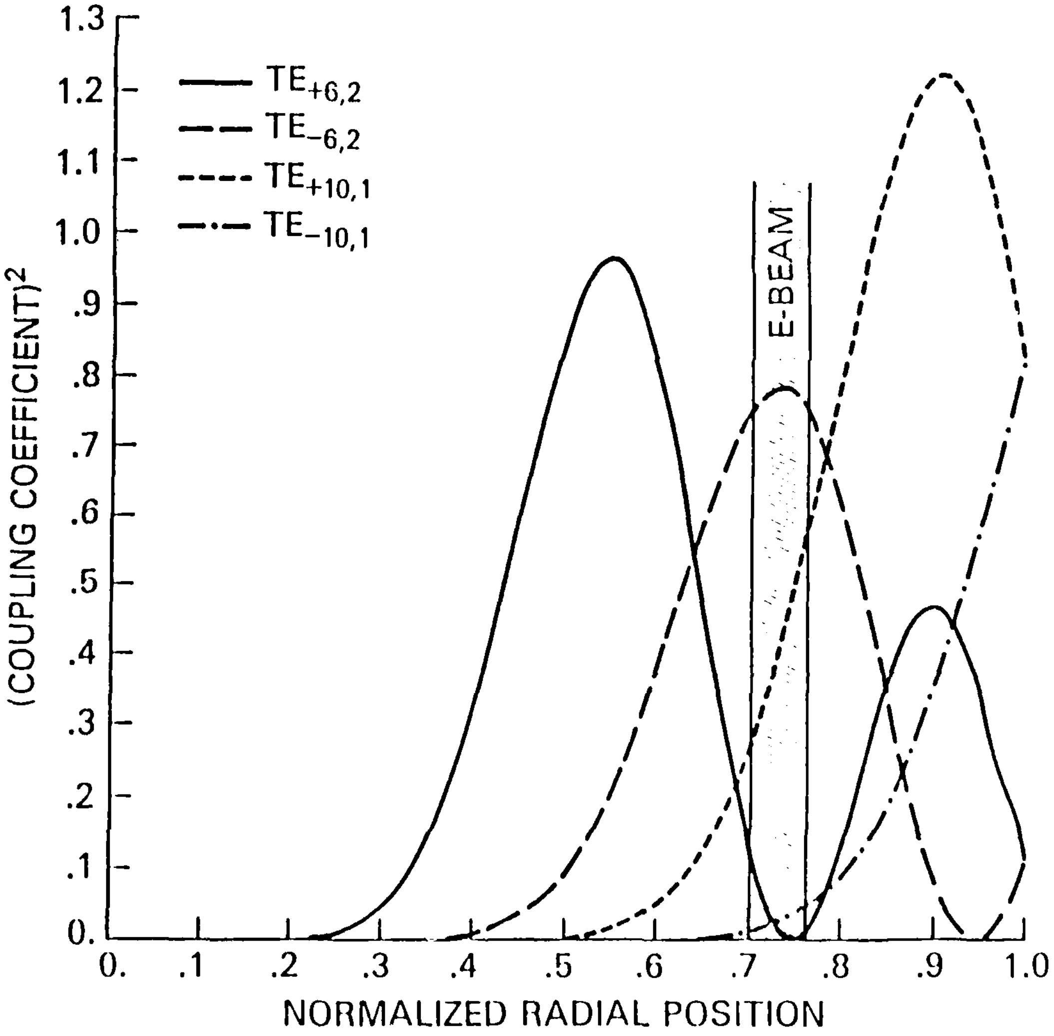

Fig. V.2. Normalized electron beam radius in the gyrotron cavity and radial dependence of gyrotron coupling coefficients for the TE$_{\pm 6\,2}$ and TE$_{\pm 10,1}$ modes.

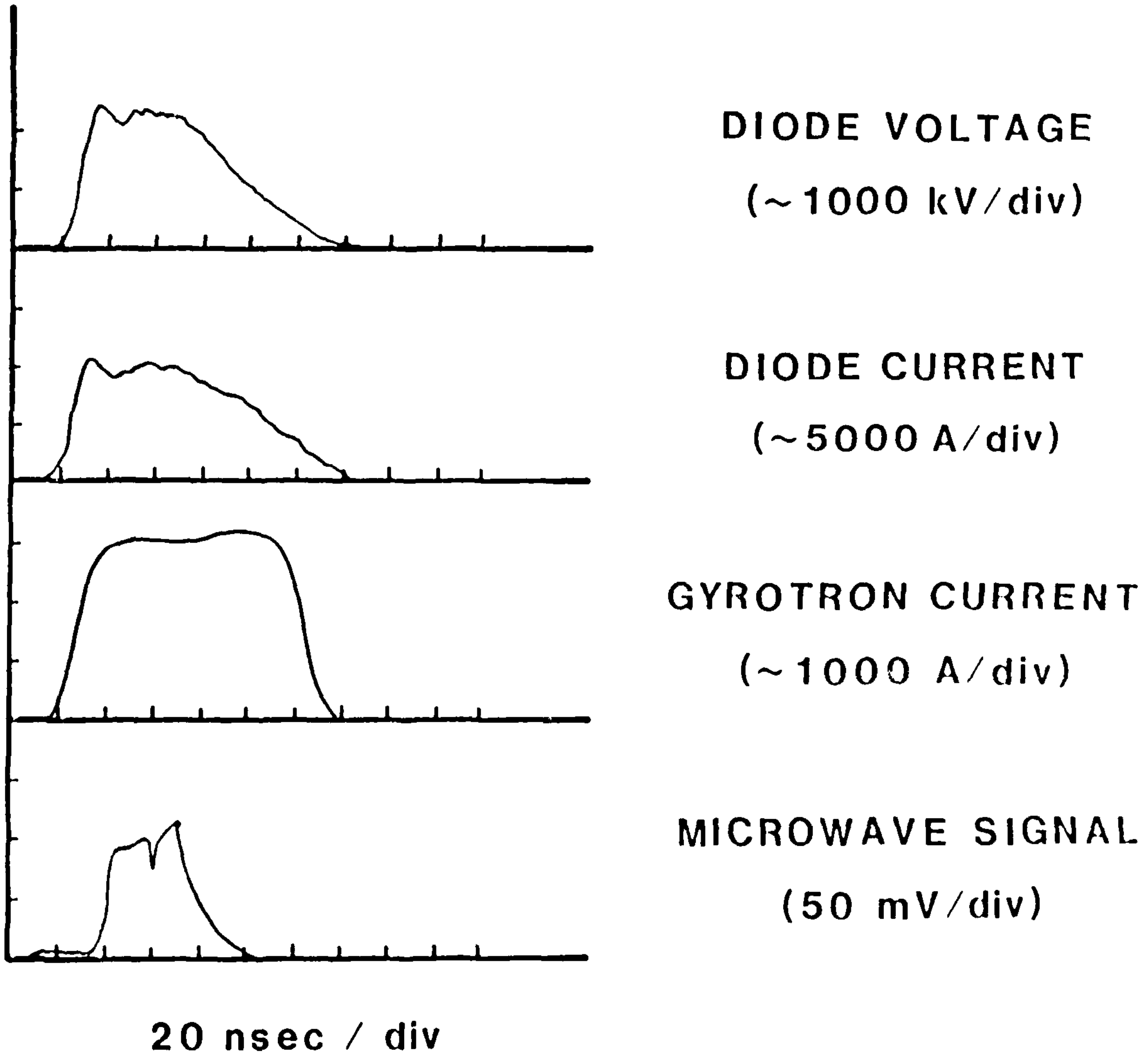

Fig. V.3. Typical experimental waveforms for diode voltage and current, gyrotron current, and microwave signal.

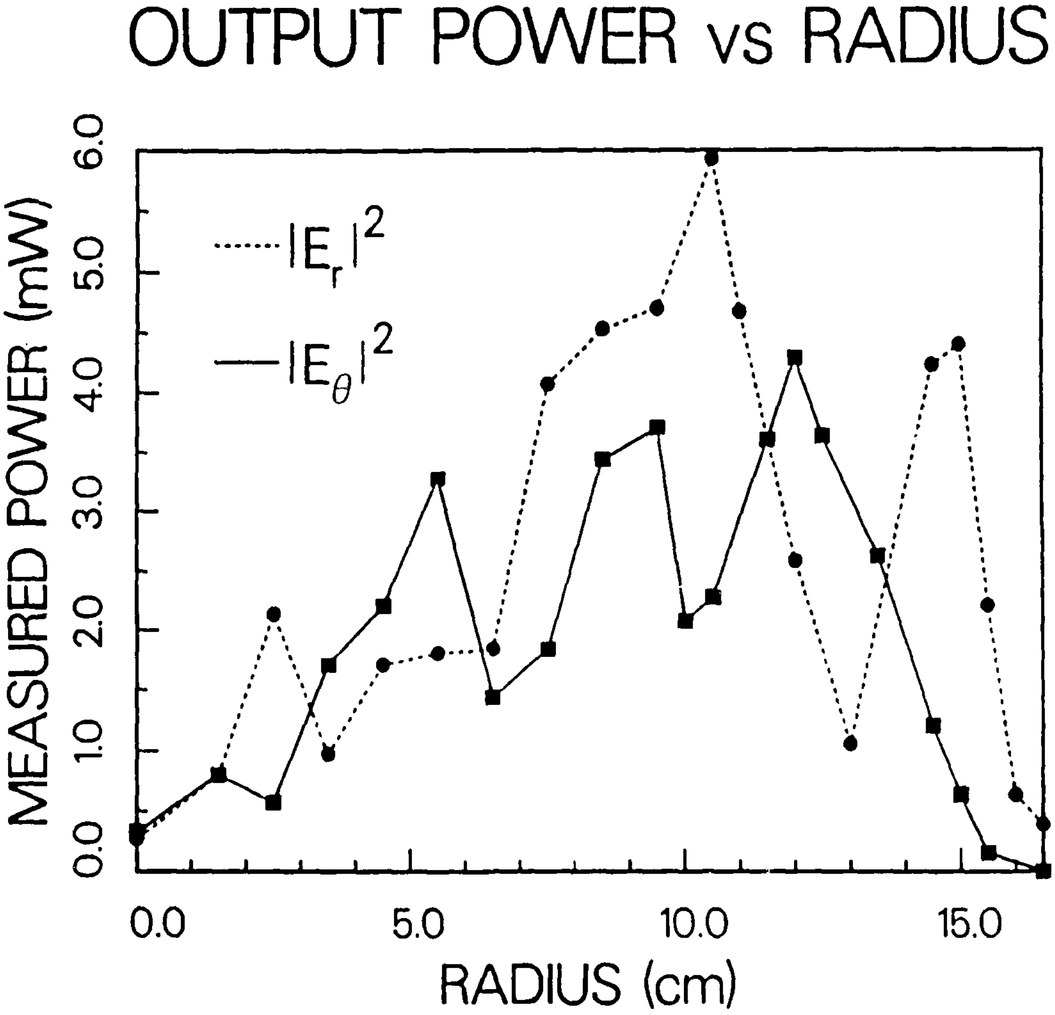

Fig. V.4. Measured output power vs radius across the 30-cm-diameter experimental output window.

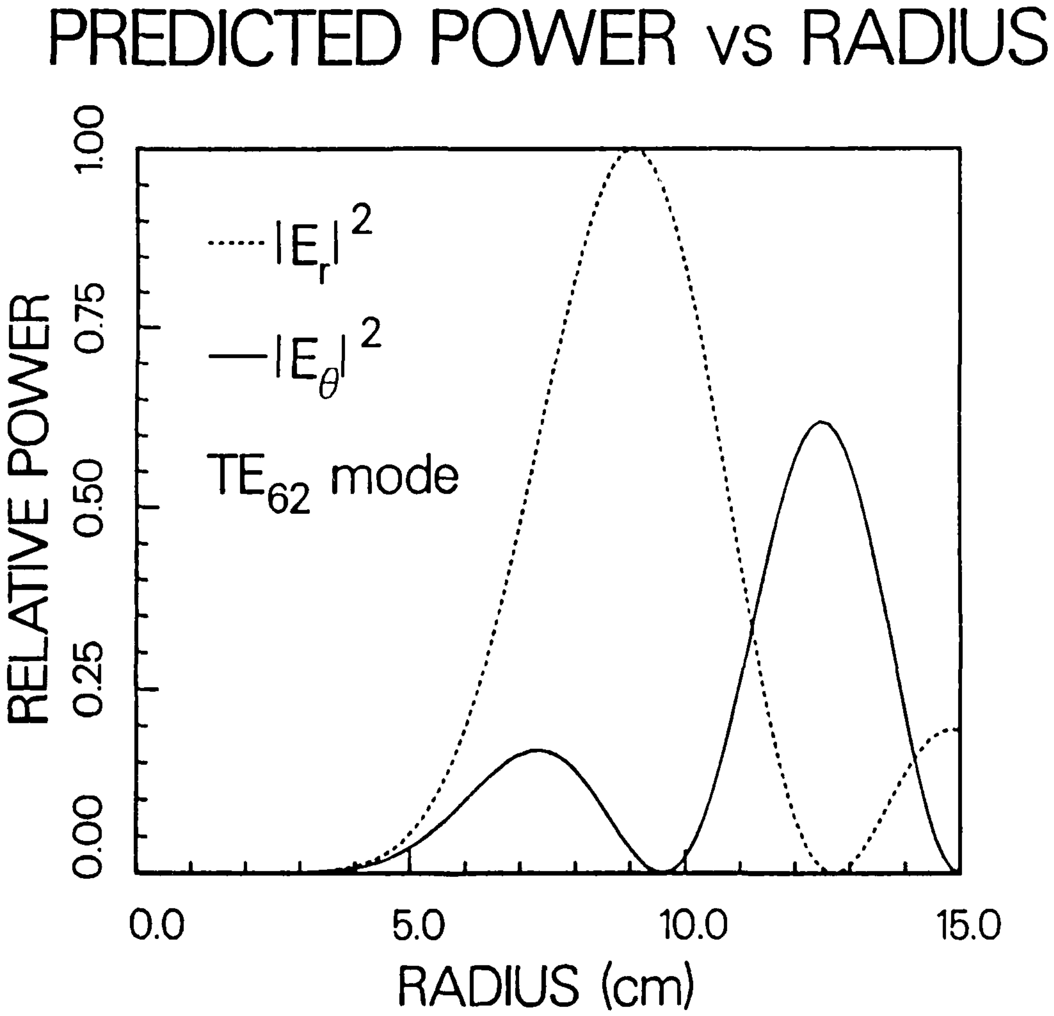

Fig. V.5. Predicted output power vs radius for the TE_{62} mode.

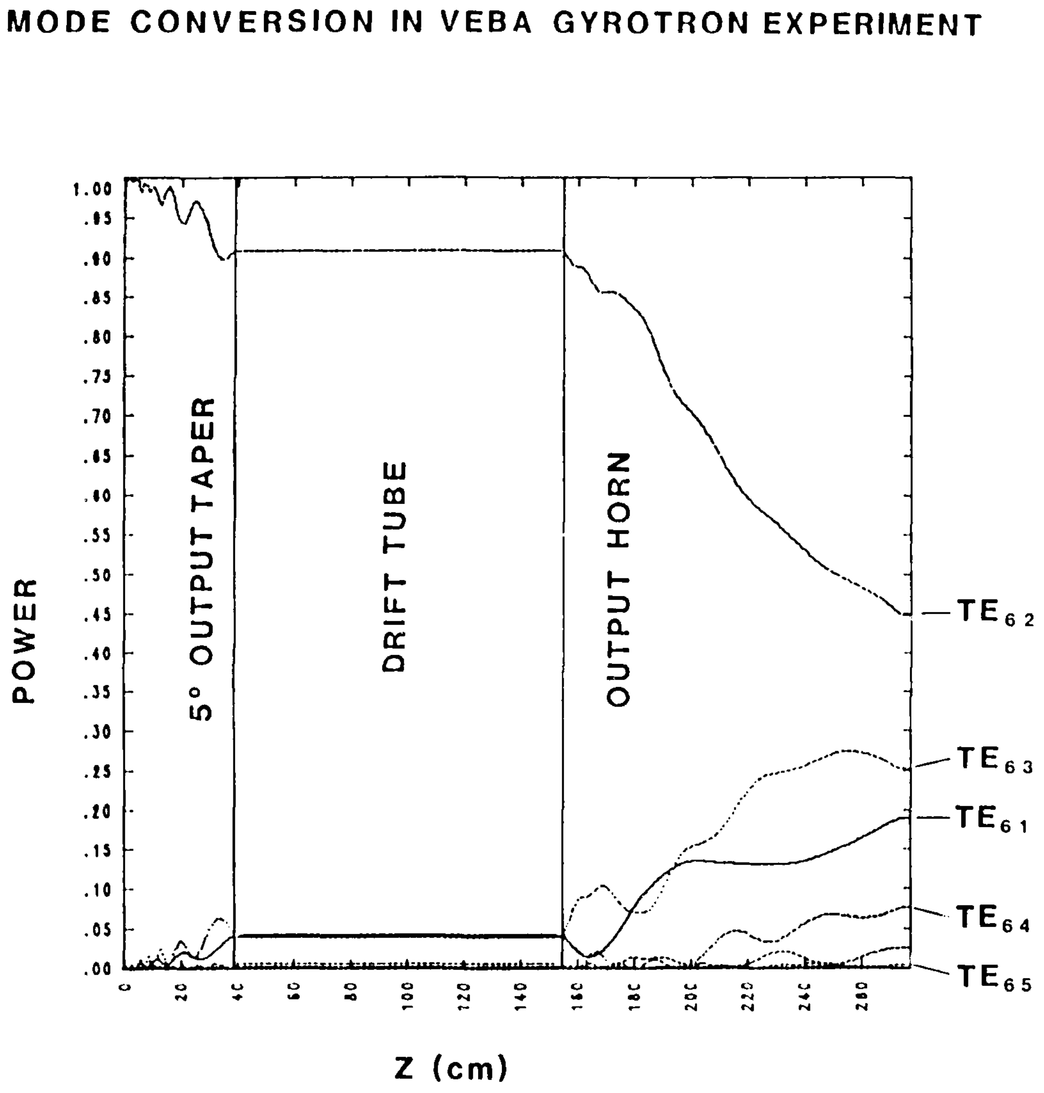

Fig. V.6. Calculated mode conversion as a function of distance along the experimental output taper, drift tube, and microwave horn.

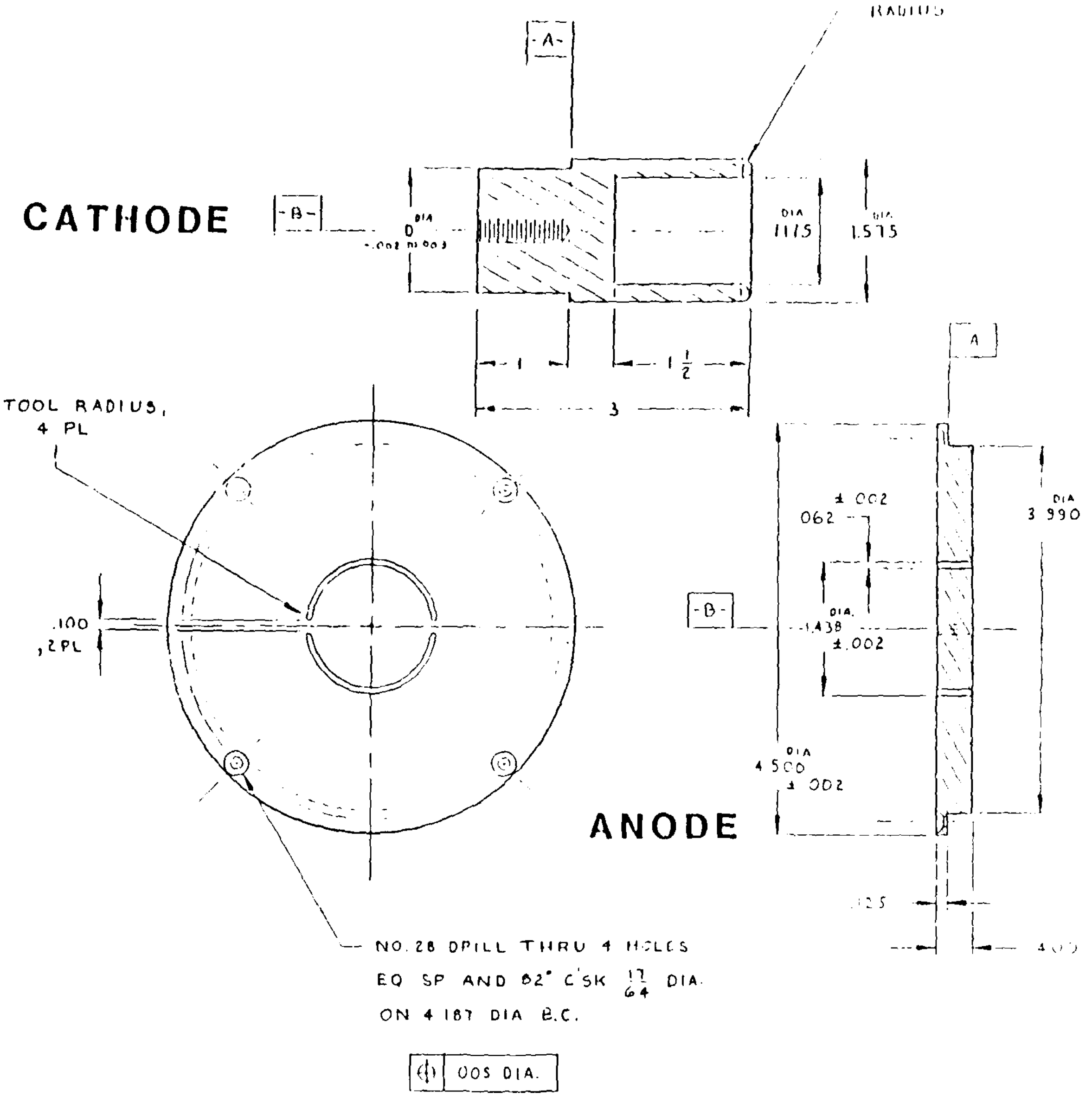

Fig. V.7. Mechanical drawing of new beam scraper cathode and anode for the VEBA gyrotron experiment.

VI. Three-Cavity Phase-Locked Gyrotron Circuit Design

This section describes the circuit design for an experimental high power, phase-locked gyrotron oscillator. The drive power is provided by a 35 GHz, 20 kW magnetron. The expected output power is in the range of 1-10 MW. The experiment is intended to serve as a testbed for the development of ultrahigh power (~ GW) pulsed gyrotron oscillators. It should allow the investigation of important elements of the design of these devices and of the diagnostics required for demonstrating phase-locked operation under short pulse, low rep-rate conditions.

A schematic of the experimental configuration is shown in Figure VI.1. A solid 1 MeV, ~ 100 Amp electron beam is produced by the NRL VEBA pulseline accelerator (voltage flattop pulselength ~ 30 nsec). The beam will be produced by a modified version of the VEBA diode previously used to produce a high quality beam for millimeter wavelength FEL experiments. The required beam transverse momentum (free energy source for CRM) is produced initially by a bifilar helix wiggler and then increased to a final momentum pitch ratio $\alpha = 0.75$ by adiabatic compression of the magnetic field. The locking signal from the magnetron is introduced via a prebunching cavity. A second (passive) bunching cavity is used to increase the locking frequency bandwidth obtainable with a given locking power. The bunching cavities are designed to operate in the fundamental TE_{111} cylindrical cavity mode. The use of this mode simplifies the problems of spurious mode excitation and cavity crosstalk. These problems are much more difficult when overmoded bunching cavities are used. Such cavities will be needed in GW power level devices and the study of their design is the objective of the NRL 85 GHz phase-locked gyrotron experiment. The bunching cavities include two axial slots to control the cavity Q factor and suppress competing modes. The output cavity operates in the TE_{121} mode since this mode is better matched to 10 MW level output power than the fundamental mode. The output cavity is also slotted to reduce competing mode excitation.

The design strategy for a multi-cavity gyrotron oscillator is similar to the design of a gyroklystron amplifier except that the output cavity is allowed to self-oscillate. As shown by Tran et al,[1] this regime leads to higher optimized efficiency than can be achieved in the amplifier regime. For given beam parameters and RF mode, the output cavity is essentially characterized by its effective interaction length (L, or μ in normalized units [see Section II]) and Q factor. The interaction length for optimum oscillator efficiency corresponds to $\mu \sim 6-12$ in the high power regime. Maximum output power and frequency bandwidth are obtained by using low Q ~ 200-500. In their investigation of gyroklystron design optimization Ganguly and Chu[2] define a phase parameter $\Phi \equiv \mu\Delta - \pi$, where Δ is the gyrotron resonance detuning parameter defined in Section II. The parameter Φ represents the phase slippage of a beam electron relative to the RF field due to kinematic effects. High efficiency is obtained by choosing $\Phi \sim \pi - 2\pi$ for the output cavity. The bunching process is most efficient when $\Phi \lesssim 0$ for the bunching cavity. The detuning parameter Δ is usually the same for both cavities and for high output cavity efficiency $\Delta \sim 1$. These conditions can be satisfied by keeping the bunching cavity short, i.e., $\mu_B \sim 2-3$.

The electron beam produced by a pulseline accelerator is characterized by voltage ripple and shot-to-shot variation which affect the resonance detuning of the interaction. For this reason it was considered highly desirable for the bunching cavities to be stable for all magnetic fields or detuning parameters. This requires that the cavity have a short interaction length and a low Q factor. Using a low Q factor also increases the bunching cavity bandwidth which ultimately limits the phase-locking bandwidth, but it decreases the bunching fields, and, hence, the beam bunching parameter q, for a given drive power. The bunching parameter and locking frequency bandwidth can be enhanced by adding a second (passive) bunching cavity as discussed below.

The design parameters of the bunching and power cavities were obtained in two steps. First, possible design configurations were obtained based on idealized cylindrical cavities with sinusoidal RF field profiles. This led to preliminary cavity lengths and Q factors and allowed the investigation of possible competing modes. Next, realistic RF field profiles were calculated numerically for actual cavity wall dimensions and the device operating parameters were recalculated. A small signal-signal threshold current code for cylindrical gyrotron cavities, developed by Chu,[3] was used to investigate possible competing modes. Figure VI.2 shows a scan of Q × threshold beam power [QP_{thr}] versus magnetic field for the TE_{111} mode (heavy line) in the prebunching cavity and for possible competing modes. The calculations assume $L/\lambda=2$ and $\alpha=0.75$. The narrow bandwidth competing modes, such as mode 5, correspond to higher harmonic interactions ($\omega \simeq 2\Omega$, etc.), and the broader bandwidth curves, such as mode 1, correspond to higher order axial modes interacting at the fundamental. The horizontal line labelled Q=200 denotes the e-beam power. Thus the cavity should be stable if its $Q \leq 200$ for all modes. This can be obtained using axial slots which can be used to reduce competing mode Q factors to values below the operating mode Q. In the present design axial slots are also used to control the Q of the operating mode. The design calculations for the cavity slots and locking signal input coupler are described in Section VII. The calculations shown in Figure VI.2 assume circular polarization. For linear polarization - to be used in the experiment - the coupling is reduced by 50% so that the starting currents are increased by a factor of 2.

A major design constraint for a fundamental mode, solid beam gyroklystron is the need to maintain adequate cavity isolation while providing sufficient clearance in the drift sections to propagate the beam. In the present case the ratio of drift tube radius to cavity wall radius $r_d/r_c=0.8$. This means that the cavity RF fields are only weakly cut-off in the drift tube and evanescent fringe fields extend well into the drift tube. This effect leads to an axial RF field profile which can be accurately modelled by a gaussian function. The axial RF field profile corresponding to particular cavity dimensions was obtained numerically using a computer code based on the theory developed in Ref. 4 modified for evanescent boundary conditions at each end of the cavity. This profile was then used in an electron trajectory integration code[5] to determine the oscillation threshold current as a function of magnetic field. The length of the cavity section above-cut-off section was varied to obtain a value for which the threshold current is greater than the beam current. In this way a cavity design having a minimum cold beam threshold current of 150 Amps and a normalized length $\mu=1.9$ for $\alpha=0.75$ was obtained. The cavity wall and RF field profiles for this design are shown in Figure VI.3. As discussed in Section VII, the cavity axial slot angle is chosen to give a cold-cavity Q factor of 200. Taking into account insertion losses, the power coupled into the interacting mode is assumed to be 5 kW. This leads to a normalized field amplitude $F_1=0.03$ in the first bunching cavity.

The primary consideration in choosing the drift tube length between cavities was providing adequate cavity isolation. It was considered prudent to keep the drift length short to minimize the deleterious effects of beam velocity spread. An effective drift tube length of $\mu_d=3$ was chosen. Actually, the boundary between the end of the cavity and the beginning of the drift is not well defined due to the strong fringe fields, however, this was taken into account in the calculations. The detuning parameter for a typical magnetic field of 32.5 kG is $\Delta=0.83$. The bunching parameter for these parameters can be calculated using Eq.(41) of Section II. The result is q=0.40.

The length of the output cavity is chosen to be $L=4.5\lambda$ or $\mu=6$. A longer cavity would give somewhat higher efficiency but would shift the optimum operating point to higher magnetic fields for which the bunching cavity is less effective. A short cavity also facilitates high power operation. An output Q factor of Q~400 was obtained by using a 5° output taper. The numerically computed axial cavity profile for the output cavity is shown in Figure VI.4. A scan of QP_{thr} vs. magnetic field is shown in Figure VI.5 for the TE_{121} mode (heavy line) and for competing modes (numbered lines). The calculation assumes $L/\lambda=4.5$ and a sinusoidal profile. The horizontal line shows the beam power for Q=400 which is well above the oscillation threshold. In this cavity the slot angle is chosen such that the axial slots have minimal effect on the TE_{121} mode while effectively suppressing competing modes. The numerically calculated threshold current vs. magnetic field curves based on realistic RF field profiles for the bunching and output cavities are shown in Figure VI.6. Figure VI.7 shows output from a steady-state nonlinear efficiency code[5] for the output cavity as a free-running oscillator (FRO). The optimum efficiency of 16%. The calculation was carried out for circular mode polarization. For linear polarization - as in the experiment - the efficiencies are the same except the beam current is multiplied by two. Thus for linear polarization the calculated FRO output power at optimum efficiency is 16 MW.

The locking frequency bandwidth of the device can be estimated using the theory developed in Section II. For a magnetic field of 32.5 kG Δ=0.83 and the FRO efficiency is 13.3%. The normalized beam current for the output cavity $I_{G3}=0.26$ and the normalized FRO RF field amplitude is $F_{o3}=0.38$. Substituting these parameters into Eq.(39) of Section II leads to the following bandwidth estimate: $|\Delta\omega|/\omega_o < 1.7\text{x}10^{-3} J_1(q)$, which is based on linear perturbation theory. The maximum value of the Bessel function $J_1=0.58$ occurs for $q=1.83$. Thus an upper limit for the bandwith at this magnetic field is 0.1% or 35 MHz based on this theory. As discussed in Section II, the bandwidth is an increasing function of the magnetic field. Some increase in bandwidth could therefore be achieved by increasing the magnetic field at the cost of somewhat reduced efficiency.

Moreover, nonlinear bandwidth calculations not based on perturbation theory tend to give larger bandwith estimates.

The estimate of maximum bandwidth obtained above assumes a bunching parameter of 1.8. This is a factor of 4.5 greater than can be achieved with a single bunching cavity using the available drive power since in this case, as discussed above, $q=0.4$. The bunching parameter can be increased considerably by adding a second bunching cavity. The principle is the same as for conventional klystrons: The ac current induced on the beam by the RF fields in the first cavity induce much stronger fields in the second cavity. These fields in turn enhance the bunching of the beam. As shown in Ref. 1, small-signal gyroklystron theory can be used to calculate the induced field F_2 in the second cavity:

$$F_2 = \sqrt{\pi}\, I_{G2}\, \mu_2\, e^{-x_2^2}\, J_1(q_2)/\sqrt{1+\delta^2} \qquad (1)$$

where $x_2=\mu_2\Delta/4$, $\delta=2Q(\omega_o-\omega_{cc})/\omega_o$ and q_2 is the bunching parameter at the input to the second cavity. The frequency ω_o is the locking signal frequency and ω_{cc} is the cold cavity resonant frequency. Since the bunching cavities are identical in the present design $I_{G2}=I_{G1}=1.1$ and $\mu_2=\mu_1=1.9$. Substituting these quantities into Eq.(1) yields $F_2\lesssim 0.33$ which is a factor of 11 higher than F_1. This analysis is supported by simulations using the STS time-dependent code. Figure VI.8 shows output from STS time-dependent code for the amplitude of the second bunching cavity field induced by beam bunching in the first cavity. The magnetic field for this run was 31 kG. The normalized amplitude increases to about F_2=0.54 in about 5 nsec. Since F_1=0.03 for the applied field in the second cavity, the field enhancement factor is about 18 in this case. Use of Eq.(41) of Section II leads to an order of magnitude increase in the bunching parameter due to the presence of the second bunching cavity. Thus the bandwidth estimate calculated in the preceding paragraph should be achievable using a second bunching cavity.

The analytical results for the locking frequency bandwidth are supported by simulations using the time-dependent STS code described in Section II. Code results not based on perturbation theory are shown in Figures VI.9-VI.11 for the output cavity driven by a beam with q=2.0. The normalized locking frequency shift is 0.1 percent and the magnetic field is 32.5 kG. The efficiency of the driven oscillator is 14.3 percent and phase-locked operation is achieved within 20 nsec. Figures VI.9, VI.10, and VI.11 show the time evolution of the driven oscillator efficiency, frequency shift, and phase, respectively.

In summary, a circuit design has been obtained for a phase-locked intense-beam gyrotron oscillator with a locking frequency bandwidth of ~0.1%. The effective gain of output power to the locking power needed to achieve this bandwidth is about 28 dB. The bunching cavities are expected to be stable for all operating magnetic fields and to have adequate RF isolation (~50 dB). The time to achieve phase-locked operation is about 20 nsec which is compatible with the 30 nsec flat top of the VEBA voltage pulse.

References for Section VI

1. T.M. Tran, B.G. Danly, K.E. Kreischer, J.B. Schutkeker, and R.J. Temkin, "Optimization of gyroklystron efficiency," Phys. Fluids <u>29</u>, 1274-1281 (1986).
2. A.K. Ganguly and K.R. CHu, "Analysis of two-cavity gyroklystron", Int. J. Elect. <u>51</u>, 503-520 (1981).
3. K.R. Chu, "Theory of electron cyclotron maser interaction in a cavity at the harmonic frequencies," Phys. Fluids <u>21</u>, 2354, (1978).
4. A.W. Fliflet and M.E. Read, "Use of weakly irregular waveguide theory to calculate eigenfrequencies, Q values, and RF field functions for gyrotron oscillators", Int. J. Electronics <u>51</u>, 475-484 (1981).
5. A.W. Fliflet, "Scaling calculations for a relativistic gyrotron," NRL Memorandum Report 5598 (1985).

NRL 35 GHz MULTI-CAVITY PHASE-LOCKED GYROTRON

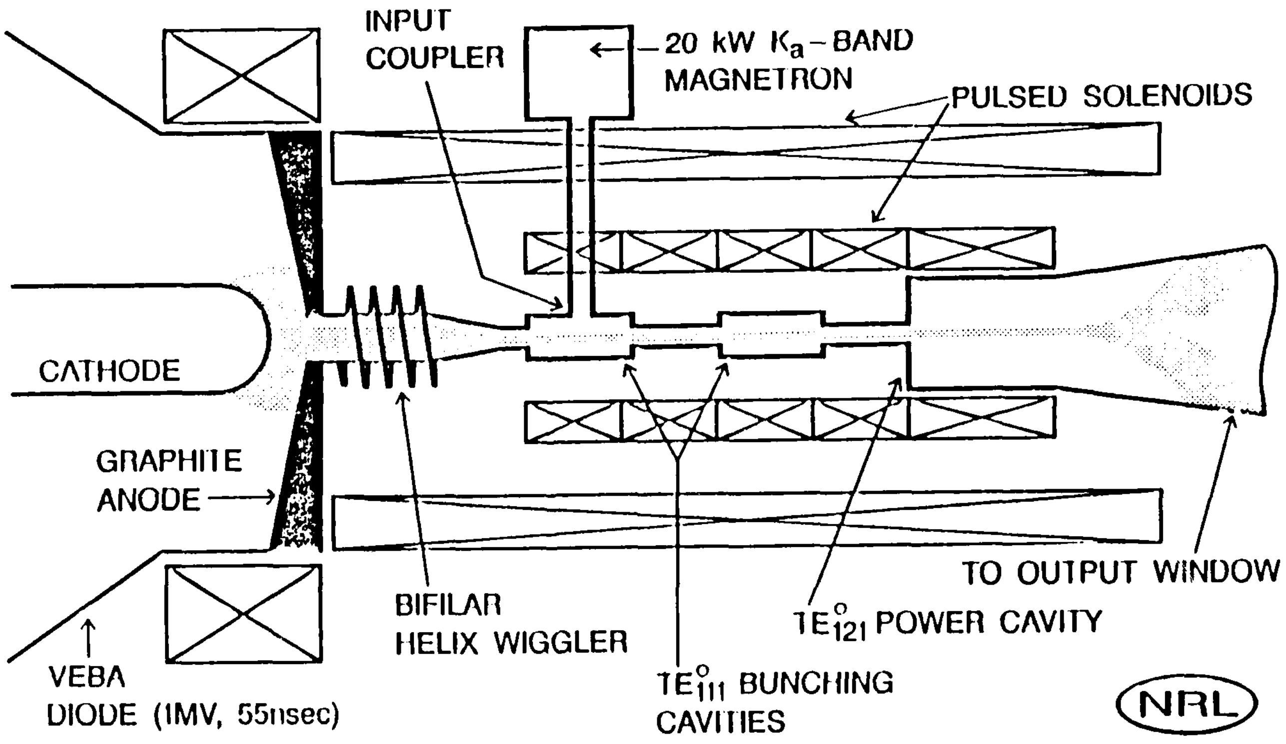

Figure VI.1. Schematic of three-cavity phase-locked gyrotron experiment.

BUNCHING CAVITY COMPETING MODE SCAN

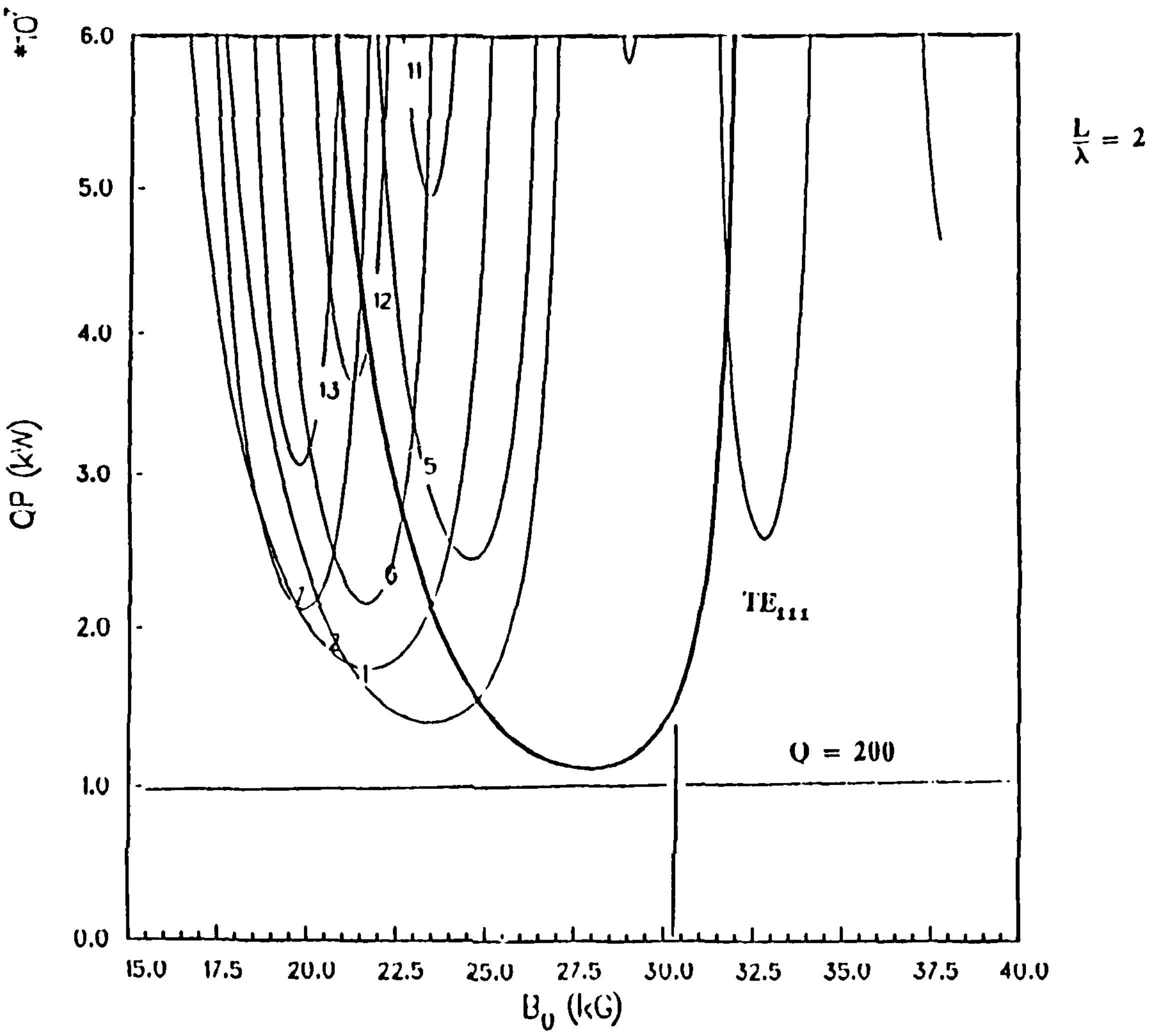

Figure VI.2. Scan of Q × threshold beam power versus magnetic field for the TE_{111} mode (heavy line) and competing modes (numbered lines) in the bunching cavity. The calculations assume a sinusoidal axial RF field profile with $L/\lambda=2$, circular polarization and $\alpha=0.75$.

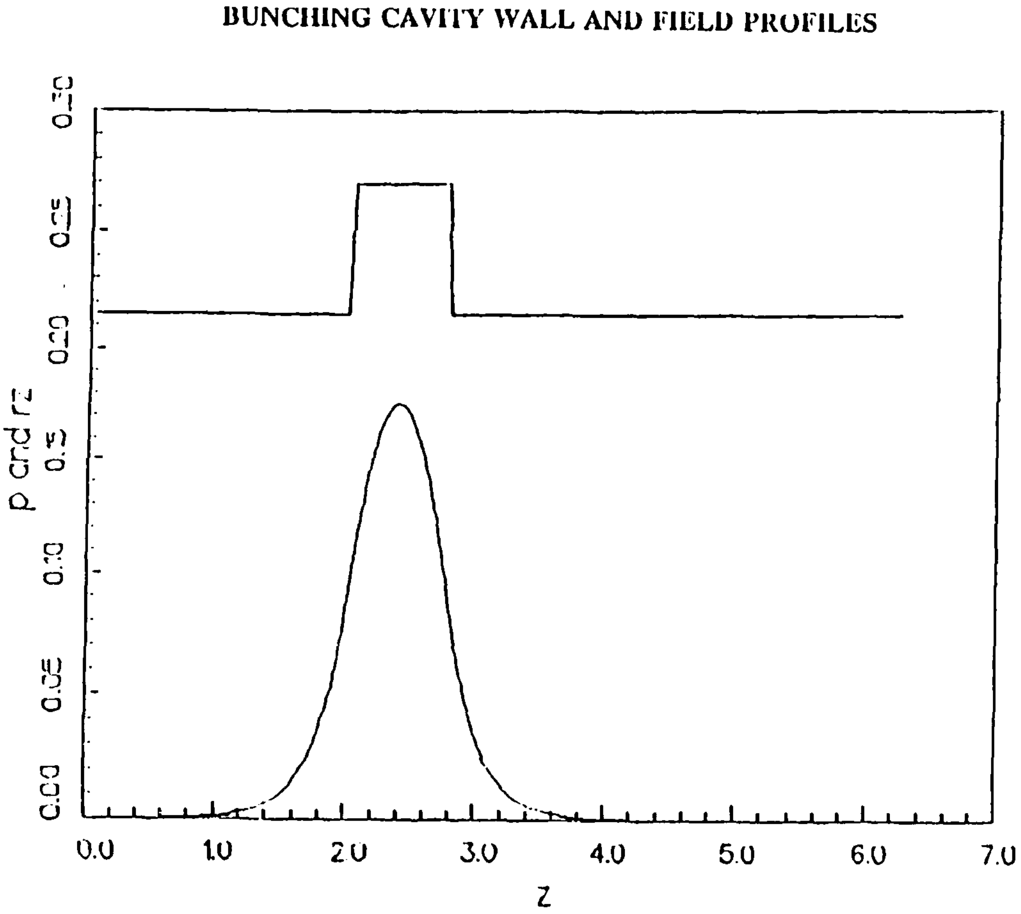

Figure VI.3. Bunching cavity wall and RF field profiles.

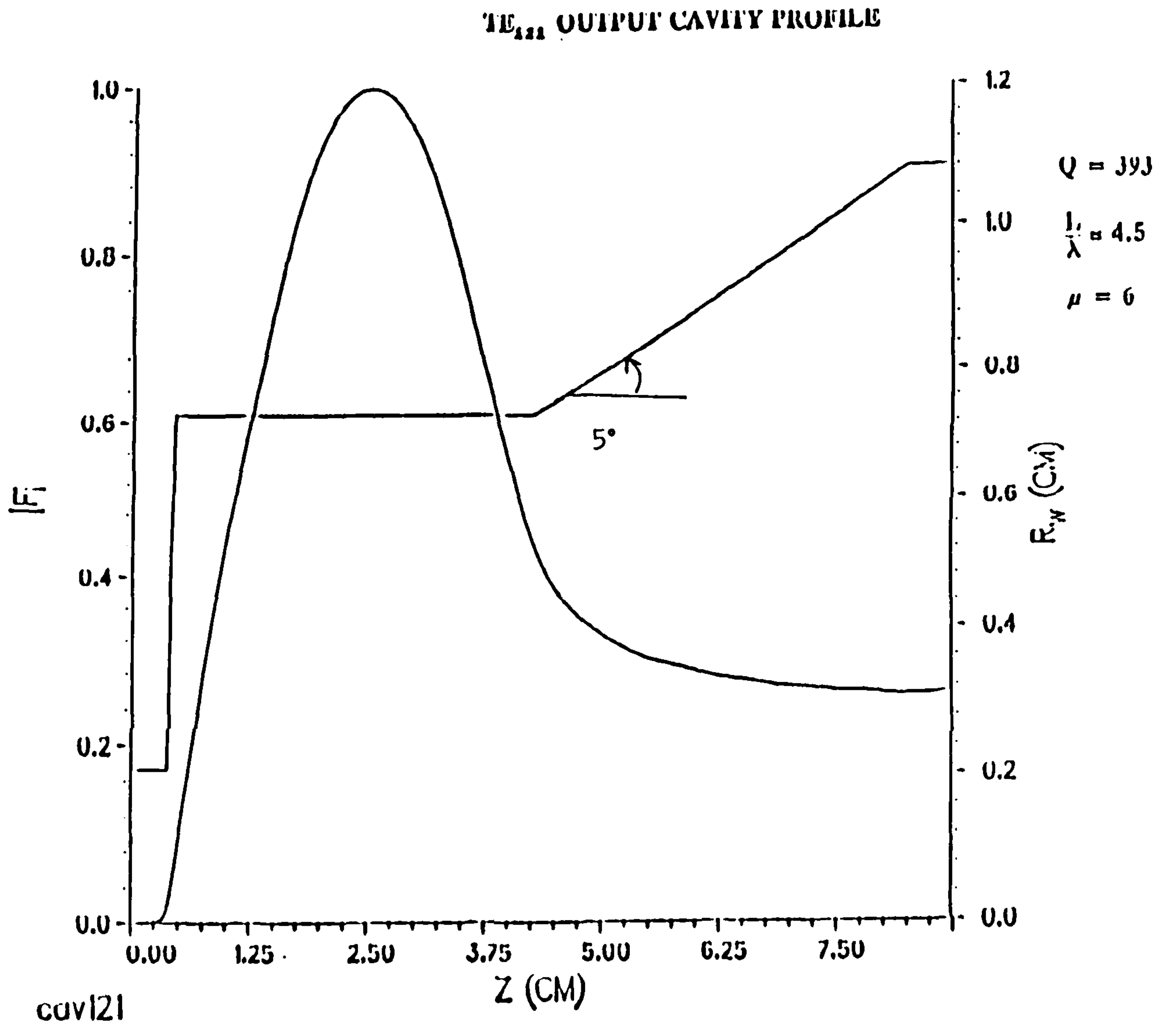

Figure VI.4. Axial RF field profile for TE_{121} output cavity.

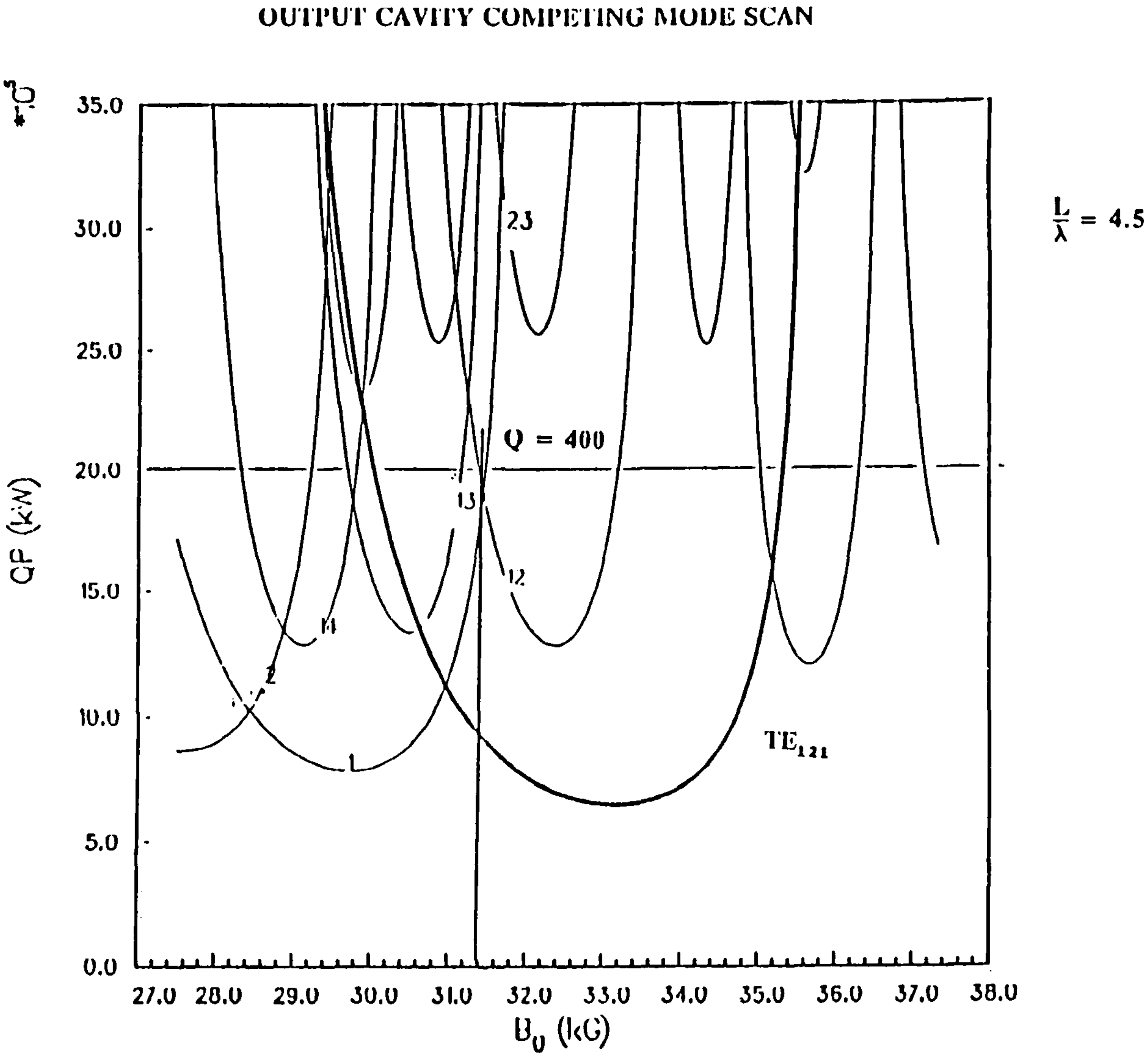

Figure VI.5. Scan of Q × threshold beam power for the TE_{121} mode (heavy line) and competing modes (numbered lines) in the output cavity. The calculations assume a sinusoidal axial profile, circular polarization, $L/\lambda=4.5$ and $\alpha=0.75$.

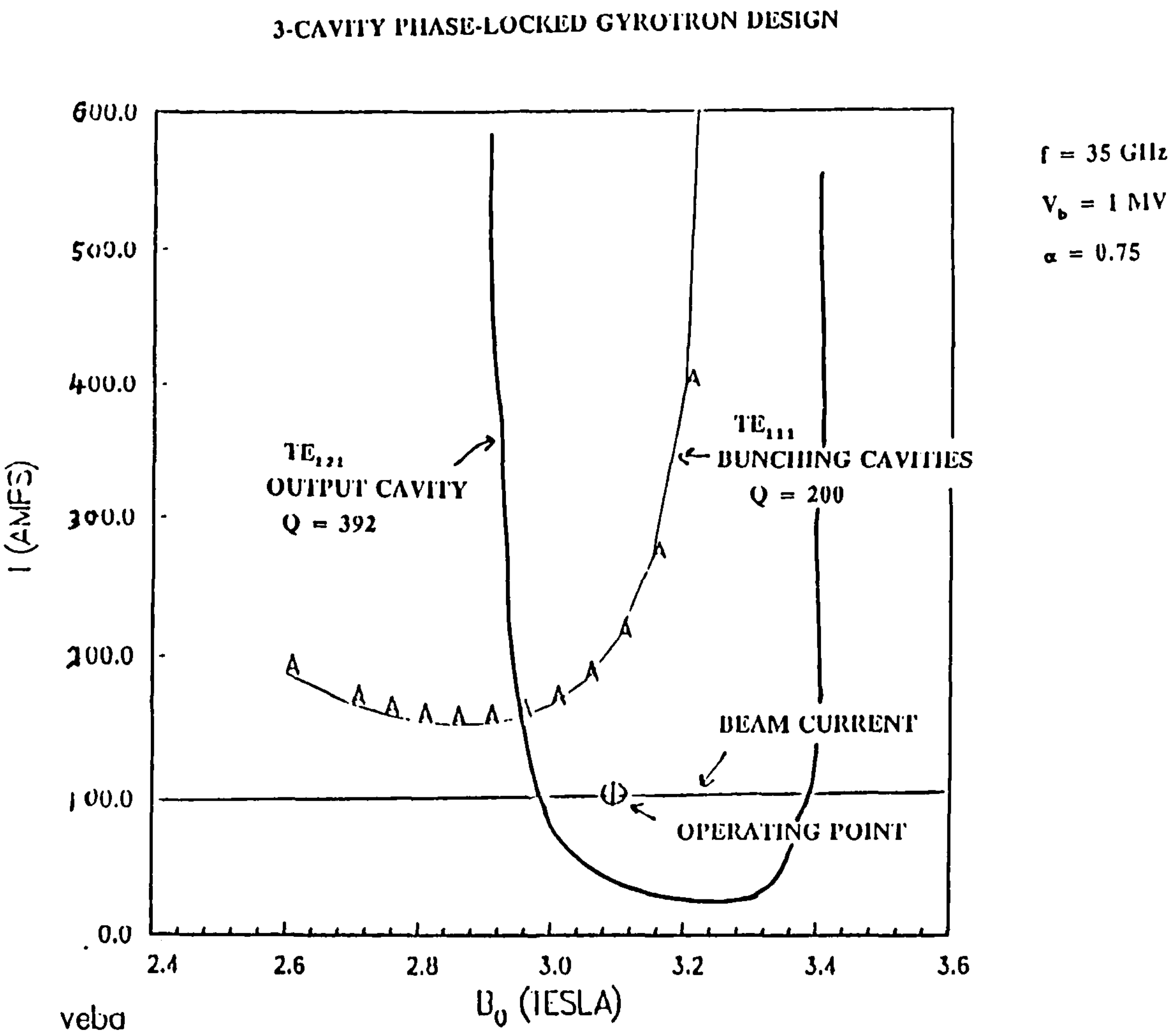

Figure VI.6. Threshold current curves for bunching and output cavities based on realistic axial RF field profiles.

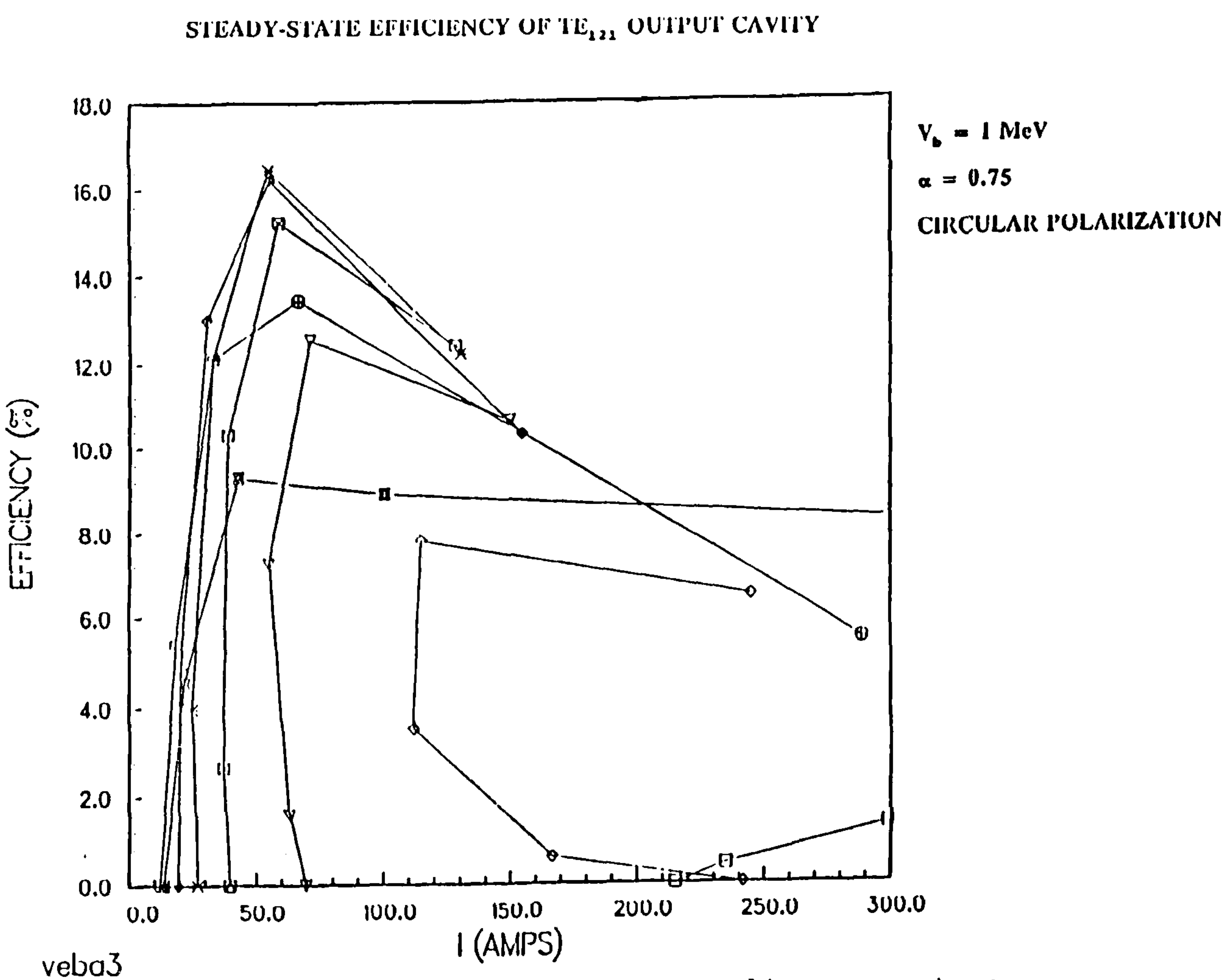

Figure VI.7. Output for steady-state nonlinear gyrotron efficiency code for output cavity as a free-running oscillator. Each curve corresponds to a different magnetic field.

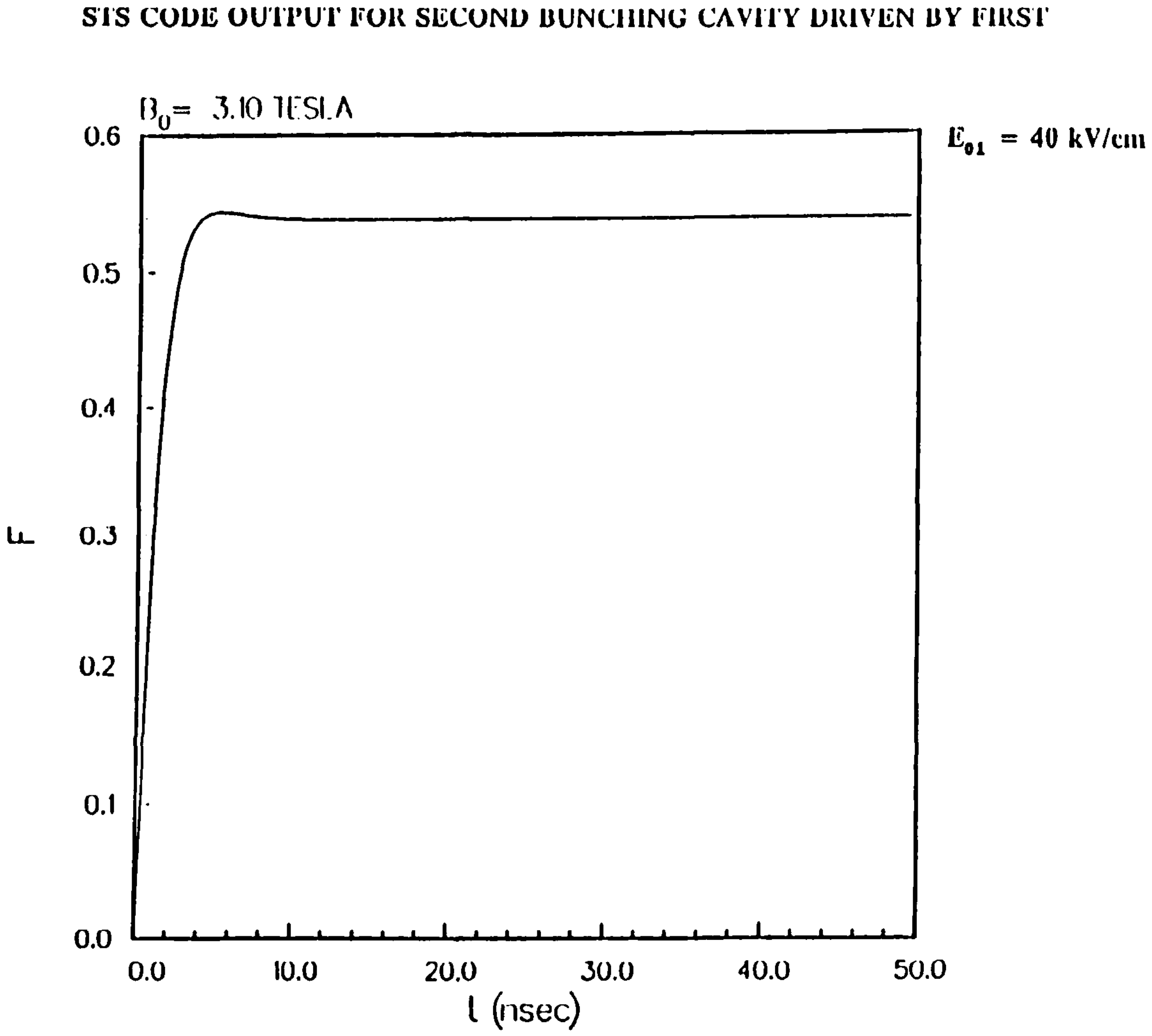

Figure VI.8. Time evolution of RF field amplitude in second bunching cavity induced by beam bunching in the first cavity. The magnetic field is 31 kG and the bunching parameter is q_2=0.36.

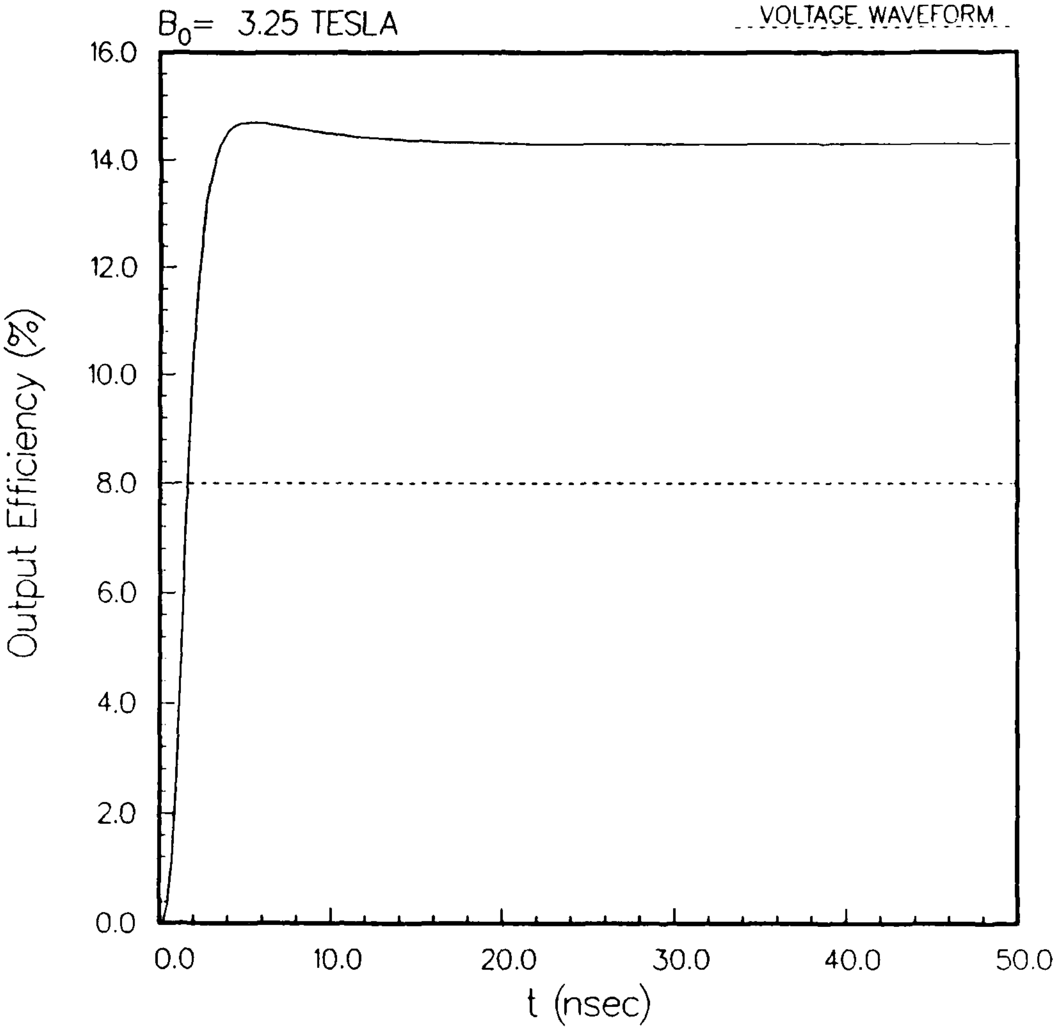

Figure VI.9. Time evolution of output cavity efficiency during phase-locked operation. The calculation assumes q_3=2.0, a magnetic field of 32.5 kG, and locking frequency shift $\Delta\omega_o/\omega_o$=0.1%.

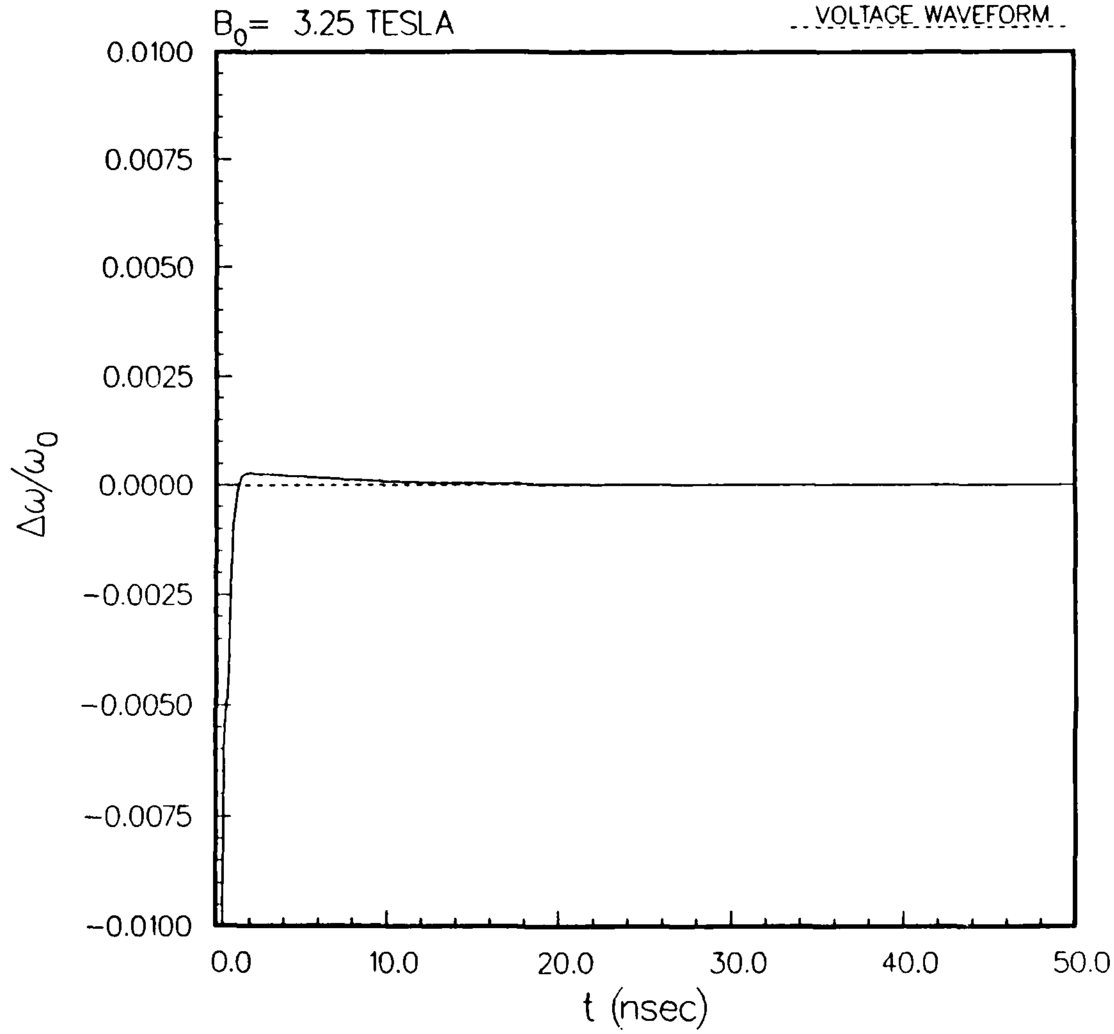

Figure VI.10. Time evolution of output cavity frequency shift relative to locking frequency for same parameters as Figure IV.9.

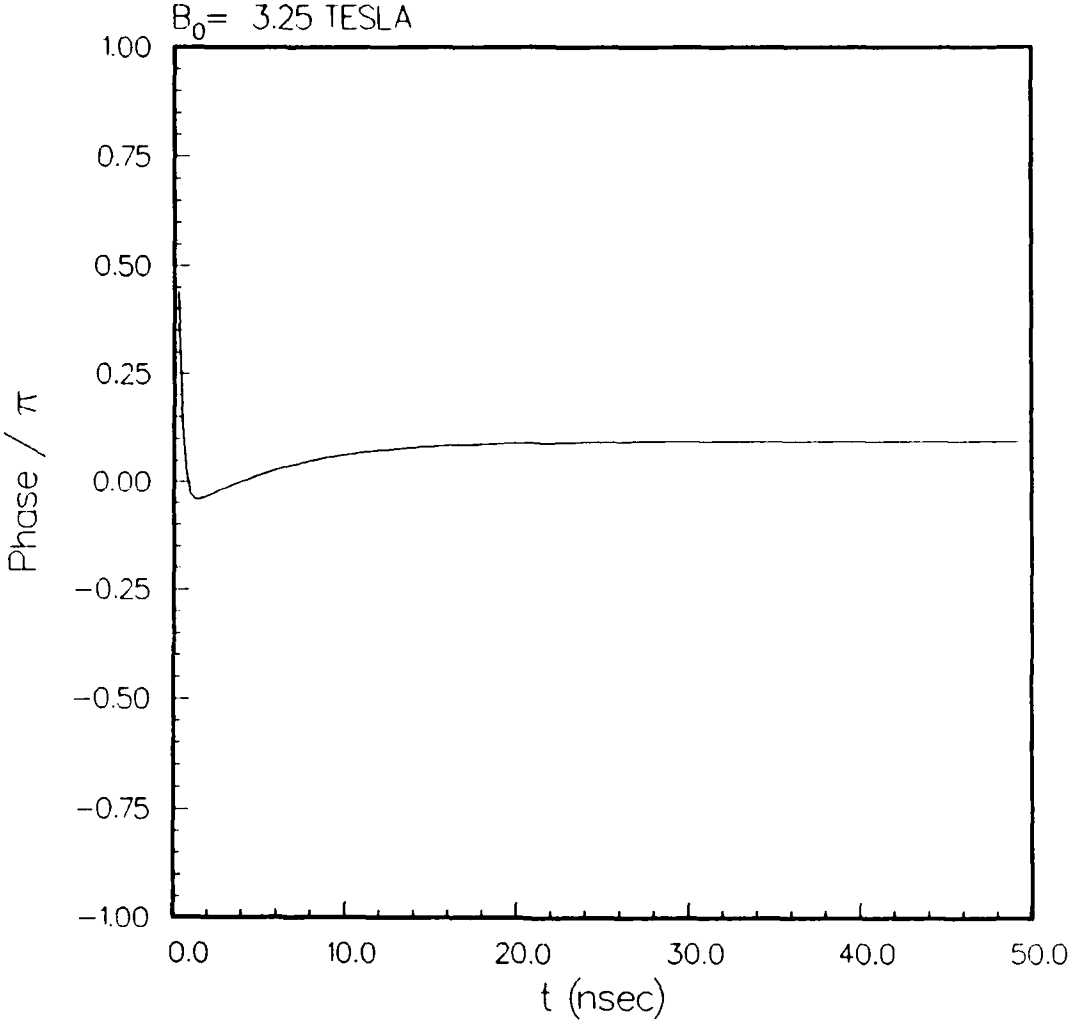

Figure VI.11. Time evolution of output cavity RF phase for same parameters as in Figure IV.9.

VII. VEBA Three-Cavity Phase-Locking Experiment

The first attempt to demonstrate phase locking on a high power gyrotron device operating from a pulseline accelerator will take place in the three-cavity phase-locking experiment described below.

A. Diagnostics

1. Frequency locking and phase locking

Frequency locking is generally diagnosed by heterodyning the oscillator output with the external drive signal using a mixer crystal. For a single-shot, short-pulse experiment, the beat signal is generally directly observed on a fast oscilloscope. If the gyrotron oscillator frequency is a frequency Δf away from the driver signal, and Δf is within the bandwidth of the oscilloscope, the microwave pulse seen on the oscilloscope will be modulated at the frequency Δf. However, if the product $\Delta f \Delta t$ is much less than 1, where Δt is the microwave pulse length, the gyrotron will appear locked to the external driver, since only a fraction of a cycle of the beat wave will be seen. That is, frequency locking can only be diagnosed to the resolution dictated by the pulse length.

The criteria for phase locking suggest that it will be necessary to drive the oscillator within 0.1% of its free-running frequency in order for phase and frequency locking to occur. Assume that the frequency detuning is 35 MHz out of 35 GHz. One full beat of the drive and oscillation frequencies would then take $\Delta t \sim 1/\Delta f \sim 30$ nsec, which probably exceeds the useful "flat-top" of the VEBA voltage waveform

For that reason, based on the parameters of a short pulse experiment, it may be much easier to observe phase locking (which for a long pulse would require frequency locking) than to observe frequency locking directly. However, it is possible than even phase locking can only be observed on a multi-shot basis, i.e. by observing that there is a fixed phase relationship on each shot between oscillator and reference signals. If the amplitude of reference and oscillator signals, at the diagnostics, can be equalized (on a shot-to-shot basis), phase locking can be observed using a hybrid coupler, such as a "magic T." This is a "four-port" device that will separate two equal signals into in-phase and out-of-phase components. To facilitate this experiment, a pair of precision direct-reading phase-shifters with an accuracy of 0.2° have been procured. This is the first phase-locking diagnostic that will be attempted. However, if the lack of shot-to-shot reproducibility makes it impossible to equalize the drive and oscillator output signals, it will be necessary to use a pair of mixer crystals, with 180° phase shift in the oscillator signal between the two crystals, combined with a differential amplifier, in order to generate a signal proportional to the sine or cosine of the phase difference. A pair of matched mixer crystals have been procured for this purpose.

B. Apparatus

1. Cavities

The first prebunching cavity must be low Q to the desired TE_{11} mode, which will be injected into the cavity from the reference source, as well as to any other modes that might oscillate in the cavity, including modes coming in in higher harmonics of the cyclotron interaction. The Q value selected to achieve this is 200. Since this cavity is closed at each end, the Q factor for a simple cylindrically symmetric cavity is determined by ohmic losses and by the input coupling aperture. These determine the internal and external Q values, Q_i and Q_e respectively, with the total $Q_T = Q_i Q_e / (Q_i + Q_e)$. Since the ohmic Q would normally be very large (>1000) unless very resistive walls were used, achieving the required Q with the coupling aperture would result in a highly overcoupled configuration ($\beta >> 1$, where $\beta = Q_i / Q_e$). Furthermore, unless great care is taken with the location of the aperture, for a Q of 200 in the TE_{111} mode, it might not load all possible oscillating modes sufficiently to prevent their oscillation. (In fact, it would not load at all the modes with linear polarization in the plane of the coupling apertures.) For that reason, it was decided to load the cavity Q by means of a pair of opposing axial slots, in order to reduce the Q_i of the TE_{111} and TE_{112} modes to 400. In that case, a coupling Q of 400 would yield a total Q of 200 at a β of 1. Figure VII.1 shows calculated "internal" Q values as a function of slot angle for the TE_{11} mode as well as for several possible competing modes. Achieving a Q_i of 400 for the TE_{111} mode by means of axial slots requires a full slot angle of 44°. This slot angle reduces the Q of the competing TE_{21} and TE_{31} to 85 and 34, respectively, and the Q of the TM_{01} mode to 65. (The TM_{01} mode was of possible concern, because it was not initially clear if axial wall slots would substantially load a mode without azimuthal wall currents.) In order to equalize the loading for the TE_{111} and for the TE_{112}, which is also cutoff in the drift spaces separating the cavities, the coupling aperture was placed one-third of the distance from the end of the cavity, rather than at the cavity midplane.

The output cavity Q of 400 should be determined principally by the output coupling. Figure VII.2 shows calculated "slot Q" versus slot half-angle for the output cavity. A full slot angle of 30° was selected to yield a slot Q of ~3000 for the preferred polarization, thus not substantially changing the overall output cavity Q, while effectively eliminating the orthogonal linear polarization.

The three microwave cavities and the connecting drift sections are shown to scale in Fig. VII.3. Because of the cavity slots, a separate vacuum enclosure surrounds the cavities. The vacuum enclosure is lined with microwave absorber, and is designed to isolate the three cavities from each other, to avoid the possibility of undesired feedback.

In order to finalize the dimensions of the cavity slots and coupling apertures, the 35 GHz prebunching cavity was scaled by a factor of 3.5 to 10 GHz in X-band, and a cold test cavity was fabricated. Using this cavity, a study was carried out of cavity Q versus coupling aperture diameter at constant wall thickness. Then, a pair of cavity slots were added to drop the total Q to ~200 according to design. The predictions of the McDonald code[1] were born out with respect to the reduction in Q due to the axial slots. However, the Code appeared to overestimate the frequency shift due to the slots. In the X-band cold test cavity, a tuning screw could be used to compensate for small errors in the cavity resonant frequency.

Before ordering the final "hot-test" cavities, a 35 GHz full scale model of the prebunching cavities was fabricated "in-house" for further testing. In these 35 GHz tests, it was discovered that the tuning screw was greatly depressing the cavity Q, presumably due to ohmic losses. In soldering the tuning screw hole shut to solve this problem, still lower Q values were found to be due to solder contamination of the cavity. Finally, the cavity was completely cleaned and then slotted, and a total Q of ~200 obtained. However, the measured input coupling was lower than predicted for a $\beta=1$ configuration. This last result is not yet understood.

Finally, precision hot test cavities were ordered, and should arrive by mid-December. They will be carefully characterized, and "trimmed" to specifications.

2. Beam formation

In order to form a cold, solid electron beam with an $\alpha \sim 0.75$, a "helix-gun" approach was chosen, in which a cold 100 A electron beam is produced by beam aperturing of a plasma-induced field emission diode, and the required beam α is induced by means of a helical wiggler magnetic field. The diode used in this device is derived from the diode used in the VEBA FEL experiment.[2] This approach is illustrated schematically in Fig. VII.4. Based on the amplitude of the axial magnetic field in the vicinity of the diode, a helix period of 4 cm was selected.

There are two basic approaches to "pumping up" the transverse momentum of an electron beam with a helical wiggler magnet. In the first approach, an untapered wiggler of fixed length is used to resonantly pump the transverse momentum. In the second approach, a tapered "adiabatic entry" wiggler is used to inject the beam into wiggler orbits closely approximating ideal, constant axial velocity wiggler orbits, and then the wiggler is abruptly terminated, releasing the electrons into the uniform axial field with the same value of transverse momentum that they had within the wiggler. Either approach should work in the current experiment, and a wiggler magnet has been ordered that should allow both approaches to be tried.

References for Section VII

1. S. McDonald, J.M. Finn, and W.M. Manheimer, "Boundary integral method for computing eigenfunctions in slotted gyrotron cavities of arbitrary cross-sections," Int. J. Electron., vol. 61, pp. 795-822, 1986.
2. R.H. Jackson, S.H. Gold, R.K. Parker, H.P. Freund, P.C. Efthimion, V.L. Granatstein, M. Herndon, A.K. Kinkead, J.E. Kosakowski, and T.J.T. Kwan, "Design and Operation of a Collective Millimeter-Wave Free-Electron Laser," IEEE J. Quantum Electron., vol. QE-19, pp. 346-356, 1983.

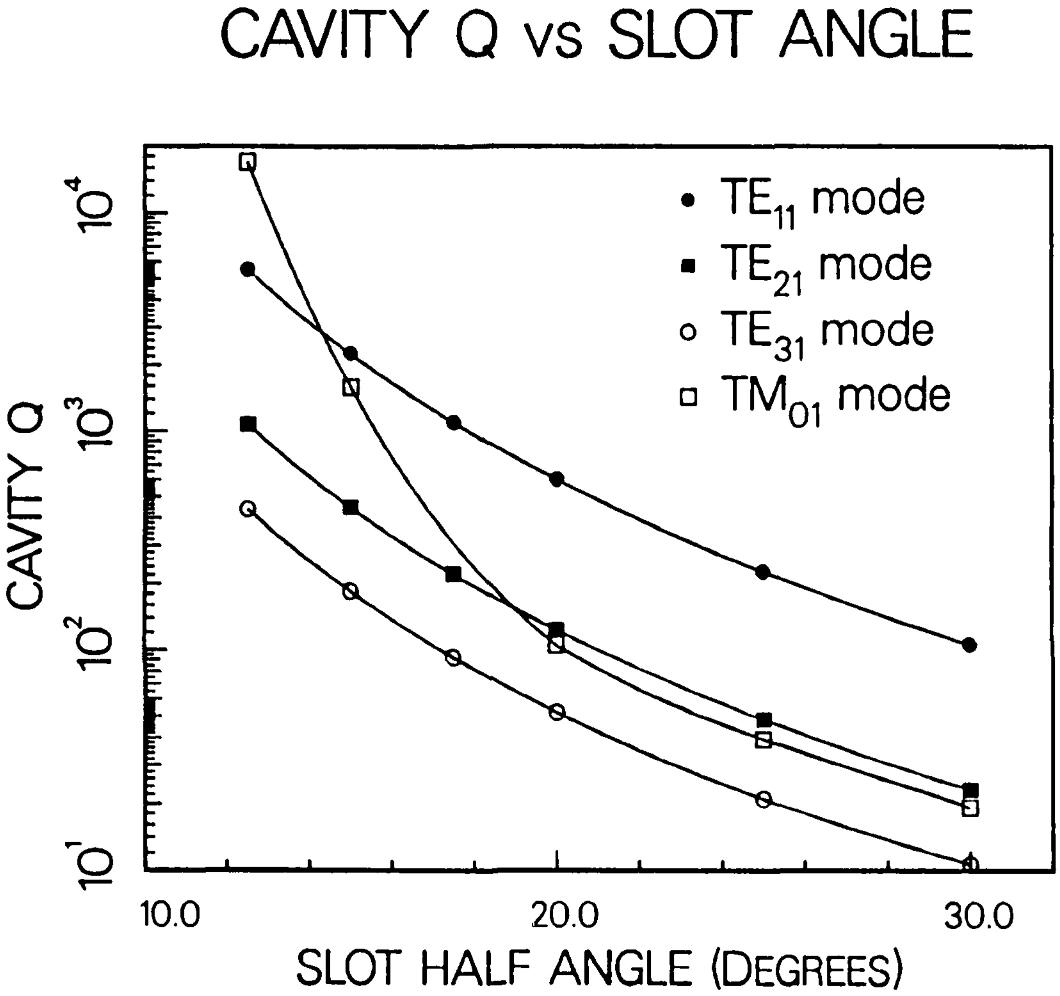

Fig. VII.1. Calculated Q-value vs slot half-angle for the TE_{11} mode and for possible competing modes in the prebunching cavities.

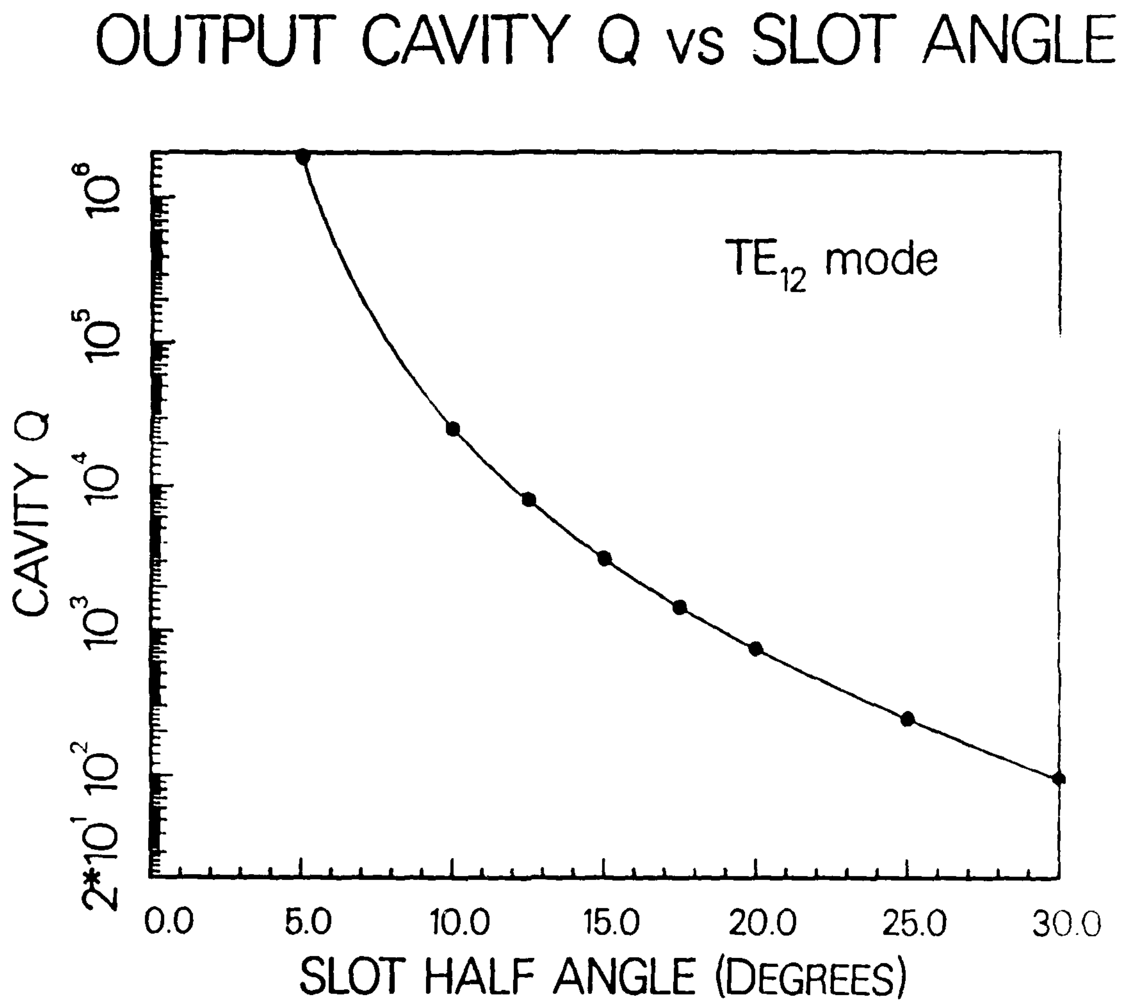

Fig. VII.2. Calculated Q-value vs slot half-angle for the TE$_{12}$ mode of the output cavity.

VEBA PHASE-LOCKING EXPERIMENT

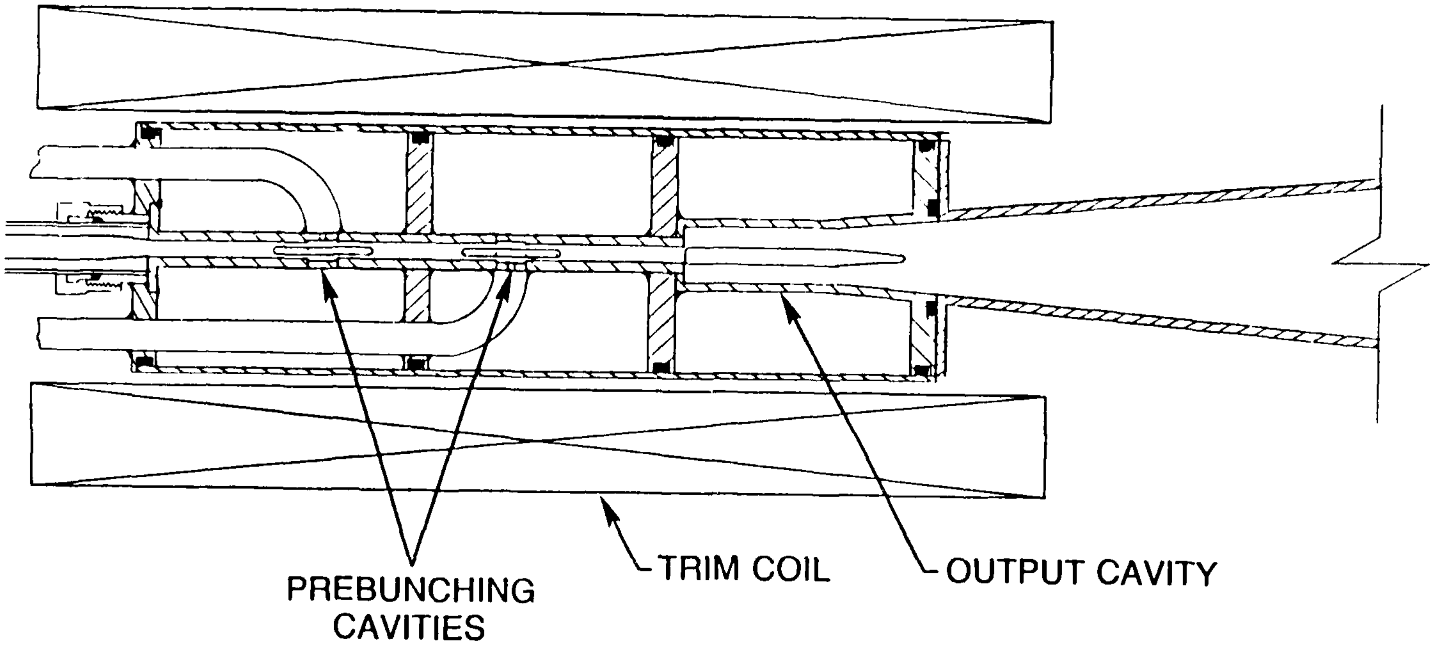

Fig. VII.3. Scale drawing of the two prebunching cavities, the output cavity, and the drift sections of the three-cavity phase-locking experiment.

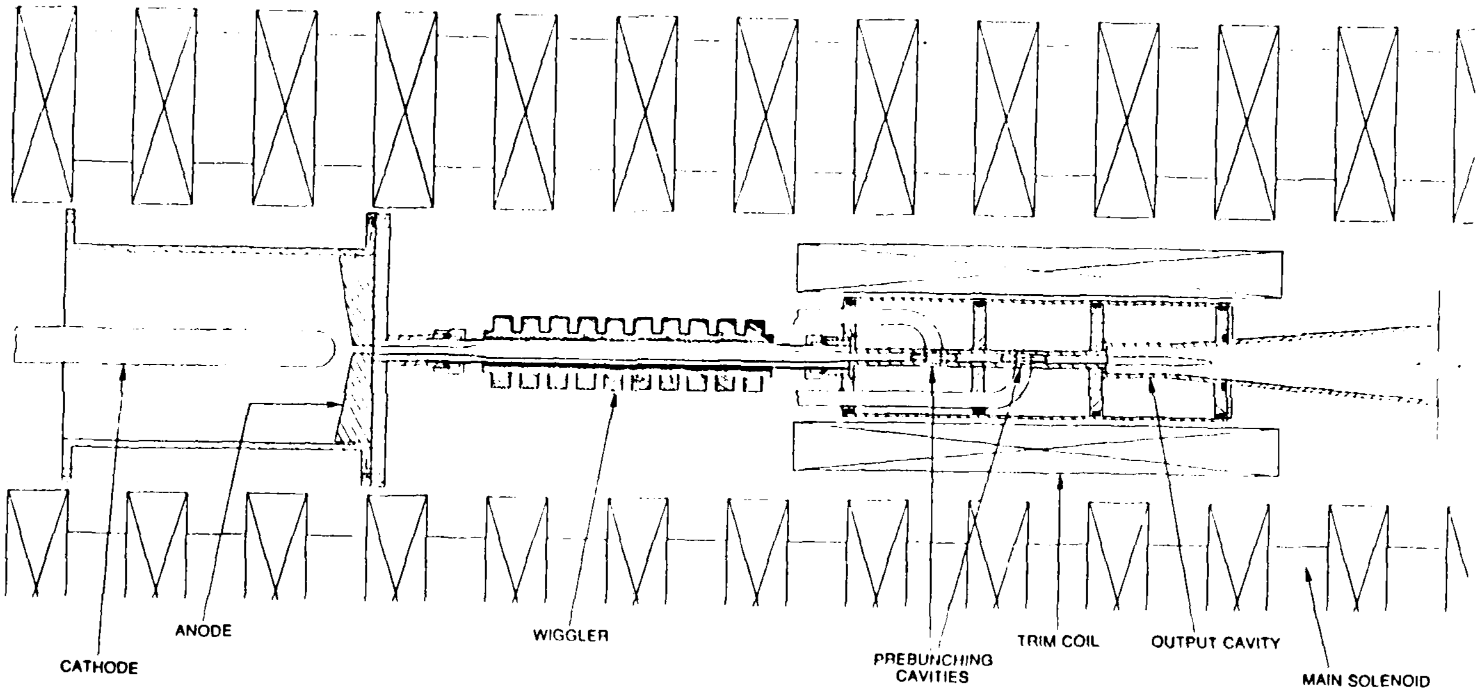
VEBA PHASE-LOCKING EXPERIMENT

Fig. VII.4. Schematic drawing of the VEBA three-cavity phase-locking experiment, showing the arrangement of diode, wiggler, and microwave cavities.

VIII. Strongly Coupled Oscillator Experiment

A direct approach to the phase locking of two or more oscillators is to link identical units together by one or more coupling cavities. The resulting system of strongly coupled oscilators has the advantage of not requiring a low power locking source with its attendant concern of isolating the low power source from the high power oscillator(s). The interest here is to couple together two or more gyrotron cavities operating in high order modes at very high power levels. This requires that the cavities efficiently couple to each other and excite the desired modes without exciting the unwanted modes. In addition, the coupling system must be able to handle the power and field strengths involved while permitting adjustments to optimize the phase locking of the gyrotrons.

The proposed initial experiment involves strongly coupling two high power gyrotron oscillators operating at 35 GHz in the TE_{62} mode. Operating alone, these oscillators have succeeded in generating 100 MW of power using a febetron (750 keV, 1-2 kA beam in the cavity) and 200 MW of power using VEBA (1.25 MeV, 3-4 kA beam in the cavity). Operating together, the oscillators will both be connected to VEBA which will provide a 1.0 to 1.5 MeV beam with ample current (6 to 10 kA) for both of the two gyrotron cavities. The diodes of both oscillators will have the same geometry on the front end of VEBA to produce two like beams. Each beam is separately directed to identical cavities with apertures designed to permit approximately 10% of the power to couple into a waveguide which links the two oscillator cavities together. In this coupling waveguide, provision is made to adjust the phase and attenuation of the coupling signal, to sample the connecting signal, and to decouple the oscillators. In a later section, the design details of the coupling cavity show that despite many competing modes, approximately 99% of the coupled energy is in the desired TE_{621} mode at 35.2 GHz.

The work completed to date includes the design of the magnetic field coils and the design of the coupling cavities and the coupling waveguide structure and components between the two oscillators. The magnetic field coils have been designed to provide the required 35 kG in the cavity region while accomodating the presence of the coupling waveguide between the coils. The windings for the main axial guide magnetic field of each oscillator will connected in series to ensure that each simultaneously produces the same current. For the same reasons, the cavity magnetic field windings will also be in series. If AWG 10 PVC wire is selected, then the peak current will occur in about 2 msecs which is an order of magnitude above the penetration time of the fields through the stainless steel vacuum enclosure. The temperature rise will be about 2 deg Celsius per pulse which should not require special cooling provisions.

Since the two oscillator cavities will be placed as close together as possible to minimize the radiation travel time between the oscillator cavities, the radial extent of the magnetic field windings around each tube has been minimized. To avoid the two magnets from interfering with one another, some magnetic shielding will be used. An aluminimum sleeve of 1/2" wall thickness will be used to surround each of the two outer magnetic field coil windings. For the cavity field which has a peak current in a time of 2 msec, the field will differ by a factor of approximately 30 on either side of two 1/2" thicknesses of Aluminum. For the main field with a maximum current at 4 msec, the ratio is about 10.

The initial fabrication and testing of the cavity and coupling structures should be completed by the end of March. Based upon the results of the cold tests, the final design and fabrication is scheduled to be completed by the end of June. Beginning in July, the experiment will then be tested to examine its phase locking capabilities in the production of microwave signals.

Coupling of High-Power High-Order-Mode Gyrotron Cavities

The coupling together of two gyrotron cavities operating in the Te_{62} modes at very high power levels of 100 MW requires consideration that the cavities efficiently couple to each other. Figure VIII.1 shows a simplified diagram of the two cavities connected with a length of waveguide and coupled via aperture(s) or slot(s). Since the desired level of power coupled from one cavity to the other is only a fraction (up to ~10 MW) of the output power (~100 MW) the coupling coefficients β_1 and β_2 between the low Q open cavities and intermediate waveguide are much less than unity (weak coupling). The matching at each end of the coupling waveguide is not perfect; therefore, the intermediate (coupling) waveguide is a cavity itself, labeled CAV3 in Fig. VIII.1. Hence, the aperture/slot arrays that are designed to excite the desired CAV1 and CAV2 modes (i.e., TE_{62}) must also excite a particular and relatively pure mode in CAV3 in order for the total coupling system from CAV1 to CAV2 to work and be efficient. Ohmic and mode conversion losses in CAV3 must be reasonably low in order for the transmission loss thru CAV3 to be low. Basically, if the aperture/slot loaded Q of CAV3 (i.e., Q_{3l}) is much lower than the unloaded Q (i.e., Q_{3u}) of CAV3 (i.e., ohmic, etc., losses), then the transmission loss will be small. This also gives a means of controlling power flow experimentally by putting in CAV3 a small variable loss to control the Q. Depending on the Q's, a few dB loss can result in tens of dB of transmission loss from CAV1 to CAV2.

Cavity Mode Excitation

The calculation of the mode excitations is done by 'normal mode theory'. This technique makes use of expanding the real cavity fields (i.e., fields that include apertures, slots, wall losses, coupling probes, etc.) as sums of normal mode fields (i.e., fields without the disturbances).

The normal mode fields $\vec{\varepsilon}_n$, $\vec{H}_n$ satisfy

$$(\nabla^2 \rightarrow k_n{}^2)\ \vec{\varepsilon}_n = 0$$

where $$k_n\ \vec{H}_n = \vec{\nabla} \times \vec{\varepsilon}_n$$

$$k_n\ \vec{\varepsilon}_n = \vec{\nabla} \times \vec{H}_n$$

$$\nabla \cdot \vec{\varepsilon}_n = 0 \text{ in } V$$

$$\hat{n} \times \vec{\varepsilon}_n = 0 \text{ on } S$$

The normal modes are normalized and orthogonal

$$\int_V \vec{H}_a \cdot H_b{}^* dv = \int_V \vec{\varepsilon}_a \cdot \vec{\varepsilon}_b{}^* dv = \delta_{ab}$$

so that the mode amplitudes

$$e_n = \int_V \vec{E} \cdot \vec{\varepsilon}_n{}^* dv$$

$$h_n = \int_V \vec{H} \cdot \vec{H}_n{}^* dv$$

where $\vec{E}$ and $\vec{H}$ are the real cavity fields (with apertures, gaps, etc.). So

$$\vec{E} = \sum_{\text{all } n} e_n \vec{\varepsilon}_n$$

$$\vec{H} = \sum_{\text{all } n} h_n \vec{H}_n$$

the power transfered into or out of the cavity via the coupling is

$$\int_V \vec{\nabla} \cdot (\vec{E} \times \vec{H}_n^{\,*}) \cdot dv = \int_S (\vec{E} \times \vec{H}_n^{\,*}) \cdot ds$$

for coupling via the $\vec{H}_n$ fields and

$$\int_V \vec{\nabla} \cdot (\vec{\varepsilon}_n^{\,*} \times \vec{H}) \cdot dv = \int_S (\varepsilon_n^{\,*} \times \vec{H}) \cdot ds$$

for coupling via the $\vec{\varepsilon}_n$ fields solving for h_n and e_n gives equations for the field amplitudes in terms of the fields at the surface of the cavity.

$$e_n = \frac{-j\omega\mu \int_S (\vec{H} \times \varepsilon_n^{\,*}) \cdot d\vec{s} + k_n \int_S (\vec{E} \times H_n^{\,*}) \cdot ds}{k^2 - k_n^{\,2}}$$

$$h_n = \frac{-j\omega\mu \int_S (\vec{H} \times \vec{\varepsilon}_n^{\,*}) \cdot d\vec{s} + k_n \int_S (\vec{E} \times \vec{H}_n^{\,*}) \cdot ds}{k^2 - k_n^{\,2}}$$

For aperture coupling (rather than probes, loops, etc.)

$\vec{H} \times \vec{\varepsilon}_n^{\,*} = 0$ at the surface of the cavity.

[If a probe or loop coupling is used, $\vec{H} \times \vec{\varepsilon}_n{}^* \neq 0$ over the probe or loop.] Also, if we only consider aperture and slots with slot field $\vec{E}_s = E_\theta \hat{\theta}$ only, (i.e., only a transverse E-field, no axial E-field) then

$$\vec{E}_s \times \vec{H}_n{}^* \neq 0 \text{ for } H_{nz}{}^* \text{ only}$$

TE mode coupling only.

Thus, if we use only axial slots and apertures in the side walls with transverse directed E-field slot excitation, then only TE modes are coupled to.

Then

$$h_n = \frac{j\omega\varepsilon\int_s (\vec{E} \times \vec{H}_n{}^*)\cdot ds}{k_n - k_n{}^2}$$

$$e_n = \frac{k_n \int_s (\vec{E} \times \vec{H}_n{}^*)\cdot ds}{k^2 - k_n{}^2}$$

for TE modes with side wall excitation. Lumping the power output of the cavity in each TE normal mode into a loaded Q_n gives expressions for the coupling in terms of the axial slot or aperture field E_s only

$$e_n = \frac{k_n \int_{\text{slot}} (\vec{E}_s \times \vec{H}_{nz}^{\,*}) \cdot ds}{k^2 - k_n^{\,2} + \dfrac{(1-j)\omega\omega_n \mu G}{Q_n}}$$

$$h_n = \frac{j\omega\varepsilon e_n}{k_n}$$

for axial slot coupling and TE modes. It is interesting to note that, at resonance, that

$$e_n \text{ (and } h_n) \propto Q_n \int_S (\vec{E}_s \times H_{nz}^{\,*}) \cdot ds$$

i.e., that the field strength of the excited nth mode (TE) is proportional to the Q of the mode, the slot E field area and strength, and to the normalized axial magnetic field strength at the wall (at the slot location). The energy stored in the cavity in the nth mode is

$$U_n = \frac{1}{4} \left(\mu \int_V |h_n \; H_n|^2 dv + \varepsilon \int_V |e_n \, \varepsilon_n|^2 dv\right) \simeq \frac{1}{2} \varepsilon |e_n|^2$$

Since power in the nth mode is (and noting $H_n \simeq j\sqrt{\varepsilon/\mu}\; e_n$ at resonance)

$$P_n = \frac{\omega U_n}{Q_n}$$

then

$$P_n \simeq \frac{\omega\varepsilon Q_n}{2k^2} \left| \int_{slot} (\vec{E}_s \times \vec{H}_{nz}^{*}) \cdot ds \right|^2$$

One would expect the coupling to whispering gallery type modes to be stronger than coupling to low order azmuthal mode as the axial H field is stronger at the wall for the higher order modes. Mode suppression of unwanted modes can be had by loading the mode by appropriate loss, slots, etc., to lower the Q and by minimizing

$$\int_{slots} \vec{E}_s \times \vec{H}_{nz}^{*} \cdot ds$$

which can be done by placing the coupling apertures at $\vec{H}_{nz}^{*}$ nulls and/or cancellation. For example, if H_{nz}^{*} varies as sin $2k_o z$ and E_s varies as sin $k_o z$, then

$$\int_0^{\lambda_o} \int_{-\theta_{s/2}}^{+\theta_{s/2}} (\vec{E}_s \times \vec{H}_{nz}^{*}) \cdot ds = 0$$

and no coupling results.

This is just like a directional coupler where the phase velocity of the desired coupled modes has to match unwanted modes phase velocity different by at least 1/2 beat wavelength over the length of the coupler. Cancellation can also be done by, for example, arranging the polarities of the driven slot field to be in opposite polarity with respect to local $\vec{H}_{n2}$ field.

Mode Suppression by the Selection and Positioning of Coupling Apertures

Figure VIII.2 shows the planned coupled gyrotron cavities physical profile with a flat middle region of ~2 cm length and 1.60 cm radius and the calculated (CAVRF) axial field profile. The middle region looks very much like the center portion of a sinusoidal cavity of ~4 cm length. As it is desired to only place the coupling slots or apertures in the middle region, for constructional convenience as much as anything, calculations have been done with sinusoidal fields. The calculations could be done for the exact calculated profile(s) but this is not necessary as the result would be very similar to a sinewave calculation.

Figure VIII.3 is a calculation for a 1 mm long axial aperture located at the center of the cavity. In this calculation all the mode Q's were assumed to be Q_n = 300, although any Q can be used (such as the Q's calculated from CAVRF). The TE_{621} mode is swamped out by a number of other modes. A decomposition of the modes at ~35.20 GHz (resonant frequency of the TE_{621}) gives a breakdown of the percentage power going into each mode. The significant modes are

$TE_{035} \approx .5\%$

$TE_{141} \approx 4.4\%$

$TE_{235} \approx 5.0\%$

$TE_{327} \approx 1.0\%$

$TE_{333} \approx .6\%$

$TE_{621} \approx 20.8\%$

$TE_{10,1,1} \approx 66.0\%$

All other modes <2%

Note that the $TE_{10,1}$ mode is very strongly coupled to and only ~21% of the power goes into TE_{62}. Obviously a single aperture excites too much of the other modes.

Figure VIII.4 shows the same cavity excited by a single 4 cm long axial slot (or line array of closely space apertures) from a waveguide of the same axial wavelength (i.e., directional coupler type coupling). Now all the higher order axial modes are suppressed. The decomposition at 35.20 GHz is then

$TE_{141} \approx 4.8\%$

$TE_{621} \approx 22.7\%$

$TE_{10,1,1} \approx 72.3\%$.

Although the spectrum is now cleaner, there is actually little difference in the power coupled into the TE_{62} mode at the Te_{62} frequency.

The relative power coupled in Figs. VIII.3 to VIII.5 is calculated for the same aperture or slot E field strength in all cases and shows the greatly increased coupling for large size and/or number of apertures or slots.

A number of slot configurations were tried to suppress the strong $TE_{10,1}$. A pair of slots are placed at .314 radians apart (azimuthally) and driven in - phase (E_θ vector polarity in same θ direction) is actually ideal for suppressing the $TE_{10,1}$ for all $TE_{10,1}$ polarizations. The decomposition at 35.20 GHz is

$TE_{141} \approx 37.0\%$
$TE_{621} \approx 62.2\%$
$TE_{10,1,1} < 1\%$

Now the TE_{621} is coupled to dominantly, but the TE_{141} is coupled to significantly. If the TE_{141} is loaded (for instance, by 4 axial slots) to a $Q \approx 30$, then at 35.2 GHz

$TE_{141} \approx 15.2\%$
$TE_{621} \approx 83.7\%$
$TE_{10,1,1} < 1\%$

This may be a suitable design depending on whether or not the TE_{14} mode can be suitably loaded without loading the TE_{62}.

A better design has been found by placing the pair of 2 cm axial slots 0.619 radians apart and fed out of phase. This is illustrated in Figure VIII.5. At 35.20 GHz the decomposition is

$TE_{621} \approx 98.9\%$
all others $\approx 1.1\%$

Thus, almost perfect mode selectivity to the TE_{621} mode can be achieved and without resorting to trying to load unwanted modes. This is not to say that some loading (slotting) is not desirable to prevent unwanted oscillations or maintain particular polarizations, but heavy loading is not necessary to minimize its coupling in the excitation.

Coupling Cavity Between Oscillators

If the standard WR28 guide (7.1 mm x 3.6 mm) is used to couple the gyrotrons at a power flow of ~10 MW (both oscillating in steady state), a peak field strength of ~ 1 MV/cm is realized in the guide. Although this is below simple theoretical multipactor breakdown (~3 MV/cm) for this gap and frequency it is not a large margin as bends, discontinuities (from components), etc., could increase the peak field strength to that level.

A somewhat better choice of waveguide is an oversized guide of 8 x 6 mm size (i.e., WR62) but operating in the TE_{01} mode. This is also convenient from the coupling aspect to achieve the effective out of phase feeds by staggering the coupling slots every $\lambda_g/2$ and ~.62 radians apart (~1 cm).

Figure VIII.6 illustrates the concept. A septum is necessary to prevent mode conversion to TE_{11} and TE_{12} in the

WR62 guide in the coupling region (not necessary elsewhere). This choice of guide not only allows convenient coupling to the TE_{62} (with Te_{14} and $TE_{10,1}$ suppression) but reduces the peak field strength in the WR62 to ~450 kV/cm. Also, since the WR62 is essentially fundamental mode (in the narrow width direction) bends and component irregularities can be introduced with minimal mode conversion and loss. Also, the loss is lower in the WR62 than the WR28, 0.0018 dB/cm vs 0.0054 dB/cm. As the guide is a resonator of Q ~ 700 (for 40 cm length and $\beta_1 = \beta_2 = 0.1$) this gives a loss of ~0.8 dB for WR28 guide and 0.3 dB for WR62 guide, or ~0.5 dB less loss. A variable attenuator (for coupling variation) with a single pass attenuation of ~5 dB would result in a Q spoiled transmission loss of ~20 dB. This would allow power coupled (steady state) from ~10 MW down to ~0.1 MW. The attenuator could be a 5 cm length of lossy wall (R ~ 1/Ω-cm) that is adjusted up and down to give ~0 to 5 dB attenuation. Also desired is a phase shifter which can consist of a split piece (in narrow walls) of WR62 guide between a caliper to adjust the phase velocity in a ~5 cm length. Also desirable is a directional coupler to sample the power flow between the gyrotrons and probably a switch to establish complete isolation. These components will be designed and made to operate in the vacuum environment.

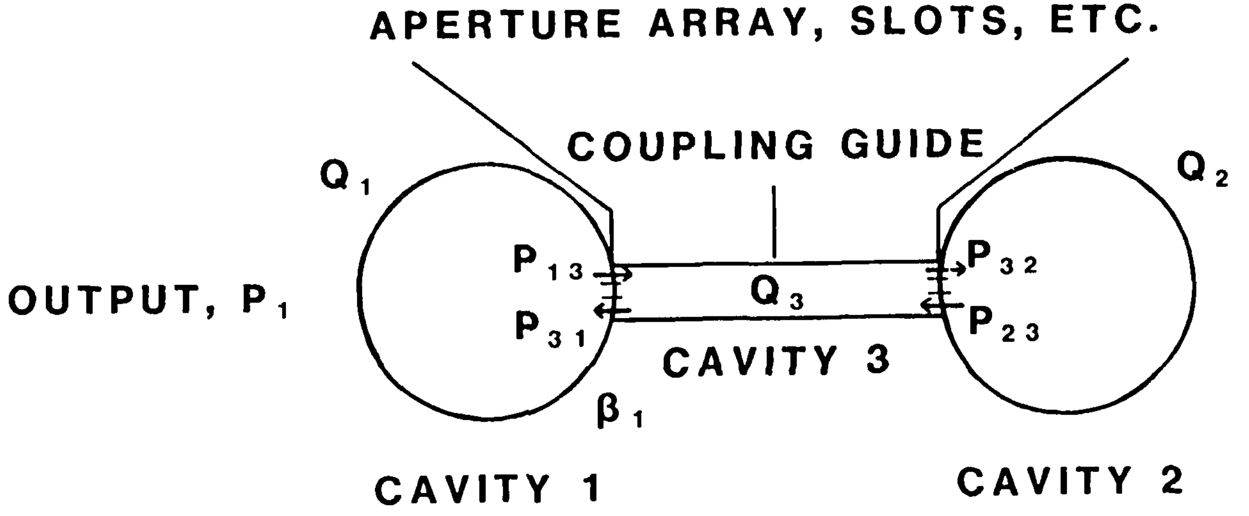

$$\beta = \beta_1 = \beta_2 << 1$$

Fig. VIII.1. Two Cavities and Intermediate Coupling Waveguide.

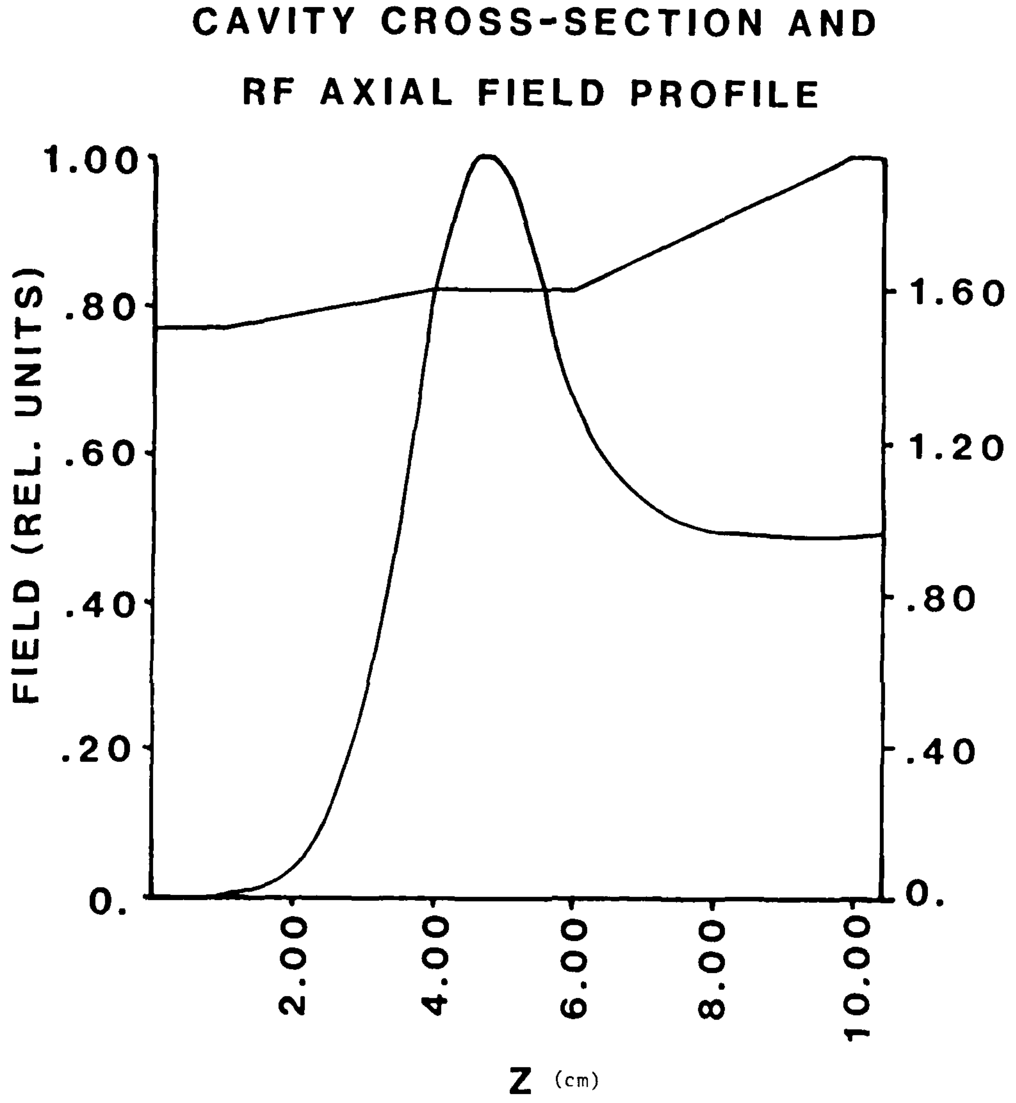

Fig. VIII.2. Cavity Cross-Section and RF Axial Field Profile.

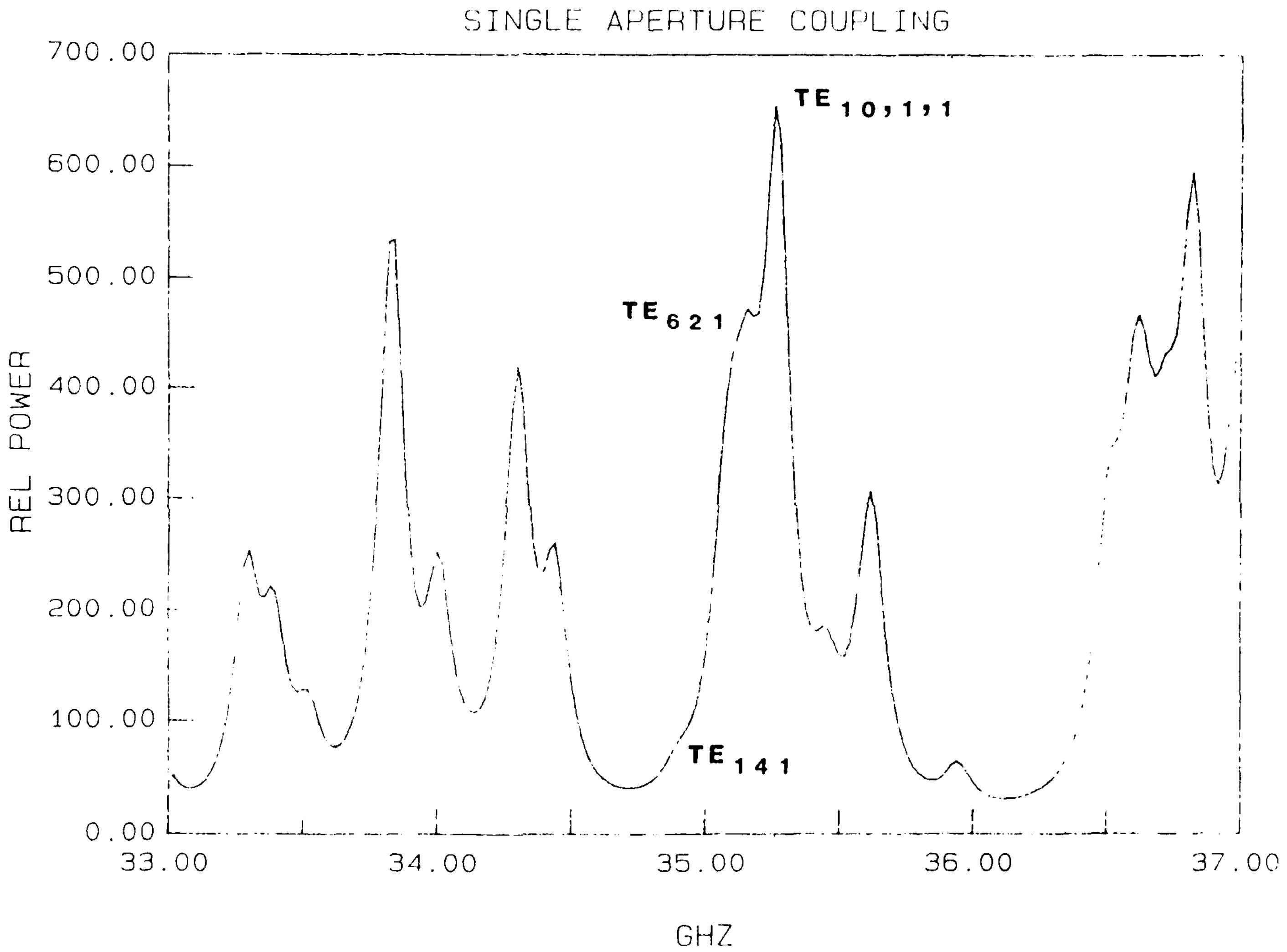

Fig. VIII.3. Cavity Excitations Near 35 GHz for a 1 mm Long Axial Aperture.

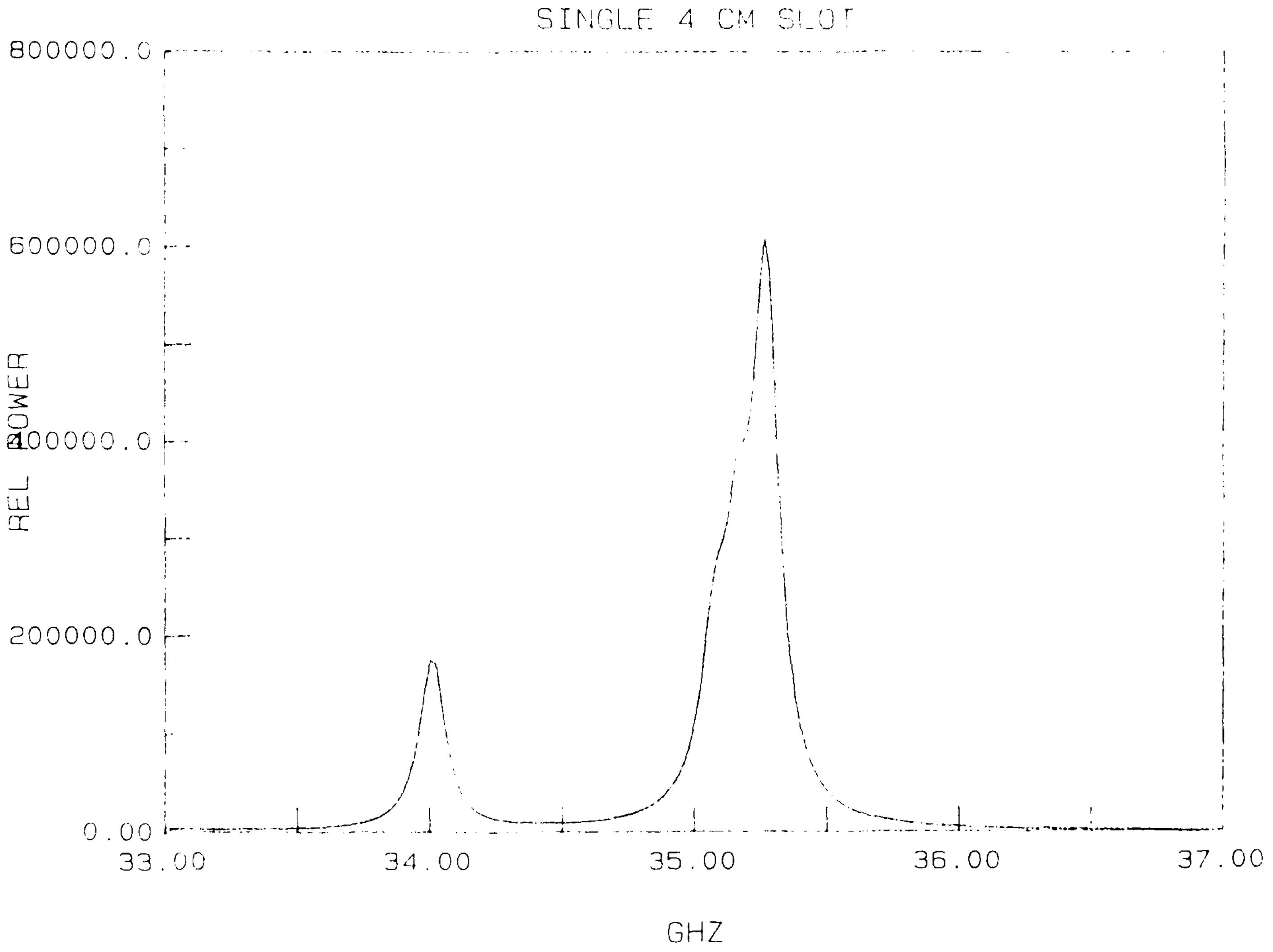

Fig. VIII.4. Cavity Excitations Near 35 GHz for a 4 cm Long Axial Slot.

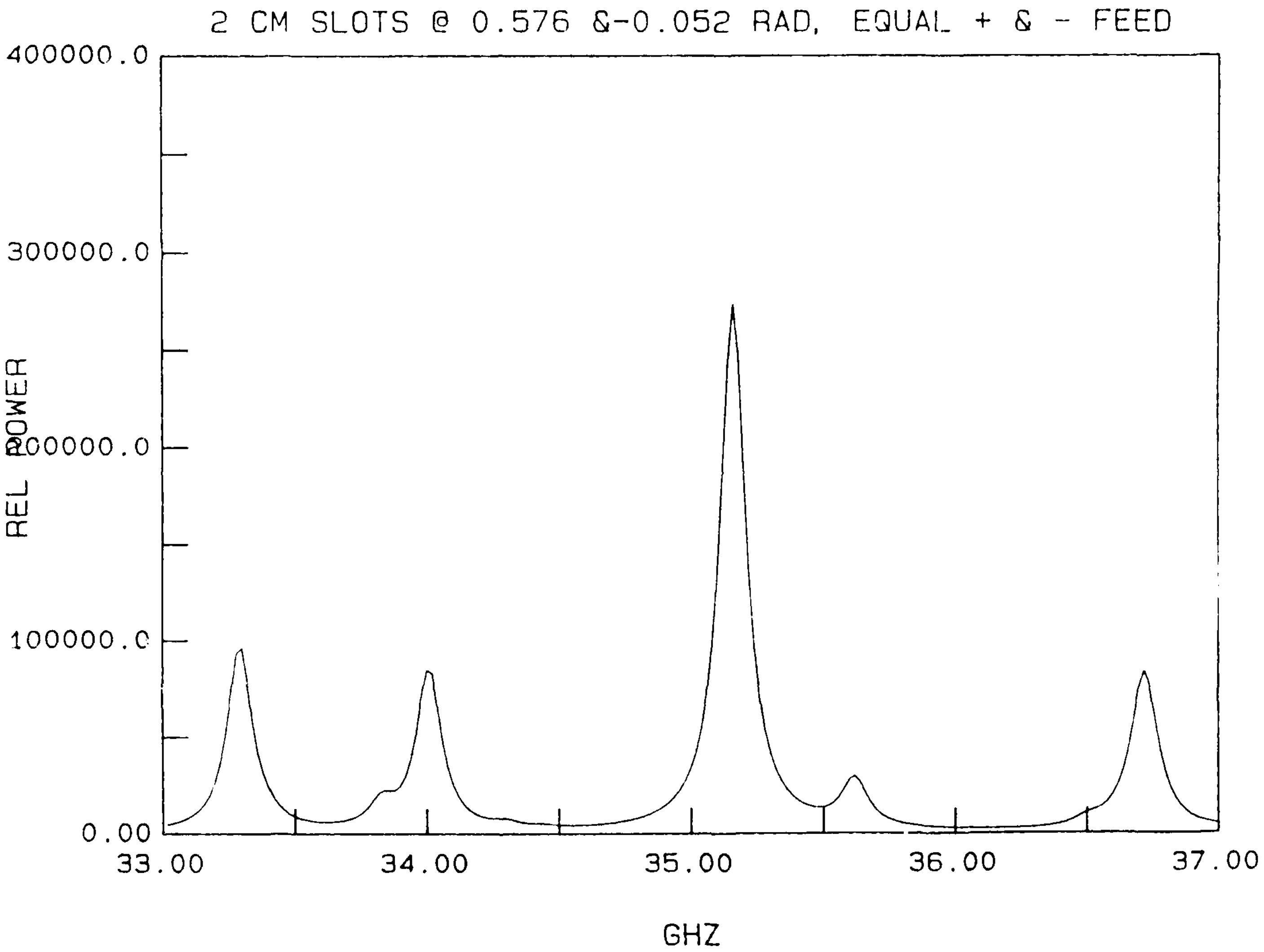

Fig. VIII.5. Cavity Excitations Near 35 GHz for a Pair of 2 cm Long Axial Slots 0.619 Radians Apart and Fed Out of Phase.

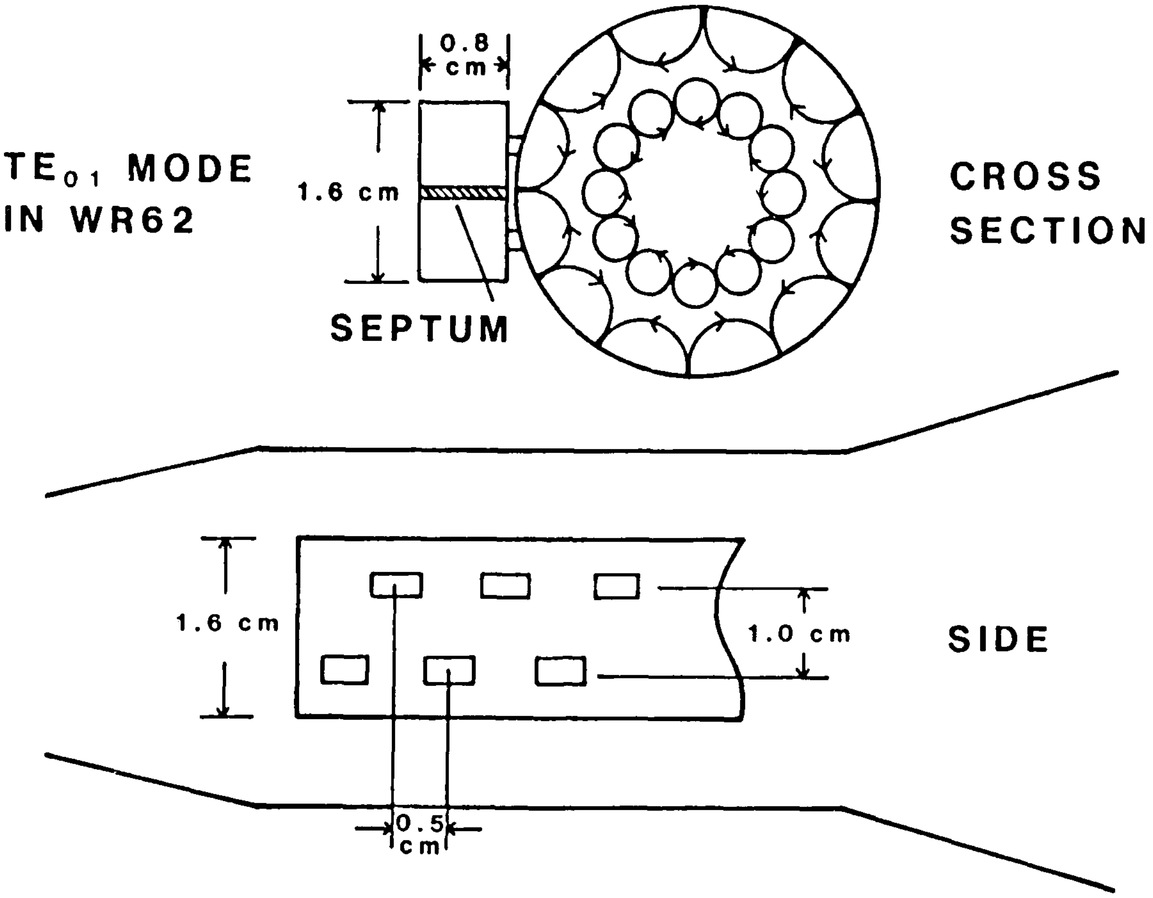

TE$_{62}$ CAVITY AND COUPLING METHOD

Fig. VIII.6. TE$_{62}$ Cavity and Coupling Method.

4740 DISTRIBUTION LIST

Air Force Avionics Laboratory
AFWAL/AADM-1
Wright/Patterson AFB, Ohio 45433
Attn: Walter Friez 1 copy

Air Force Office of
Scientific Research
Bolling AFB
Washington, D.C. 20332
Attn: H. Schlossberg 1 copy

Air Force Weapons Lab
Kirkland AFB
Albuquerque, New Mexico 87117
Attn: Dr. William Baker 2 copies

Columbia University
520 West 120th Street
Department of Electrical Engineering
New York, N.Y. 10027
Attn: Dr. S.P. Schlesinger 1 copy
A. Sen

Columbia University
520 West 120th Street
Department of Applied Physics
and Nuclear Engineering
New York, New York 10027
Attn: T.C. Marshall 1 copy
R. Gross

Cornell University
School of Applied and Engineering Physics
Ithica, New York 14853
Attn: Prof. Hans H. Fleischmann 1 copy
John Nation 1 copy
R. N. Sudan 1 copy

Dartmouth College
18 Wilder, Box 6127
Hanover, New Hampshire 03755
Attn: Dr. John E. Walsh 1 copy

Department of Energy
Washington, D.C. 20545
Attn: T.V. George/ER-531, GTN 1 copy

Defense Advanced Research Project Agency/DEO
1400 Wilson Blvd.
Arlington, Virginia 22209
Attn: Dr. S. Shey 1 copy
Dr. L. Buchanan 1 copy

Defense Communications Agency
Washington, D.C. 20305
Attn: Dr. Pravin C. Jain
Assistant for Communications
Technology 1 copy

Defense Nuclear Agency
Washington, D.C. 20305
Attn: Mr. J. Farber 1 copy
Mr. Lloyd Stossell 1 copy

Defense Technical Information Center
Cameron Station
5010 Duke Street
Alexandria, Virginia 22314 2 copies

Georgia Tech. EES-EOD
Baker Building
Atlanta, Georgia 30332
Attn: Dr. James J. Gallagher 1 copy

Hanscomb Air Force Base
Stop 21, Massachusetts 01731
Attn: Lt. Rich Nielson/ESD/INK 1 copy

Hughes Aircraft Co.
Electron Dynamics Division
3100 West Lomita Boulevard
Torrance, California 90509
Attn: J. Christiansen 1 copy
J.J. Tancredi 1 copy

KMS Fusion, Inc.
3941 Research Park Dr.
P.O. Box 1567
Ann Arbor, Michigan 48106
Attn: S.B. Segall 1 copy

Lawrence Livermore National Laboratory
P.O. Box 808
Livermore, California 94550
Attn: Dr. D. Prosnitz 1 copy
Dr. T.J. Orzechowski 1 copy
Dr. J. Chase 1 copy
Dr. M. Caplan 1 copy

Los Alamos Scientific Laboratory
P.O. Box 1663, AT5-827
Los Alamos, New Mexico 87545
Attn: Dr. J.C. Goldstein 1 copy

Dr. T.J.T. Kwan	1 copy
Dr. L. Thode	1 copy
Dr. C. Brau	1 copy
Dr. R. R. Bartsch	1 copy
Massachusetts Institute of Technology	
Department of Physics	
Cambridge, Massachusetts 02139	
Attn: Dr. G. Bekefi/36-213	1 copy
Dr. M. Porkolab/NW 36-213	1 copy
Dr. R. Davidson/NW 16-206	1 copy
Dr. A. Bers/NW 38-260	1 copy
Dr. K. Kreischer	1 copy
Massachusetts Institute of Technology	
167 Albany St., N.W. 16-200	
Cambridge, Massachusetts 02139	
Attn: Dr. R. Temkin/NW 14-4107	1 copy
Dr. B. Danley	1 copy
Spectra Technologies	
2755 Northup Way	
Bellevue, Washington 98004	
Attn: Dr. J.M. Slater	1 copy
Mission Research Corporation	
Suite 201	
5503 Cherokee Avenue	
Alexandria, Virginia 22312	
Attn: Dr. M. Bollen	1 copy
Dr. Tom Hargreaves	1 copy
Mission Research Corporation	
1720 Randolph Road, S.E.	
Albuquerque, New Mexico 87106	
Attn: Dr. Ken Busby	1 copy
Mr. Brendan B. Godfrey	1 copy
SPAWAR	
Washington, D.C. 20363	
Attn: E. Warden	
Code PDE 106-3113	1 copy
G. Bates	
PMW 145	1 copy
Naval Research Laboratory	
Addressee: Attn: Name/Code	
Code 1001 - T. Coffey	1 copy
Code 1220 - Security	1 copy
Code 2628 - TID Distribution	22 copies
Code 4000 - W. Ellis	1 copy
Code 4600 - D. Nagel	1 copy
Code 4700 - S. Ossakow	26 copies
Code 4700.1 - A.W. Ali	1 copy
Code 4710 - C. Kapetanakos	1 copy
Code 4740 - Branch Office	25 copies
Code 4740 - W. Black	1 copy

[illegible] RESEARCH
[illegible] ACADEMY
[illegible]
2 COPIES

Code 4740 - A. Fliflet	1 copy
Code 4740 - S. Gold	1 copy
Code 4740 - A. Kinkead	1 copy
Code 4740 - W.M. Manheimer	1 copy
Code 4740 - M. Rhinewine	1 copy
Code 4770 - G. Cooperstein	1 copy
Code 4790 - B. Hui	1 copy
Code 4790 - C.M. Hui	1 copy
Code 4790 - Y.Y. Lau	1 copy
Code 4790 - P. Sprangle	1 copy
Code 5700 - J. Montgomery	1 copy
Code 6840 - S.Y. Ahn	1 copy
Code 6840 - A. Ganguly	1 copy
Code 6840 - R.K. Parker	1 copy
Code 6840 - N.R. Vanderplaats	1 copy
Code 6850 - L.R. Whicker	1 copy
Code 6875 - R. Wagner	1 copy

Northrop Corporation
Defense Systems Division
600 Hicks Rd.
Rolling Meadows, Illinois 60008
Attn: Dr. Gunter Dohler — 1 copy

Oak Ridge National Laboratory
P.O. Box Y
Mail Stop 3
Building 9201-2
Oak Ridge, Tennessee 37830
Attn: Dr. A. England — 1 copy

Office of Naval Research
800 N. Quincy Street
Arlington, Va. 22217
Attn: Dr. C. Roberson — 1 copy
Dr. W. Condell — 1 copy
Dr. T. Berlincourt — 1 copy

Office of Naval Research
1030 E. Green Street
Pasadena, CA 91106
Attn: Dr. R. Behringer — 1 copy

Optical Sciences Center
University of Arizona
Tucson, Arizona 85721
Attn: Dr. Willis E. Lamb, Jr. — 1 copy

OSD/SDIO

Attn: IST (Dr. H. Brandt)
Washington, D.C. 20301-7100 — 5 copies

Pacific Missile Test Center
Code 0141-5
Point Mugu, California 93042
Attn: Will E. Chandler — 1 copy

Physical Dynamics, Inc.
P.O. Box 10367
Oakland, California 94610
Attn: A. Thomson 1 copy

Physics International
2700 Merced Street
San Leandro, California 94577
Attn: Dr. J. Benford 1 copy

Princeton Plasma
Plasma Physics Laboratory
James Forrestal Campus
P.O. Box 451
Princeton, New Jersey 08544
Attn: Dr. J. Doane 1 copy

Quantum Institute
University of California
Santa Barbara, California 93106
Attn: Dr. L. Elias 1 copy

Raytheon Company
Microwave Power Tube Division
Foundry Avenue
Waltham, Massachusetts 02154
Attn: N. Dionne 1 copy

Sandia National Laboratories
ORG. 1231, P.O. Box 5800
Albuquerque, New Mexico 87185
Attn: Dr. Thomas P. Wright 1 copy
Mr. J.E. Powell 1 copy
Dr. J. Hoffman 1 copy
Dr. W.P. Ballard 1 copy
Dr. C. Clark 1 copy

Science Applications, Inc.
1710 Goodridge Dr.
McLean, Virginia 22102
Attn: Adam Drobot 1 copy
D. Bacon 1 copy

Stanford University
High Energy Physics Laboratory
Stanford, California 94305
Attn: Dr. T.I. Smith 1 copy

TRW, Inc.
Space and Technology Group
Suite 2600
1000 Wilson Boulevard
Arlington, VA 22209
Attn: Dr. Neil C. Schoen 1 copy

TRW, Inc.
Redondo Beach, California 90278
Attn: Dr. H. Boehmer 1 copy
Dr. T. Romisser 1 copy

University of California
Physics Department
Irvine, California 92717
Attn: Dr. G. Benford 1 copy
Dr. N. Rostoker 1 copy

University of California
Department of Physics
Los Angeles, CA 90024
Attn: Dr. A.T. Lin 1 copy
Dr. N. Luhmann 1 copy
Dr. D. McDermott 1 copy

University of Maryland
Department of Electrical Engineering
College Park, Maryland 20742
Attn: Dr. V. L. Granatstein 1 copy
Dr. W. W. Destler 1 copy

University of Maryland
Laboratory for Plasma and Fusion Energy Studies
College Park, Maryland 20742
Attn: Dr. Jhan Varyan Hellman 1 copy
Dr. John Finn 1 copy
Dr. Baruch Levush 1 copy
Dr. Tom Antonsen 1 copy
Dr. Edward Ott 1 copy

University of Tennessee
Dept. of Electrical Engr.
Knoxville, Tennessee 37916

Attn: Dr. I. Alexeff 1 copy

University of New Mexico
Department of Physics and Astronomy
800 Yale Blvd, N.E.
Albuquerque, New Mexico 87131
Attn: Dr. Gerald T. Moore 1 copy
Dr. Stan Humphries 1 copy

University of Utah
Department of Electrical Engineering
3053 Merrill Engineering Bldg.
Salt Lake City, Utah 84112
Attn: Dr. Larry Barnett 1 copy
Dr. J. Mark Baird 1 copy

U. S. Naval Academy
Annapolis, Maryland 21402-5021 1 copy

U. S. Army
Harry Diamond Labs
2800 Powder Mill Road
Adelphi, Maryland 20783-1145
Attn: Dr. Edward Brown 1 copy
Dr. Michael Chaffey 1 copy
Dr. Howard Brandt 1 copy

Varian Associates
611 Hansen Way
Palo Alto, California 94303
Attn: Dr. H. Jory 1 copy
Dr. David Stone 1 copy
Dr. Kevin Felch 1 copy
Dr. A. Salop 1 copy

Varian Eimac San Carlos Division
301 Industrial Way
San Carlos, California 94070
Attn: C. Marshall Loring 1 copy

Yale University
Applied Physics
Madison Lab
P.O. Box 2159
Yale Station
New Haven, Connecticut 06520
Attn: Dr. N. Ebrahim 1 copy
Dr. I. Bernstein 1 copy